

Aus dem Bereich Medizinische Biochemie und Molekularbiologie
Theoretische Medizin und Biowissenschaften
der Medizinischen Fakultät
der Universität des Saarlandes, Homburg/Saar

**Assembly, regulation and molecular architecture of
mitochondrial cristae organising systems**

**Dissertation zur Erlangung des Grades eines Doktors der
Naturwissenschaften
der Medizinischen Fakultät der
UNIVERSITÄT DES SAARLANDES
2020**

vorgelegt von: Florian J.A. Wollweber
geb. am: 31.03.1993 in Solingen

Tag der Promotion: 03.02.2021

Dekan: Prof. Dr. M. D. Menger

1. Berichterstatter: Prof. Dr. M. van der Laan

2. Berichterstatter: Prof. Dr. M. Hoth

3. Berichterstatter: Prof. Dr. C. Ungermann

Table of contents

1. Summary.....	5
2. Zusammenfassung.....	6
3. Introduction	7
3.1.Mitochondria are multifunctional, semi-autonomous organelles	7
3.2.Cristae are bioenergetic micro-compartments	9
3.3.Large assemblies of ATP-synthase dimers shape cristae membranes	11
3.4.A dynamin-like GTPase actively remodels cristae membranes	13
3.5.The mitochondrial contact site and cristae organising system forms the proteinaceous scaffold of crista junctions	14
3.6.MICOS has multiple connections to protein biogenesis machineries.....	17
3.7.Crosstalk of cristae organising systems and dynamic remodelling of mitochondrial membranes	19
4. Aims	20
5. Materials and Methods	21
5.1.Materials	21
5.1.1. Reagents and critical equipment.....	21
5.1.2. Antibodies	25
5.1.3. Plasmids	27
5.1.4. Yeast strains	28
5.1.5. Cell lines	31
5.2.Methods	32
5.2.1. Biochemistry	32
5.2.2. Yeast assays.....	37
5.2.3. Generation and culture of human cell lines.....	39
6. Results	41
6.1.MICOS core subunits are required for efficient metabolic adaptation in yeast .	41
6.2.A Mic10-ATP synthase interaction is crucial for metabolic adaptation.....	45
6.3.Mic10 oligomerisation is regulated by Mic26-Mic27 antagonism.....	48
6.4.MICOS organisation is conserved from yeast to man	53
6.5.Human MIC10 affects cristae organising proteins of the inner membrane	56
6.6.Hierarchical organisation of the MIC10 subcomplex	59
6.7.The human MICOS/MIB complex and DNAJC11 spatially coordinate β -barrel biogenesis in the outer mitochondrial membrane.....	62
6.8. Assembly mechanism of the cristae-shaping dymanin-like GTPase Mgm1	65
7. Discussion.....	72
7.1.MICOS core subunits are required for efficient adaptation to respiratory metabolism in yeast.....	72
7.2.The Mic10-ATP synthase interaction is crucial for metabolic adaptation.....	73

7.3.Mic10 oligomerisation is regulated by Mic26-27 antagonism and cardiolipin..	74
7.4.MICOS organisation is conserved from yeast to man	76
7.5.The MIB complex and DNAJC11 spatially coordinate mitochondrial protein biogenesis	78
7.6.Helical arrays of Mgm1 tetramers shape the inner mitochondrial membrane ...	82
7.7.Conclusion	85
8. References	87
9. Abbreviations.....	104
10. List of figures.....	107
11. List of tables	107
12. Acknowledgements	108
13. Publications	109
14. Curriculum vitae	110

1. Summary

Mitochondria are double-membrane bound organelles with a plethora of metabolic and signalling functions, which are facilitated by their complex micro-architecture. The mitochondrial inner membrane possesses an intricate ultrastructure and is divided into a boundary membrane and specialized membrane invaginations, termed cristae, which are optimised for oxidative phosphorylation and a universal structural feature of aerobic eukaryotes. Several protein machineries help to shape cristae. Dimers of the ATP synthase create membrane curvature to stabilise cristae tips and rims, while the *mitochondrial contact site and cristae organising system* (MICOS) stabilises crista junctions and links inner and outer membrane. In addition, dynamin-like GTPases of the OPA1/Mgm1 family dynamically remodel cristae shape by a poorly characterised mechanism.

The work described in this thesis further elucidates the assembly mechanisms of MICOS and Mgm1 using a combination of genetic and biochemical approaches in yeast and human cell lines. Studies in yeast reveal that the MICOS core subunits Mic10 and Mic60 are essential for the efficient adaptation to respiratory metabolism. A moonlighting function of Mic10 in modulating ATP synthase assembly appears to be particularly important for this process. The assembly of Mic10 can be regulated by the two paralogous MICOS subunits Mic26 and Mic27 in an antagonistic manner, possibly to coordinate Mic10 functions. The second core subunit Mic60 forms stable supercomplexes with the β -barrel biogenesis machinery of the outer membrane in human cells. A detailed analysis of knockout cell lines revealed that a lack of Mic60 leads to protein biogenesis defects and that a J-protein of the outer membrane interacts with MICOS to spatially coordinate protein biogenesis at import sites.

The dynamic remodelling of cristae membranes is mostly mediated by proteins of the Mgm1/OPA1 family. The crystal structure of Mgm1 described here revealed a tetrameric assembly and cryo-electron tomography reconstructions of membrane-bound Mgm1 showed that these tetramers assemble into helical filaments on the inside and outside of membrane tubes. Mgm1 yeast mutants demonstrated that the assembly of Mgm1 into dimers and tetramers is essential for the maintenance of cristae architecture and respiratory growth.

The work described here shed light on the assembly of MICOS and Mgm1, which are two major cristae organising systems. A structural biology approach combined with data from yeast mutants revealed how Mgm1 filaments can remodel cristae membranes. A comparative approach in yeast and human cells showed that MICOS organisation is evolutionarily conserved and that both core subunits affect distinct mitochondrial pathways. While Mic60 is directly involved in protein biogenesis of outer membrane proteins, Mic10 affects the assembly of inner membrane complexes such as the ATP synthase. Future work will have to dissect how the membrane-shaping protein machineries of the inner membrane coordinate their activities to control cristae shape in a regulated manner.

2. Zusammenfassung

Mitochondrien sind von zwei Membranen umschlossene Organellen aller eukaryotischen Zellen mit einer Vielzahl an Funktionen im zellulären Metabolismus und in Signalwegen. Die innere Membran formt Einstülpungen oder Cristae mit einer für die zelluläre Atmung optimierten Form. Ein großer Proteinkomplex (MICOS; *mitochondrial contact site and cristae organising system*) formt die Verbindung zwischen Cristae und dem Rest der Innenmembrane und verbindet außerdem Außen- und Innenmembran. Dimere der ATP-Synthase stabilisieren die Membrankrümmung in Cristae. Zusätzlich können Cristae durch die Dynamin-ähnliche GTPase Mgm1 verformt werden.

Mit Hilfe genetischer und biochemischer Ansätze in Hefen und humanen Zelllinien konnten in dieser Arbeit detaillierte Modelle der Assemblierung von MICOS und Mgm1 erstellt werden. Experimente in Hefe zeigen, dass die zentralen MICOS Untereinheiten Mic10 und Mic60 in der Anpassung an respiratorischen Metabolismus beteiligt sind. Eine Zusatzfunktion von Mic10, welches auch die Assemblierung der ATP-Synthase beeinflusst, scheint hier besonders wichtig zu sein. Die Assemblierung von Mic10 wird auch aus diesem Grund von zwei anderen MICOS Untereinheiten, den paralogen Proteinen Mic26 und Mic27, in einer antagonistischen Weise reguliert. Die zweite zentrale Untereinheit Mic60 bildet in humanen Zellen sehr stabile Kontakte mit der β -barrel Proteinbiogenesemaschinerie der Außenmembran und koordiniert, zusammen mit einem hier charakterisiertem J-Protein, die Proteinbiogenese auf der Mitochondrienoberfläche.

Die dynamische Veränderung der Cristaestruktur wird hauptsächlich durch die Dynamin-ähnliche GTPase Mgm1 vollzogen. Basierend auf einer Mgm1 Kristallstruktur und Kryoelektronen-Tomographie Daten konnte ein modularer Aufbau in Dimere, Tetramere und helikale Filamente auf der Außen- und Innenseite von Membranröhrchen gezeigt werden. Die hier beschriebenen Experimente mit Hefe Mgm1 Mutanten konnten zeigen, dass dieser modulare Aufbau essenziell für die Aufrechterhaltung der Cristaestruktur ist.

Die hier dargestellten Arbeiten beschreiben neue Details des Aufbaus von MICOS und Mgm1. Mittels einer Kombination aus strukturbioologischen Daten und genetischen Ansätzen in Hefe konnte gezeigt werden wie Mgm1-Filamente Cristae verformen können. Ein Vergleich des molekularen Aufbaus des MICOS Komplexes in Hefe- und Säugerzellen offenbarte, dass MICOS hochkonserviert ist und dass die zentralen MICOS Untereinheiten unterschiedliche Prozesse in Mitochondrien beeinflussen. Während Mic60 die Biogenese mitochondrialer Außenmembranproteine steuert, hat Mic10 einen Einfluss auf die Assemblierung von Innenmembrankomplexen, wie zum Beispiel der ATP-Synthase. Zukünftige Studien müssen versuchen, das Zusammenspiel der verschiedenen cristaeverformenden Proteinkomplexe besser zu verstehen.

3. Introduction

3.1. *Mitochondria are multifunctional, semi-autonomous organelles*

The defining feature of eukaryotes is their sub-cellular compartmentalisation into membrane-bound organelles, which spatially restrict metabolic processes and signalling events. Eukaryotes evolved from a single endosymbiotic event approximately 2 billion years ago, during which a gram-negative bacterium related to modern alphaproteobacteria was engulfed by a proto-eukaryote. This endosymbiotic ancestor of modern mitochondria then integrated into the host cells metabolism and physiology and evolved into a permanent organelle (Roger et al, 2017). During this process, mitochondrial genes were transferred to the nuclear genome, sophisticated machineries evolved for the import of proteins from the cytosol (Dolezal et al, 2006) and the metabolic activities of both cells were integrated, enabling the development of complex life. Even though mitochondria have lost the majority of their genome, they cannot be formed *de novo* but rely on fission and fusion events (Giacomello et al, 2020) as a relic of their endosymbiotic ancestry. Mitochondria form a reticulated network within cells and it is very likely that cells possess several mitochondrial subspecies with distinct properties, depending on their contact to other organelles (Benador et al, 2018) or their subcellular localisation. A complex regulatory network coordinates both cellular genomes to fine-tune metabolism (Mottis et al, 2019). Furthermore, mitochondria of modern eukaryotes still show signs of bacterial origin, as they possess two membranes which contain the non-bilayer forming phospholipid cardiolipin (Ikon & Ryan, 2017) and many proteins typical for bacterial cells, such as β -barrel proteins of the outer membrane (Pfanner et al, 2019).

Virtually all known eukaryotes contain mitochondria or mitochondria-like organelles. Modern mitochondria are best known for their role in generating the vast amount of cellular ATP by aerobic respiration, but are also involved in many metabolic pathways, cell fate decisions and signalling processes (McBride et al, 2006). This functional diversity is reflected in the size of the mitochondrial proteome, which encompasses more than 1,000 different proteins in a simple eukaryote such as baker's yeast (Sickmann et al, 2003; Morgenstern et al, 2017). Due to the multifaceted role of mitochondria in many different cellular processes, mitochondrial dysfunction has been implicated as causative in a plethora of diseases, collectively termed mitochondriopathies (Vafai & Mootha, 2012). These monogenic defects of either nuclear or mtDNA encoded mitochondrial proteins affect multiple organ systems, particularly the peripheral and central nervous system as well as heart, liver and kidney function. As a result, mitochondriopathies can cause a wide variety of symptoms, which poses a challenge in diagnosis and causative care.

The diverse array of mitochondrial functions is also facilitated by the complex double-membrane microarchitecture of mitochondria (Figure 1). The two mitochondrial membranes enclose two aqueous compartments, the intermembrane space as well as the matrix. The outer mitochondrial membrane separates the organelle from the cytosol and contains protein

machineries that are responsible for the import of proteins and the exchange of metabolites. In addition, the outer membrane mediates the contact to other organelles (Eisenberg-Bord et al, 2016; Murley & Nunnari, 2016) and between mitochondria (Picard et al, 2015). Outer membrane mediated contact to other organelles, especially to the endoplasmic reticulum, is necessary for mitochondrial signalling and lipid exchange (Wu et al, 2018), but also for mitochondrial fusion and fission (Lewis et al, 2016; Abrisch et al, 2020; Nagashima et al, 2020) and mtDNA replication and distribution (Murley et al, 2013; Lewis et al, 2016).

The extremely protein-rich inner mitochondrial membrane encloses the matrix space and is highly folded. It can be divided into the inner boundary membrane (IBM) and cristae membranes, which protrude into the matrix space and are the main site for oxidative phosphorylation (Gilkerson et al, 2003). This architectural feature is pivotal for the mitochondrion's main function in oxidative phosphorylation, as it extends the membrane surface area and creates a specialized compartment optimised for ATP generation (Strauss et al, 2008; Rieger et al, 2014). The transition between both inner membrane subcompartments, termed crista junction (CJ), possesses a high degree of membrane curvature (Frey & Mannella, 2000). This elaborate intraorganellar compartmentalisation is a necessity for fulfilling the large number of mitochondrial functions, since the spatial protein distribution within the mitochondrial inner membrane is highly asymmetric (Figure 1; Gilkerson et al, 2003; Vogel et al, 2006; Wurm & Jakobs, 2006; Stoldt et al, 2018; Busch, 2020). While the inner boundary membrane harbours metabolite and protein transporters, cristae membranes contain the majority of the respiratory chain. This micro-compartmentalisation likely increases the efficiency of oxidative phosphorylation and represents a common feature of bioenergetic membranes (Busch et al, 2013). In addition to its unusual protein abundance and distribution, the inner membrane possesses a unique lipid composition as a result of its bacterial ancestry. Approximately 50% of the membrane is composed of the non-bilayer forming lipids phosphatidylethanolamine and cardiolipin which help to maintain the high degrees of membrane curvature found in the inner membrane (Ikon & Ryan, 2017). These lipids also directly affect the stability and localisation of the protein complexes found in the inner membrane (Zhang et al, 2002; Pfeiffer et al, 2003; Tamura et al, 2006; Kutik et al, 2008; Acehan et al, 2011; Böttinger et al, 2012; Bazán et al, 2013; Friedman et al, 2015) and cardiolipin influences the assembly and activity of all major proteinaceous cristae organising systems (Acehan et al, 2011; Friedman et al, 2015; Ban et al, 2017). Cardiolipin and a local pH gradient might be sufficient for promoting membrane invaginations in a minimal membrane system (Khalifat et al, 2008), demonstrating an intrinsic link between lipid composition and the unique membrane structure of mitochondria.

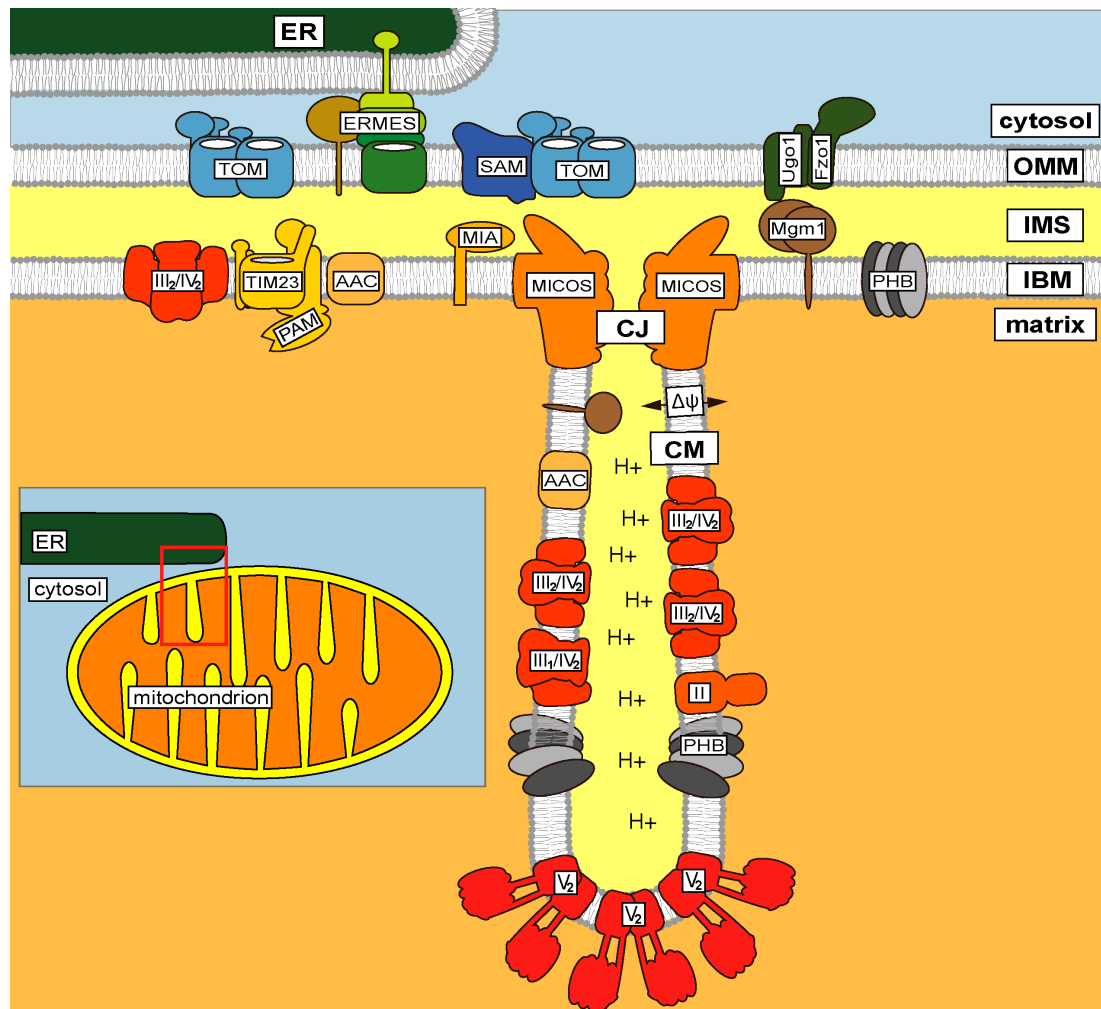


Figure 1 Asymmetry of mitochondrial membranes in yeast (adapted from Wollweber et al, 2017)

The double-membrane architecture of mitochondria enables a spatial compartmentalisation of metabolic processes. The two mitochondrial membranes enclose two aqueous compartments, the intermembrane space (IMS) and the matrix. The outer membrane (OMM) contains protein complexes that mediate contact sites to other organelles, such as the ER-mitochondria encounter structure (ERMES) and the fission and fusion (Ugo1/Fzo1/Mgm1) machinery. The outer membrane and the inner boundary membrane (IBM) contain metabolite transporters, such as VDAC/porin or the ATP/ADP carrier (AAC), as well as protein translocases. Protein translocases, such as TOM (translocase of the outer membrane) and SAM (sorting and assembly machinery), form supercomplexes in the outer membrane. The TOM complex also forms transient interactions with the presequence translocase of the inner membrane (TIM23/PAM). IMM/OMM tethering is also mediated by the mitochondrial contact site and cristae organising system (MICOS) at crista junctions (CJ) with its outer-membrane interaction partners. The cristae membranes (CM) of mitochondria contain the majority of respiratory chain supercomplexes for the generation of ATP by oxidative phosphorylation (in red: II, III, IV), which generate the membrane potential ($\Delta\psi$) that is used by the ATP synthase (V_2) for the generation of ATP.

3.2. Cristae are bioenergetic micro-compartments

Mitochondrial cristae are a universal feature of aerobic eukaryotes and of crucial importance for efficient oxidative phosphorylation (Cogliati et al, 2013). Cristae are likely structural homologues of alphaproteobacterial intracytoplasmic membranes (Muñoz-Gómez et al, 2017). These membrane systems evolved to increase the surface area available for certain bioenergetic processes and to increase their efficiency by compartmentalisation. Cristae contain the majority of the respiratory chain (Gilkerson et al, 2003), which consists of four

protein complexes that couple electron transport to the translocation of protons across the inner membrane. The resulting chemiosmotic membrane potential can be used for the generation of ATP by the ATP synthase but also fuels processes such as protein import. The respiratory chain can be divided into four separate entities: Complex I transfers electrons from NADH to ubiquinone, which are transferred to cytochrome c by complex III. Complex IV catalyses the final reaction, in which electrons are transferred to oxygen. Complex II does not contribute to proton translocation but transfers electrons from succinate to ubiquinone as part of the TCA cycle. A number of experiments used blue-native PAGE (Cruciat et al, 2000; Schägger & Pfeiffer, 2000), electron microscopy (Schäfer et al, 2006) and in situ cryo-electron tomography (Davies et al, 2018) to show that respiratory complexes I, III and IV are not exclusively present as separate entities, but rather form stable assemblies. Impairment of one complex can destabilise another complex (Schägger et al, 2004; Diaz et al, 2006; Vempati et al, 2009) and isolated supercomplexes are catalytically active (Acín-Pérez et al, 2008). Several hypotheses have been developed to explain the occurrence of respiratory supercomplexes (Milenkovic et al, 2017). One of the most prominent explanations is substrate channelling, based on a proposed partitioning of substrate pools (Lapuente-Brun et al, 2013). This view has however been challenged (Trouillard et al, 2011; Blaza et al, 2014). Another hypothesis suggests that supercomplex formation minimises and controls ROS production (Maranzana et al, 2013), which is a side effect of oxidative phosphorylation. Finally, it has been proposed that the high protein density of the mitochondrial inner membrane requires the formation of defined but weak interactions between complexes to prevent protein aggregation (Blaza et al, 2014). Following this hypothesis, supercomplex formation would not only be a consequence of the special properties of the IMM but would also be involved in maintaining its architecture and functionality. Importantly, mitochondrial cristae shape affects the organisation and assembly of supercomplexes with a profound influence on mitochondrial function and cell growth (Cogliati et al., 2013).

Mitochondrial cristae membranes show a remarkable ultrastructural diversity depending on the organism (Muñoz-Gómez et al, 2017; Hashimi, 2019; Pánek et al, 2020) and cell type, ranging from tubular to discoidal or lamellar shapes. Ultrastructural aberrations are frequently observed in mitochondriopathies (Vincent et al, 2016) and cristae shape changes during ageing (Brandt et al, 2017). The molecular basis as well as the functional relevance of these different shapes is still unknown. Crista junctions, which connect inner boundary and cristae membranes, possess a very defined and stable structure (Renken et al, 2002) with a narrow diameter. The shape appears to vary from circular to slot-like openings, depending on the organism or tissue (Mannella, 2006; Pánek et al, 2020). Even though cristae are ubiquitous structures among aerobic eukaryotes (Muñoz-Gómez et al, 2017), which underlines their importance for oxidative phosphorylation, the exact molecular advantages of the ultrastructural compartmentalisation into two inner membrane subcompartments are still

under debate. They clearly increase the surface area available for oxidative phosphorylation and form a microcompartment that enables a dense packing and a close spatial proximity of respiratory chain complexes. Cristae shape therefore enables kinetic coupling of proton pumping and ATP generation, even though the crista lumen might not represent a microscopic proton trap (Toth et al, 2020). Very recent super resolution microscopy data suggests that individual cristae are energetically isolated units, which supposedly prevents a collapse of aerobic respiration within an entire mitochondrion after local disturbances of the membrane potential (Wolf et al, 2019).

Cristae shape appears to vary depending on the metabolic state of the cell. Early experiments using isolated mitochondria showed that mitochondrial ultrastructure can reversibly transition from orthodox to condensed states (Hackenbrock, 1966, 1968), depending on the respiratory activity. Furthermore, experiments in yeast showed that mitochondrial ultrastructure varied during different growth phases (Yotsuyanagi, 1962). These findings demonstrated that inner membrane architecture is not static, but dynamically responds to metabolic states. In higher eukaryotes, cristae are also remodelled to mobilise cytochrome c during apoptosis (Scorrano et al, 2002; Frezza et al, 2006). Recently, super-resolution imaging was successfully applied for the visualization of cristae in living cells (Stephan et al, 2019; Wang et al, 2019a). These approaches revealed that cristae are dynamically remodelled and might undergo fusion events (Kondadi et al, 2020), which possibly explains the dynamic alteration of membrane shape described in the 1960s (Hackenbrock, 1966, 1968). The molecular bases of these phenomena and the formation of cristae are still largely unexplored.

3.3. Large assemblies of ATP-synthase dimers shape cristae membranes

The generation of ATP by oxidative phosphorylation is catalysed by respiratory supercomplexes, which create a proton gradient across the IMM that is utilised by a conserved F_1F_0 ATP-synthase to synthesize ATP. This highly conserved complex can be divided into two entities (reviewed in Walker, 2013; Kühlbrandt, 2019), a membrane-bound F_0 moiety and the catalytic and soluble F_1 part. F_1 is mainly formed by a hexamer of three α and three β subunits, which can hydrolyse ATP. F_1 is connected to F_0 by a central and peripheral stalk. Proton translocation via F_0 creates a torque on the central stator, which leads to conformational changes in F_1 that allow the phosphorylation of ADP. The central F_0 subunit c forms a ring, whose stoichiometry determines the ATP synthesis rate per translocated proton and varies between species. In addition to the catalytic function of ATP synthase, more recent evidence demonstrated an essential function in shaping mitochondrial cristae membranes. Early electron-microscopy studies suggested the existence of non-randomly distributed and highly-ordered supramolecular ATP synthase assemblies along tubular cristae in *Paramecium* (Allen et al, 1989). Monomeric complexes are able to deform lipid bilayers, suggesting an intrinsic role of the structure in cristae shaping (Jiko et al, 2015). Biochemical studies in yeast using

mild detergents and native gel electrophoresis showed the existence of dimeric species of the complex containing dimer-specific subunits e, g and k (Arnold et al, 1998; Donzeau et al, 2000; Brunner et al, 2002; Everard-Gigot et al, 2005). Both dimer-specific subunits harbour a GxxxG motif (Russ & Engelman, 2000), which is located at the dimerisation interface and essential for the function of both subunits (Arselin et al, 2003; Bustos & Velours, 2005). Structures of dimeric ATP synthases helped to unravel the molecular basis of its cristae shaping activity by local membrane bending (Dudkina et al, 2005; Hahn et al, 2016; Guo et al, 2017). Deletion of subunit e or g in yeast causes a destabilisation of the dimers and drastically altered membrane architecture including inflated and deformed cristae (Paumard et al, 2002; Arselin et al, 2004) and a decreased mitochondrial membrane potential (Bornhövd et al, 2006). Dimerisation and oligomerisation of the complex is not thought to influence its catalytic activity, but rather confer an additional function in allowing to shape mitochondrial cristae, which explains the striking phenotype of dimerisation-deficient mutant mitochondria. Interestingly, the amount of dimer-specific subunits directly correlates to the architecture of the inner membrane as shown by inducible expression systems (Arselin et al, 2004). Electron microscopy studies showed that ATP synthase dimers assemble into even larger structures along cristae (Paumard et al, 2002; Buzhynskyy et al, 2007; Strauss et al, 2008; Davies et al, 2012; Blum et al, 2019). Recent studies using cryo-electron tomography suggested that this assembly does not depend on protein-protein interactions between dimers, but rather relies on the local membrane curvature of dimers which leads to a self-association into dimer rows (Anselmi et al, 2018; Blum et al, 2019).

ATP synthase clustering is thought to be regulated depending on the metabolic requirements of the cell (Jimenez et al, 2014; Plecítá-Hlavatá et al, 2016) and the suborganellar localisation of the complex might change in different metabolic conditions (Salewskij et al, 2020). Multiple lines of evidence now suggest that supra-molecular assemblies of ATP synthase are important for shaping the cristae membrane, but the physiological benefits of local membrane bending are still not fully explored. To date, no diseases have been associated with a specific defect in dimerisation, which possibly underlines the fundamental nature of this function. However, a variety of physiological processes were found to be dependent on the membrane-shaping activity of ATP synthase: IF_1 dependent dimerisation was suggested to inhibit apoptosis by preventing cytochrome c release (Faccenda et al, 2013). ATP synthase dimerisation status changes in ageing (Daum et al, 2013). Finally, a study suggested that germline differentiation requires ATP synthase oligomerisation, but is not dependent on the catalytic activity (Teixeira et al, 2015). These examples demonstrate the importance of the membrane-shaping activity of the complex independently of its role in energy conversion.

3.4. A dynamin-like GTPase actively remodels cristae membranes

While the ATP synthase is essential for the maintenance of cristae architecture, it is not the only complex involved in the remodelling of cristae membranes. One of the main proteins implicated in cristae remodelling is the dynamin-like GTPase Mgm1 in yeast and the closely related OPA1 protein in mammals. Yeast Mgm1 was first identified as an essential protein for the maintenance of mitochondrial DNA (Jones & Fangman, 1992). Mutations of the human OPA1 gene were identified as a cause of optical atrophy (Alexander et al, 2000; Delettre et al, 2000). Mgm1 and OPA1 have at least two functions in mediating the fusion of the mitochondrial inner membrane (Wong et al, 2003; Cipolat et al, 2004; Meeusen et al, 2006) as well as the remodelling of cristae during processes such as apoptosis (Olichon et al, 2002; Frezza et al, 2006) or metabolic adaptation (Patten et al, 2014). Mgm1 and OPA1 interact with the outer membrane fusion machinery to mediate fusion of both mitochondrial membranes (Wong et al, 2003; Cipolat et al, 2004). Mgm1 might also be important for the biogenesis of lamellar cristae via partial inner membrane fusion (Harner et al, 2016). Unlike other dynamin-like GTPases, both proteins are present in soluble short forms as well as membrane-bound long forms. The short form of Mgm1 (s-Mgm1) is generated by intra-membrane proteolysis by the rhomboid protease Pcp1 during import (Herlan et al, 2003; McQuibban et al, 2003). OPA1 forms are generated by alternative splicing as well as proteolytic processing by at least three proteases (Del Dotto et al, 2018a) and different tissues express a distinct combination of isoforms (Olichon et al, 2007). Isoform processing is also closely linked to metabolic activity (Mishra et al, 2014). The different forms of the protein possess partially overlapping essential functions and additionally carry out specialized functions. Fusion requires Mgm1-mediated local deformation of the membrane (Rujiviphat et al, 2015). During fusion, membrane-bound l-Mgm1 is thought to anchor the catalytically active soluble Mgm1 (DeVay et al, 2009; Zick et al, 2009). In agreement with this model, recent *in vitro* evidence showed that a combination of membrane-bound and soluble forms is essential for successful mitochondrial fusion (Ge et al, 2020). While only the combined expression of long and short forms can fully rescue mitochondrial network morphology in OPA1 knockout cells (Song et al, 2007; Del Dotto et al, 2017), short OPA1 isoforms can sustain cristae structure and the bioenergetic properties of mitochondria (Lee et al, 2017). In addition, the proteolytic generation of s-OPA1 can support cell survival during oxidative stress (Lee et al, 2020).

Since OPA1/Mgm1 proteins possess such a complex biogenesis and diverse array of functions, their contribution to membrane fusion and cristae shaping still remain poorly understood. A mechanistic understanding is further complicated by the observation that some OPA1 functions require not only homo-typic interactions but also specific contacts with lipids (Ban et al, 2017) and other cristae organising complexes (Glytsou et al, 2016; Quintana-Cabrera et al, 2018; chapter 3.7). A detailed mechanistic understanding of OPA1/Mgm1 mediated membrane remodelling is not only pivotal for the elucidation of processes such as cristae

formation and mitochondrial adaptation to metabolic demands, but also for the potential treatment of diverse mitochondriopathies, since OPA1 dependent cristae shaping is crucial for respiratory chain supercomplex stability (Cogliati et al, 2013). OPA1 overexpression in mice, which leads to a stabilisation and tightening of cristae, was found to be beneficial in two mitochondrial disease models (Civiletto et al, 2015) and to prevent apoptosis and ischemic tissue damage (Varanita et al, 2015). As a result, OPA1 was proposed as a potential target for gene therapy in mitochondrial diseases (Del Dotto et al, 2018b).

3.5. *The mitochondrial contact site and cristae organising system forms the proteinaceous scaffold of crista junctions*

The crista junction is a critical region of the mitochondrial inner membrane, since it not only separates two functionally distinct compartments, but also allows for a regulated lipid, metabolite and possibly protein exchange. This region is characterised by an unusually high membrane curvature and has to be maintained by a specialized protein machinery. Studies in yeast (Rabl et al, 2009) and mammalian cells (John et al, 2005) identified the protein mitofilin (later termed Mic60) as crucial component of this putative protein complex. Several independent approaches (Harner et al, 2011; Hoppins et al, 2011; von der Malsburg et al, 2011; Alkhaja et al, 2012) then led to the identification of a large multi-protein complex located at CJs, later termed *mitochondrial contact site and cristae organising system* (MICOS). It consists of at least six genuine subunits in yeast (7 in mammals), which were termed Mic10 – Mic60 (Pfanner et al, 2014). Furthermore, MICOS-interacting proteins with so far poorly-defined functions have been identified (reviewed in Eramo et al, 2020), including the J-domain containing protein DNAJC11 (Xie et al, 2007; Ioakeimidis et al, 2014) and the carrier-like protein SLC25A46 (Abrams et al, 2015; Janer et al, 2016; Steffen et al, 2017) in the outer membrane. Depleting the core components Mic10 or Mic60 results in the same phenotype, cristae detach from the IBM, creating internal stacks of cristae membranes with a number of secondary effects on mitochondrial functionality (Harner et al, 2011; Hoppins et al, 2011; von der Malsburg et al, 2011; Alkhaja et al, 2012). This striking phenotype indicated that MICOS forms the protein backbone of cristae junctions, enabling the maintenance of the exceptionally high degree of membrane curvature in these regions. MICOS subunits have been identified in all aerobic eukaryotes, supporting an essential function in the maintenance of mitochondrial ultrastructure. Furthermore, Mic60 orthologues were identified in alphaproteobacteria, which are related to the mitochondrial ancestor, indicating a pre-endosymbiotic origin of MICOS (Muñoz-Gómez et al, 2015). These bacteria possess intracytoplasmic membranes which strongly resemble modern cristae. The identification of ancestral Mic60 thus supports the hypothesis that bacterial intracytoplasmic membranes are structural homologues of modern cristae (Muñoz-Gómez et al, 2015, 2017). Further studies in yeast and mammalian cells could differentiate two MICOS subcomplexes, both containing one of the two core components

(Figure 2): The membrane-bridging Mic60-19/25 subcomplex and the membrane-shaping Mic10-12-26-27 subcomplex (Bohnert et al, 2015; Friedman et al, 2015; Guarani et al, 2015). The Mic60 subcomplex appears to be primarily involved in mediating the numerous contacts with other protein machineries (Xie et al, 2007; Harner et al, 2011; Hoppins et al, 2011; von der Malsburg et al, 2011; Alkhaja et al, 2012; Ott et al, 2012; Friedman et al, 2015), especially of the outer membrane, such as porin/VDAC and the protein translocases TOM and SAM. The highly conserved C-terminal region of Mic60 seems to be particularly important for this function (Korner et al, 2012; Zerbès et al, 2012). It is tempting to speculate that Mic60 strategically positions the protein import machinery at crista junctions to promote protein (complex) biogenesis. The highly organised subcellular and sub-organellar distribution of MICOS (Jans et al, 2013; Stoldt et al, 2019) would allow to spatially coordinate mitochondrial biogenesis, including lipid transport (Aaltonen et al, 2016; Michaud et al, 2016). Importantly, its interaction with the outer membrane SAM complex appears to be conserved throughout eukaryotic evolution (Kaurov et al, 2018) and seems to be much stronger in metazoans than in yeast (Xie et al, 2007; Ott et al, 2012, 2015; Ding et al, 2015; Huynen et al, 2016; Tang et al, 2020). This stronger interaction leads to the formation of a stable two-membrane spanning complex, sometimes referred to as mitochondrial intermembrane space bridging (MIB) complex (Ott et al, 2012, 2015; Huynen et al, 2016). In addition to membrane bridging, Mic60 also shapes the inner membrane. For instance, Mic60 overexpression results in cristae branching (Rabl et al, 2009), leading to a potential role in the initiation of cristae formation. Mic60 can induce membrane invaginations when expressed in *E. coli* and tubulate liposomes *in vitro* (Hessenberger et al, 2017; Tarasenko et al, 2017), providing direct evidence for membrane shaping. Remarkably, this membrane-shaping activity is a highly conserved feature of bacterial and mitochondrial Mic60 orthologues, since bacterial Mic60 can partially rescue the phenotype of *mic60* Δ yeast (Tarasenko et al, 2017). It is currently unclear how this activity is spatiotemporally controlled to prevent excessive cristae branching while assuring CJ stability. Mic19, the only peripheral membrane protein of the MICOS complex, has a yet to be fully elucidated regulatory function on complex stability and subcomplex association. It is itself regulated in a redox-dependent manner, containing an intra-molecular disulphide bond (Sakowska et al, 2015). In yeast, Mic19 modulates the membrane-shaping activity of Mic60 (Hessenberger et al, 2017). The mammalian homologue is important for the interaction with SAM (Darshi et al, 2011; Tang et al, 2020) and was found to be cleaved by the stress-induced protease OMA1 (Tang et al, 2020), while its vertebrate-specific paralogue Mic25 lacks the cleavage site. This proteolytic cleavage might represent a potential pathway for the rapid disassembly of the MIB complex.

The second subcomplex contains oligomers of Mic10. Mic10 is a small and highly hydrophobic protein with two transmembrane segments connected by a short, positively charged loop. Oligomerisation is mediated by strictly conserved glycine motifs in both trans-

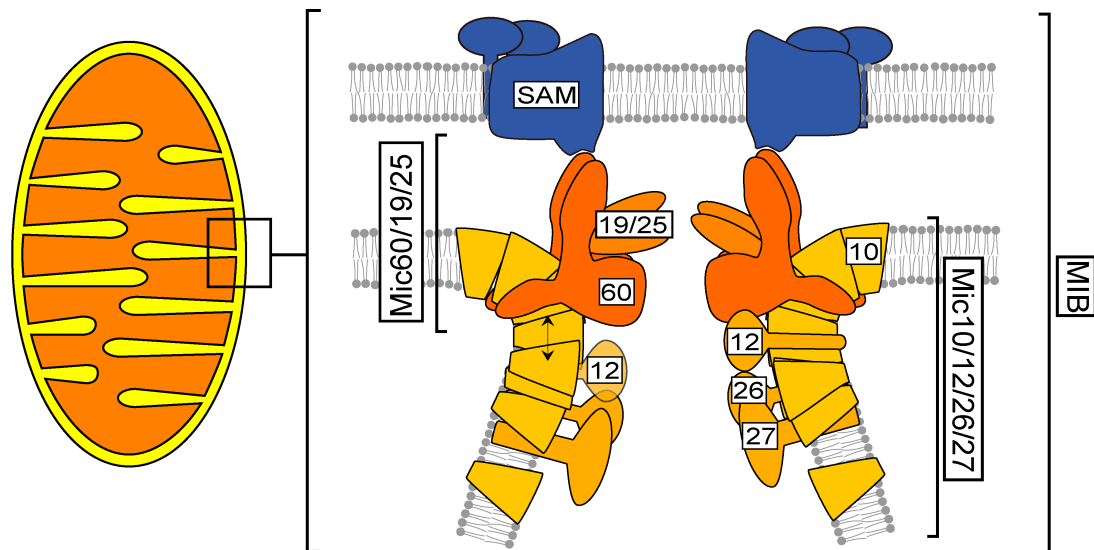


Figure 2 Organisation of the MICOS/MIB complex at crista junctions (modified from Wollweber et al, 2017)

Hypothetical model of the MICOS/MIB complex in human mitochondria. MICOS is located at crista junctions in the inner mitochondrial membrane and consists of at least 6 (in yeast) or 7 (in humans) genuine subunits. The human MICOS complex stably interacts with the SAM complex in the outer membrane to form the mitochondrial intermembrane space bridging (MIB) complex. One core subunit, Mic60, mediates the contact to the outer membrane and forms a subcomplex with Mic19 and Mic25. The other core subunit, Mic10, forms a proteinaceous scaffold at crista junctions by homo-oligomerisation and exists in a subcomplex with Mic12 (termed Mic13 in human cells), Mic26 and Mic27.

membrane segments. Due to its unique topology, Mic10 oligomerisation can stabilise and induce membrane curvature *in vitro* and *in vivo* (Barbot et al, 2015; Bohnert et al, 2015). Its levels have to be highly regulated, as overexpression resulted in a drastic expansion of cristae membranes and disorganised CJs (Bohnert et al, 2015). The additional subunits, Mic12, Mic26 and Mic27, are thought to regulate the membrane-bending activity of Mic10. Mic12 stabilises the Mic10 subcomplex and is necessary for linking both MICOS subcomplexes (Zerbes et al, 2016). The mammalian protein QIL1 (sometimes referred to as MIC13) was found to link MICOS subcomplexes in mammalian cells (Guarani et al, 2015), similarly to yeast Mic12 (Zerbes et al, 2016), and loss-of-function mutations in MIC13/QIL1 lead to hepatocerebralopathy (Anand et al, 2016; Guarani et al, 2016). Despite the similar function, the phylogenetic relationship is still under debate. The paralogous subunits Mic26 and Mic27 are apolipoprotein-O-like proteins with lipid binding domains (Weber et al, 2013; Koob et al, 2015). In yeast, Mic27 was shown to stabilise Mic10 oligomers (Zerbes et al, 2016), which could possibly help to dynamically remodel cristae junctions. Interestingly, Mic26 is the only known MICOS subunits in yeast that is not required for crista junction stability. A correlation of their function in different organisms is complicated by the observation that the paralogous subunits in yeast and metazoans originate from separate genome duplication events (Muñoz-Gómez et al, 2015; Huynen et al, 2016) and their exact function remains to be elucidated. Mammalian Mic27 can bind cardiolipin *in vitro* (Weber et al, 2013) and cardiolipin was suggested to be required for the stability of the Mic10 (but not the Mic60) subcomplex

(Friedman et al, 2015). Mic26 and Mic27 might therefore be involved in creating the lipid environment necessary for membrane bending at CJs.

3.6. *MICOS has multiple connections to protein biogenesis machineries*

Even though mitochondria possess their own genome, only a small number of mitochondrial proteins are mitochondrially encoded. The vast majority of the mitochondrial proteome is encoded in the nuclear genome and synthesised by cytosolic ribosomes. Mitochondrial proteins, which are often highly hydrophobic, are then shielded by cytosolic chaperones of the Hsp70 family and J-protein co-chaperones (Becker et al, 2019) or ubiquilins (Itakura et al, 2016) to prevent aggregation in the aqueous cytosol and keep precursors in an unfolded state. Some mitochondrial proteins might also be synthesised at mitochondria and could therefore be translocated in a co-translational manner. A recent study also demonstrated a transient J-protein mediated interaction of mitochondrial precursor proteins with the ER prior to transfer to mitochondria (Hansen et al, 2018). After arrival at the mitochondrial surface, proteins are imported, sorted and assembled by a sophisticated network of protein translocases (recently reviewed in: Wiedemann & Pfanner, 2017; Hansen & Herrmann, 2019). Incoming mitochondrial precursors bind to receptors of the translocase of the outer membrane (TOM) complex, which represents the general import pore of mitochondria. Its central subunit Tom40 is a β -barrel protein which creates a hydrophilic channel for the import of unfolded polypeptides. The subsequent steps depend on the suborganellar destination of the precursor and require the concerted action of different translocase complexes. The majority of mitochondrial precursor proteins carry amino-terminal presequences. After transit through TOM, they are handed over to the inner membrane presequence translocase (TIM23) complex, which mediates their translocation to the matrix or the lateral release into the inner membrane. This import reaction utilises the membrane potential across the inner membrane and an Hsp70-based motor complex termed PAM. TIM23 was found to interact with the respiratory chain (van der Laan et al, 2006; Gebert et al, 2012) as well as the ADP/ATP carrier (Mehnert et al, 2014), presumably to optimise the efficiency of membrane potential dependent protein import. Upon import, the presequence is cleaved off. Protein destined to the intermembrane space frequently carry internal disulphide bridges which are formed by a disulphide relay system formed by the MIA machinery, which catalyses efficient folding in the IMS after transit through TOM. Hydrophobic carrier proteins of the inner membrane, which include essential proteins such as the ATP/ADP carrier, the mitochondrial calcium uniporter as well as the mitochondrial pyruvate carrier (Gomkale et al, 2020; Rampelt et al, 2020), are chaperoned through the hydrophilic environment of the intermembrane space by small TIM chaperones. These hexameric assemblies of Tim8/13 or Tim9/10 (Weinhäupl et al, 2018) guide the proteins to the carrier translocase of the inner membrane (TIM22) complex, that subsequently mediates their assembly. β -barrel proteins of the outer mitochondrial membrane share a similar

biogenesis pathway. After transit through TOM, the hydrophobic precursors are bound by small TIM chaperones until they are inserted by the sorting and assembly machinery (SAM) complex. The core subunit SAM50 itself is a β -barrel protein and the major interaction partner of MICOS in human cells (chapter 3.5).

To enable efficient substrate channelling, various protein translocation machineries assemble into supercomplexes (reviewed in Horvath *et al*, 2015). Some contacts are of rather transient nature, such as the interaction of the presequence translocases of the outer and inner membrane. A TOM-TIM23 supercomplex can be stabilised by arresting preproteins during their import (Schleyer & Neupert, 1985; Pfanner *et al*, 1987; Dekker *et al*, 1997; Gold *et al*, 2014). These two-membrane spanning translocation sites are micro-clustered in vicinity of crista junctions (Harner *et al*, 2011; Gold *et al*, 2014). Later studies found that the IMS domains of TIM and TOM interact even in a passive state (Shiota *et al*, 2011; Waegemann *et al*, 2014). In yeast, the TOM complex forms a supercomplex with SAM during the assembly of β -barrel proteins to enable efficient substrate channelling (Qiu *et al*, 2013). These examples of stable interactions between mitochondrial protein translocation machineries demonstrate the importance of functional supercomplexes in mitochondrial biogenesis. Most likely, many more transient interactions exist, which cannot easily be detected biochemically but might be equally important.

The MICOS complex was found to interact with a large number of protein transport complexes of both mitochondrial membranes and the intermembrane space, possibly to coordinate the assembly of proteins at its strategic position at crista junctions and bridge both mitochondrial membranes (Reichert & Neupert, 2002). An interaction with Mia40 and the TOM complex presumably promotes efficient transfer of IMS proteins from TOM to MIA (von der Malsburg *et al*, 2011; Varabyova *et al*, 2013). The significance of this finding was recently supported by the observation that MIA is an integral component of MICOS in the excavate *Trypanosoma brucei* (Kaurov *et al*, 2018), suggesting an evolutionarily conserved relationship between cristae architecture and IMS protein biogenesis. Mic60 was also found to interact with TOM and SAM complexes in yeast to promote the biogenesis of outer membrane proteins (Bohnert *et al*, 2012; Korner *et al*, 2012; Zerbes *et al*, 2012). The human MICOS complex forms a highly stable contact with the SAM machinery of the outer membrane, which is essential for crista junction architecture (Xie *et al*, 2007; Ott *et al*, 2012, 2015; Ding *et al*, 2015; Huynen *et al*, 2016; Tang *et al*, 2020). However, it is currently unclear whether this connection is also required for outer membrane protein biogenesis. It is not clear whether MICOS is actively involved in the presequence pathway, even though the TIM23 complex appears to be enriched at crista junctions (Harner *et al*, 2011; Gold *et al*, 2014) and was found to interact with MICOS in yeast (Callegari *et al*, 2019) and human cells (Ding *et al*, 2015). Importantly, the human MICOS complex also interacts with the carrier translocase of the inner membrane, presumably to spatially restrict the assembly of highly hydrophobic inner membrane precursor proteins

(Callegari et al, 2019). The plethora of interactions between MICOS and protein translocases and the evolutionarily conserved nature of these interactions demonstrate the benefits of spatial coordination of protein biogenesis at crista junctions.

3.7. Crosstalk of cristae organising systems and dynamic remodelling of mitochondrial membranes

Cristae shaping machineries such as MICOS and the ATP synthase cannot be regarded as fully separate entities but appear to coordinate their activities. In the past years, numerous connections between cristae shaping machineries have been identified. In yeast, Mic10 interacts with subunit e of the ATP synthase (Eydt et al, 2017; Rampelt et al, 2017). Mic10 at the ATP synthase modulates its assembly into oligomers and thus directly contributes to its membrane-shaping activity. Crosslinking data suggests that this interaction might be conserved in metazoans (Schweppe et al, 2017). It is still unclear how Mic10 affects ATP synthase oligomerisation and whether this interaction is physiologically significant. A recent study also revealed an influence of OPA1 on ATP synthase oligomerisation. These data also suggested that OPA1-mediated cristae shaping, rather than a direct interaction, impacts ATP synthase assembly, which in turn has bioenergetic benefits (Quintana-Cabrera et al, 2018). OPA1 also interacts with the MICOS core subunit Mic60 in a complex that is remodelled during apoptotic cristae opening (Barrera et al, 2016; Glytsou et al, 2016). OPA1 dynamically alters cristae junction width during e.g. apoptosis, while Mic60 provides a stable structural scaffold at the crista junction. OPA1 processing is also influenced by prohibitins (Merkwirth et al, 2008), which might also shape cristae (Osman et al, 2009). In addition to the canonical cristae organising proteins, several novel proteins have recently been implicated in cristae shaping, including the BAR-domain containing protein FAM92A (Wang et al, 2019b), MICU1, which is a subunit of the mitochondrial calcium uniporter complex (Gottschalk et al, 2019) and the conserved and clinically relevant LETM1 protein (Nakamura et al, 2020). It is currently unclear how these proteins interact with known cristae organising systems. Most importantly, only very little is known about cristae formation and how membrane-shaping proteins orchestrate this process. Most likely, several processes exist, depending on the cristae shape (Harner et al, 2016). Discoidal cristae could theoretically be formed by Mgm1-dependent partial inner membrane fusion (Harner et al, 2016) or the fusion of tubular cristae (Kondadi et al, 2020), while local assembly of ATP synthase oligomers might trigger the biogenesis of tubular cristae (Anselmi et al, 2018; Blum et al, 2019).

4. Aims

Seminal studies in the field of mitochondrial membrane organisation of the past decade defined the major cristae organising complexes, namely MICOS, Mgm1/OPA1 and the ATP synthase. These studies focussed on the identification of novel components and their connections to other mitochondrial processes such as protein biogenesis. Importantly, many of these protein machineries are essential for all complex eukaryotic life and are therefore highly conserved throughout evolution. While it appears that most proteins involved in cristae biogenesis and remodelling have been identified, many open questions remain:

i.) It is still unclear how cristae are initially formed and which proteins are involved in distinct steps of cristae biogenesis. This process likely requires a coordination of the various membrane-shaping activities of different protein complexes, but their interplay remains poorly defined. ii) Cristae remodelling during processes such as apoptosis and metabolic transitions, as described several decades ago, likely requires a spatiotemporal regulation of membrane shaping by MICOS, the ATP synthase and Mgm1/OPA1. However, the assembly mechanism of Mgm1/OPA1 and MICOS core subunits is poorly defined. Furthermore, it is unclear how the activity of these oligomeric protein assemblies can be regulated. iii) All known cristae organising protein machineries possess multiple and seemingly unrelated functions. Mgm1/OPA1 is involved in inner membrane fusion and possibly fission, but also determines cristae shape in response to e.g. altered metabolic conditions. MICOS stabilises crista junctions, but additionally spatially controls protein biogenesis. The core subunit Mic10 also modulates the assembly of the ATP synthase. MICOS therefore influences multiple pathways at different sub-mitochondrial locations. The ATP synthase is best known for its role in generating ATP, but forms dimers and oligomers to shape and generate cristae. Most likely, many more additional functions of these proteins can be defined in different tissues or organisms. Currently, it is mostly unknown how and why cristae organising proteins integrate such a large number of distinct functions.

This work attempts to address some of these questions using a combination of experimental approaches in yeast and mammalian cell lines. Firstly, the ability of MICOS yeast mutants to adapt their metabolism to respiratory conditions will be analysed. During this transition, mitochondrial and cristae biogenesis is stimulated and potential defects in these processes would lead to an inefficient metabolic adaptation. Furthermore, the different functions of MICOS and its interaction partners will be genetically dissected to define core functions that are important for mitochondrial biogenesis. Secondly, the effect of accessory MICOS subunits on the assembly of MICOS core subunits will be analysed, since the spatiotemporal regulation of MICOS assembly is poorly defined. In addition, MICOS organisation and interaction partners in yeast will be compared to the human MICOS complex to define conserved and divergent features of the complex. Finally, the assembly mechanism of Mgm1/OPA1 will be analysed in detail to shed light on the mechanism of dynamic cristae remodelling.

5. Materials and Methods

5.1. Materials

5.1.1. Reagents and critical equipment

Table 1 Reagents and critical equipment

Reagents	
reagent	supplier
[³⁵ S]-Methionine	Perkin Elmer
3xFLAG-peptide	Sigma-Aldrich
6-Aminocaproic acid	Sigma-Aldrich
Acetic acid	Carl Roth
Acrylamide 4x crist.	Carl Roth
AcTEV protease	Invitrogen/Thermo Fisher
Albumin from bovine serum (BSA)	Sigma-Aldrich
Ammonium chloride	Sigma-Aldrich
Ammonium persulfate (APS)	Carl Roth
Ampicillin sodium salt	Carl Roth
Anti-FLAG M2 affinity gel	Sigma-Aldrich
ATP	Roche
Bacto Agar	Becton Dickinson
Bambanker freezing media	Wako
beta-Mercaptoethanol	Carl Roth
Bis-Tris	Carl Roth
BN-PAGE HMW native marker kit	GE Healthcare
Bromophenol blue	Sigma-Aldrich
Calcium chloride dihydrate	Carl Roth
Complete EDTA free Protease inhibitor	Roche
Complete supplement mixture (CSM) (-URA; -LEU; -TRP)	MP Biomedicals
Coomassie brilliant blue G250	Serva
Coomassie brilliant blue R250	Carl Roth
Crystal violet	Carl Roth
DAPI (4',6-diamidino-2-phenylindole)	Thermo Fisher
di-Potassium hydrogen phosphate	Carl Roth
Difco Yeast Nitrogen Base w/o amino acids	Becton Dickinson
Digitonin	Calbiochem

DiOC ₆ (3) (3,3'-Dihexyloxacarbocyanine Iodide)	Invitrogen/Thermo Fisher
DMEM (Dulbecco's Modified Eagle Media)	Gibco/Thermo Fisher
DMSO (Dimethyl sulfoxide)	Carl Roth
Dounce homogeniser (glass/teflon)	Sartorius
DSG (Disuccinimidyl glutarate)	Thermo Fisher
DTT (Dithiothreitol)	Carl Roth
ECL western blotting detection reagents	Pierce
EDTA (Ethylenediaminetetraacetic acid)	Carl Roth
Ethanol	Sigma-Aldrich
FCS (Fetal calf serum)	Gibco/Thermo Fisher
Formaldehyde	Polyscience
FuGene 6 HD transfection reagent	Promega
G-418 (Geniticinsulfat)	Carl Roth
Galactose	Sigma-Aldrich
Gibson assembly mix enzymes (T5 exonuclease, Phusion polymerase, Taq Ligase)	NEB
Glucose	Carl Roth
Glutaraldehyde (EM grade)	Science Services
Glycerol	Sigma-Aldrich
Glycine	MP Biomedicals
Goat anti-mouse-IgG antibody coupled to peroxidase	Merck
Goat anti-rabbit-IgG antibody coupled to peroxidase	Merck
HEPES	Roth
Herring sperm DNA	Sigma-Aldrich
Hydrochloric acid	Carl Roth
Hyperfilm ECL	GE Healthcare
Imidazole	Carl Roth
L-Methionine	Carl Roth
LE agarose	Biozym
LidBacs	Eppendorf
Lithium acetate	Carl Roth
Lithium chloride	Carl Roth
Magnesium acetate	Carl Roth
Magnesium chloride	Carl Roth
MES (2-(N-morpholino)-ethanesulfonic acid)	Carl Roth

Milk powder (skimmed)	Neuform, Sucofin
MOPS (3-(N-morpholino)-propanesulfonic acid)	Carl Roth
N,N'-Methylenebisacrylamide 2x	Serva
NiNTA resin	Qiagen
NuPAGE BisTris 4-12% gels	Thermo Fisher
Oligonucleotides, salt free	Eurofins Genomics; Sigma-Aldrich
PBS (Phosphate buffered saline, pH 7.2)	Gibco/Thermo Fisher
PCR Purification Kit, Gel Extraction Kit, MiniPrep Kit	Qiagen; NEB
Peptone	Becton Dickinson
PMSF (phenylmethanesulfonyl fluoride)	Carl Roth
poly-L-lysine	Sigma-Aldrich
Polybrene	Sigma-Aldrich
Polyethylene glycol 4000	Merck
Potassium acetate	Carl Roth
Potassium chloride	Carl Roth
Potassium dihydrogen phosphate	Carl Roth
Potassium hydroxide	Carl Roth
Proteinase K	Roche
PVDF membranes	Millipore
Q5 2x Hot Start Master Mix	NEB
Quick Ligase	NEB
Raffinose	Sigma-Aldrich
Restriction enzymes	NEB
Rotiphorese Gel 30 (37.5:1) acrylamide solution	Carl Roth
RotiQuant Bradford reagent	Carl Roth
SDS (Sodium dodecyl sulfate)	Carl Roth
SDS-PAGE standards, broad range	Thermo Fisher; Biorad
Sodium carbonate	Carl Roth
Sodium chloride	Carl Roth
Sodium citrate	Carl Roth
Sodium hydrogen carbonate	Carl Roth
Sodium hydroxide	Carl Roth
Sodium succinate	MP Biomedicals
Sorbitol	Carl Roth
Spin column	MobiTech

Sucrose	MP Biomedicals
T4 PNK	NEB
TEMED	Carl Roth
TNT SP6 Transcription/Translation Kit	Promega
Trichloroacetic acid	Sigma-Aldrich
Tricine	Carl Roth
Tris	MP Biomedicals
Triton X-100	Sigma-Aldrich
Trypsin-EDTA	Gibco/Thermo Fisher
Tryptone	Becton Dickinson
Tween 20	Sigma-Aldrich
Uridine	Sigma-Aldrich
Yeast extract	Becton Dickinson
Zymolyase 20T (from <i>Arthrobacter luteus</i>)	Nacalai Tesque
Critical equipment	
blotting chamber for semidry transfer (Owl-Hep1)	Thermo Fisher
blotting chamber for wet transfer (Mini-Trans Blot cell)	Biorad
SDS PAGE running apparatus (Mini-Protean system)	Biorad
Blue native PAGE running apparatus (SE600X)	Hoefler
Microplate reader (Spark 10M)	Tecan
Typhoon scanner (9410)	GE Healthcare
Western Blot Imaging system (ImageQuant 680)	GE Healthcare
Software	
Benchling (Molecular Biology Software)	https://benchling.com
Excel	Microsoft
Fiji/ImageJ 1.51s	(Schindelin et al, 2012)
Huygens Essential v17.04	Scientific Volume Imaging
Illustrator CC	Adobe
Photoshop CC	Adobe
Prism v6.0	GraphPad

5.1.2. Antibodies

Table 2 Antibodies

Antibodies against yeast proteins			
Target	Identifier or cat. number	Dilution	Source or supplier
α -phospho-AMPK	2535 (40H9)	1:500	Cell Signaling Technologies
α -AAC	115B	1:250	Laboratory of Nikolaus Pfanner (University of Freiburg) & Martin van der Laan
α -Aco1	945-7	1:1000	
α -Atp18	1962-4	1:500	
α -Atp19	1961-3	1:500	
α -Atp2	861-3	1:500	
α -Atp20	1516-4	1:500	
α -Atp21	138-9	1:500	
α -Cor1	371-5	1:500	
α -Cox1	1538-4	1:500	
α -Cox4	578-5	1:500	
α -Cox4	578-4	1:500	
α -Mgm1	796-5	1:500	
α -Mic10	3367-7	1:1000	
α -Mic12	3336-6	1:500	
α -Mic19	3358-2	1:250	
α -Mic26	3335-3	1:500	
α -Mic27	3357-2	1:250	
α -Mic60	857-5	1:500	
α -Porin	3622-3	1:500	
α -Rip1	543-5	1:500	
α -Sam50	312-15	1:500	
α -Ssc1	119-3	1:1000	
α -Tim13	238-6	1:500	
α -Tim23	3878-4	1:500	
α -Tom40	168-4	1:500	
α -Tom70	657-4	1:500	
Antibodies against human proteins			
α -ATP5B	4826	1:5000	laboratory of Peter Rehling, Göttingen

α -ATP5I	ab122241	1:500	abcam
α -COX4-I	1522	1:500	laboratory of Peter Rehling, Göttingen
α -DNAJC11	ab183518	1:500	abcam
α -FLAG M2	A2220	1:500	Sigma-Aldrich
α -HSPA9	ab227215	1:500	abcam
α -MIC10	5031	1:500	Laboratory of Nikolaus Pfanner (University of Freiburg) & Martin van der Laan
α -MIC13	5033	1:500	
α -MIC60	5041	1:500	
α -MIC19	HPA042935	1:500	Sigma-Aldrich
α -MIC25	HPA051975	1:500	Sigma-Aldrich
α -MIC26	HPA003187	1:500	Sigma-Aldrich
α -MIC27	HPA000612	1:500	Sigma-Aldrich
α -NDUFB8	3764	1:400	laboratory of Peter Rehling, Göttingen
α -OPA1	612607	1:500	BD Biosciences
α -SAM50	-	1:500	laboratory of Mike T. Ryan, Melbourne
α -SAM50	ab246987	1:500	abcam
α -TOM22	ab179826	1:500	abcam
α -TOM40	ab185543	1:500	abcam
α -UQCRC1	1512	1:500	laboratory of Peter Rehling, Göttingen
α -VDAC	PC548	1:500	Merck
total OXPHOS (α -ATP5A; α -UQCRC2; α -MTCO1; α -SDHB; α -NDUFB8)	ab110413	1:500	abcam

5.1.3. Plasmids

Table 3 Plasmids

Plasmid	Source
pRS426	(Sikorski & Hieter, 1989)
pRS414	(Sikorski & Hieter, 1989)
pFL36	(Bohnert et al, 2015)
pFL36-Mic10	(Bohnert et al, 2015)
pFL36-Mic10 ^{G76A}	(Bohnert et al, 2015)
pFL36-Atp21-Mic10	Heike Rampelt, University of Freiburg
pFL36-Atp21-STOP-Mic10	This work, stop codon inserted by site directed mutagenesis
pFL36-Atp21-Mic10 ^{G76A}	This work, mutation generated by site directed mutagenesis
pRS426-Mic10	(Bohnert et al, 2015)
pRS426-Mic60	(Bohnert et al, 2015)
pRS414-Mgm1	(Ieva et al, 2014)
pRS414-Mgm1 D542A	This work (Faelber et al, 2019), mutations generated by site directed mutagenesis
pRS414-Mgm1 K545A	
pRS414-Mgm1 N675A	
pRS414-Mgm1 F805D	
pRS414-Mgm1 Y520A	
pRS414-Mgm1 R621A	
pRS414-Mgm1 M745D, S756D	
pSpCas9-(BB)-2A-GFP	(Ran et al, 2013)
pBABE (puro) MIC10-FLAG	Plasmid for retroviral transduction, created by Ralf Zerbes, University of Freiburg
pBABE (puro) DNAJC11-FLAG	Plasmids for retroviral transduction, created by Alexander von der Malsburg, Saarland University
pBABE (puro) FLAG-SAM50	

5.1.4. Yeast strains

Table 4 Yeast strains

Yeast strain	Reference/ created by
YPH499 (WT)	(Sikorski & Hieter, 1989)
YPH499pRS426	(Bohnert et al, 2015)
YPH499 <i>mic10</i> Δ pRS426	(Bohnert et al, 2015)
YPH499 pRS426-Mic10	(Bohnert et al, 2015)
YPH499 <i>mic10</i> Δ	(von der Malsburg et al, 2011)
YPH499 <i>mic12</i> Δ	(von der Malsburg et al, 2011)
YPH499 <i>mic19</i> Δ	(von der Malsburg et al, 2011)
YPH499 <i>mic26</i> Δ	(von der Malsburg et al, 2011)
YPH499 <i>mic27</i> Δ	(von der Malsburg et al, 2011)
YPH499 <i>mic60</i> Δ	(von der Malsburg et al, 2011)
YPH499 <i>mic60</i> Δ pRS426	(Bohnert et al, 2015)
YPH499 pRS426-Mic60	(Bohnert et al, 2015)
YPH499 Mic60-TEV-ProtA-7xHis pRS426	(von der Malsburg et al, 2011)
YPH499 <i>mic26</i> Δ Mic60-TEV-ProtA-7xHis pRS426	This work, (Rampelt et al, 2018)
YPH499 <i>mic27</i> Δ Mic60-TEV-ProtA-7xHis pRS426	This work, (Rampelt et al, 2018)
YPH499 <i>mic26</i> Δ pRS426	This work, (Rampelt et al, 2018)
YPH499 <i>mic27</i> Δ pRS426	This work, (Rampelt et al, 2018)
YPH499 Mic10-10xHis pRS426	(Bohnert et al, 2015)
YPH499 <i>mic26</i> Δ Mic10-10xHis pRS426	(Bohnert et al, 2015)
YPH499 <i>mic27</i> Δ Mic10-10xHis pRS426	(Bohnert et al, 2015)
YPH499 <i>crd1</i> Δ pRS426	This work, (Rampelt et al, 2018)
YPH499 <i>crd1</i> Δ Mic60-TEV-ProtA-7xHis pRS426	This work, (Rampelt et al, 2018)
YPH499 <i>mic26</i> Δ <i>crd1</i> Δ Mic60-TEV-ProtA-7xHis pRS426	This work, (Rampelt et al, 2018)

YPH499 <i>mic27Δcrd1Δ</i> Mic60-TEV-ProtA-7xHis pRS426	This work, (Rampelt et al, 2018)
YPH499 <i>mic10Δ</i> Mic60- TEV-ProtA-7xHis pRS426	(Bohnert et al, 2015)
YPH499 <i>mic10Δ</i> Mic60- TEV-ProtA-7xHis pFL36Mic10	(Bohnert et al, 2015)
YPH499 <i>mic10Δ</i> Mic60- TEV-ProtA-7xHis pFL36Atp21-Mic10	This work, Heike Rampelt (Univ. of Freiburg) & F.W.
YPH499 <i>mic10Δ</i> Mic60- TEV-ProtA-7xHis pFL36Atp21-STOP-Mic10	This work
YPH499 pFL36	(Bohnert et al, 2015)
YPH499 <i>mic10Δ</i> pFL36- Mic10	(Bohnert et al, 2015)
YPH499 <i>mic10Δ</i> pFL36- Atp21-Mic10	This work, Heike Rampelt (Univ. of Freiburg) & F.W.
YPH499 <i>mic10Δ</i> pFL36- Atp21-STOP-Mic10	This work
YPH499 <i>mic10Δ</i> pFL36- Mic10 ^{G76A}	(Bohnert et al, 2015)
YPH499 <i>mic10Δ</i> pFL36- Atp21- Mic10 ^{G76A}	This work
YPH499 <i>PGALI-MGMI</i>	This work, (Faelber et al, 2019)
YPH499 pRS414	This work, (Faelber et al, 2019)
YPH499 <i>PGALI-MGMI</i> pRS414	This work, (Faelber et al, 2019)
YPH499 <i>PGALI-MGMI</i> pRS414-Mgm1	This work, (Faelber et al, 2019)
YPH499 <i>PGALI-MGMI</i> pRS414-Mgm1 D542A	This work, (Faelber et al, 2019)
YPH499 <i>PGALI-MGMI</i> pRS414-Mgm1 K545A	This work, (Faelber et al, 2019)
YPH499 <i>PGALI-MGMI</i> pRS414-Mgm1 N675A	This work, (Faelber et al, 2019)

YPH499 <i>PGALI-MGMI</i> pRS414-Mgm1 F805D	This work, (Faelber et al, 2019)
YPH499 <i>PGALI-MGMI</i> pRS414-Mgm1 Y520A	This work, (Faelber et al, 2019)
YPH499 <i>PGALI-MGMI</i> pRS414-Mgm1 R621A	This work, (Faelber et al, 2019)
YPH499 <i>PGALI-MGMI</i> pRS414-Mgm1 M745D, S746D	This work, (Faelber et al, 2019)

5.1.5. Cell lines

Table 5 Mammalian cell lines

Cell line	sgRNA or retroviral construct	Source/ created by
HEK293T	-	Laboratory of Michael T. Ryan, Melbourne, Australia (Stroud et al, 2016)
HEK293T MIC10-6	sgRNA: AGTCGGAGCTCGGCAGGAAG	Ralf Zerbes, University of Freiburg, Germany
HEK293T MIC60-22	sgRNA: CAGCATCTCGGTCAAGCGGA	Alexander von der Malsburg, Saarland University, Germany
HEK293T MIC13-9	sgRNA: GTTCCATCAAGGGAAGTG	Ralf Zerbes, University of Freiburg, Germany
HEK293T MIC26-18	sgRNA: GAACATGTCGCTGGCAGCGG	Ralf Zerbes, University of Freiburg, Germany and F.W.
HEK293T MIC27-10	sgRNA: TGTAACAACCAGTTGCAGTG	Ralf Zerbes, University of Freiburg, Germany
HEK293T DNAJC11-5	sgRNA: CGGTGGGGCAGCACTCACAG	Stefan Schorr and Alexander von der Malsburg, Saarland University, Germany
HEK293T MIC10-6 + MIC10-FLAG cl. 6	MIC10-6 transduced with MIC10- FLAG (clonal population)	Ralf Zerbes, University of Freiburg, Germany
HEK293T + FLAG-SAM50	HEK293T transduced with FLAG- SAM50 (non-clonal population)	Alexander von der Malsburg, Saarland University, Germany
HEK293T DNAJC11-5 cl. 19	DNAJC11-5 transduced with DNAJC11-FLAG (clonal population)	Alexander von der Malsburg, Saarland University, Germany

5.2. Methods

5.2.1. Biochemistry

5.2.1.1. Isolation of mitochondria from yeast

Yeast were grown in YPG medium or synthetic defined media containing 3% [v/v] glycerol and 0.1% [w/v] glucose (see section 5.2.2.1 for details) at 30°C and 130 rpm to mid-logarithmic phase and mitochondria were isolated using a protocol modified from Meisinger et al, 2006. Cells were harvested by centrifugation for 10 min at 1,200 x g, washed with water and incubated in DTT buffer (100 mM Tris/H₂SO₄ pH 9.4, 10 mM DTT; 2 ml per gram wet weight) for 20 min at 30°C. Cells were re-isolated by centrifugation (5 minutes at 2,000 x g), washed in zymolyase buffer (1.2 M sorbitol, 20 mM potassium phosphate pH 7.4) and incubated in zymolyase buffer containing 4 mg per gram wet weight zymolyase 20T for 30 – 45 min. After a wash in zymolyase buffer, spheroplasts were resuspended in homogenisation buffer (0.6 M sorbitol, 10 mM Tris-HCl pH 7.4, 1 mM EDTA, 0.2% [w/v] BSA, 1 mM PMSF) and homogenised in a glass-teflon dounce homogeniser (Sartorius) on ice. The cell lysate was then centrifuged for 10 min at 1,000 x g and crude mitochondria were isolated from the supernatant by centrifugation at 17,000 x g for 10 min. The pellet was washed in SEM buffer (250 mM sucrose, 1 mM EDTA, 10 mM MOPS-KOH pH 7.2), the protein concentration was determined using the Bradford assay by adding 1 µl of mitochondria in 50 µl water to 800 µl of 1x RotiQuant and comparing the absorbance at 595 nm to an IgG standard curve. The concentration was adjusted to 10 mg/ml with SEM buffer, mitochondrial fractions were snap frozen in liquid nitrogen and stored at -80°C.

5.2.1.2. Isolation of mitochondria from mammalian cell lines

HEK293T cells were grown in 145 mm dishes and harvested in ice-cold PBS by centrifugation (800 x g, 5 min) and cell pellets were stored at -80°C. For all assays except import and assembly experiments, mitochondria were isolated by differential centrifugation as described in Acín-Pérez et al, 2008. Cells were resuspended in buffer A (83 mM sucrose, 10 mM HEPES-KOH pH 7.2) and homogenised in a glass-teflon dounce homogeniser on ice. After homogenisation, an equal volume buffer B (250 mM sucrose, 30 mM HEPES-KOH pH 7.2) was added to the cell homogenate, which was subsequently centrifuged at 1,000 x g for 5 min. Crude mitochondrial fractions were isolated from the supernatant by centrifugation at 20,000 x g for 5 min and resuspended in S₃₂₀EM buffer (320 mM sucrose, 1 mM EDTA, 10 mM MOPS-KOH pH 7.2). Protein concentration was estimated by the Bradford assay and aliquots of crude mitochondria were stored at -80°C. For mitochondrial import assays, mitochondria were isolated according to Johnston et al, 2002. Cells were harvested in PBS and resuspended in isolation buffer (20 mM HEPES-KOH pH 7.6, 220 mM mannitol, 70 mM sucrose, 1 mM EDTA) containing 2 mg/ml [w/v] BSA and 0.5 mM PMSF and homogenised as above. After centrifugation at 800 x g for 5 min, crude mitochondria were isolated by

centrifugation at 10,000 x g for 10 min, the protein concentration was determined by a Bradford assay and mitochondria were kept on ice until the start of the assay.

5.2.1.3. *SDS-PAGE and immunoblotting*

Lysates of isolated mitochondria or yeast cells were prepared in SDS sample buffer (Laemmli, 1970) (2% [w/v] SDS, 10% [v/v] glycerol, 60 mM Tris-HCl pH 6.8, 0.01% [w/v] bromophenole blue, 1% [v/v] β -mercaptoethanol) and incubated at 95°C for 5 min or 65°C for 15 min (to prevent aggregation of hydrophobic proteins). Bis-Tris SDS polyacrylamide gels (as described in: https://openwetware.org/wiki/Sauer:bis-Tris_SDS-PAGE,_the_very_best) were prepared using a 3x Bis-Tris gel buffer (1 M Bis-Tris HCl pH 6.8) and acrylamide/bisacrylamide (37.5:1) at a final concentration of 10% [w/v]. Gels were run either in MES low-molecular weight running buffer (50 mM MES, 50 mM Tris, 1 mM EDTA, 0.1% [w/v] SDS) or MOPS high-molecular weight running buffer (50 mM MOPS, 50 mM Tris, 1 mM EDTA, 0.1% [w/v] SDS) at a constant voltage of 150 – 200 V. Proteins were then transferred to PVDF membranes with a semi-dry blotting system at a constant current of 300-400 mA in semidry transfer buffer (20 mM Tris, 150 mM glycine, 0.02% [w/v] SDS, 10% [v/v] ethanol). For analysis of OPA1 isoforms, commercially available NuPAGE 4-12% Bis-Tris gradient gels were used and transferred to nitrocellulose membranes in a wet-transfer system at a constant voltage of 100 V for 1 h in wet-transfer buffer (25 mM Tris, 192 mM glycine, 10% [v/v] ethanol). To assess equal loading of PVDF membranes, membranes were stained with Coomassie brilliant blue R250 (0.3% [w/v] in 40% [v/v] ethanol, 10% [v/v] acetic acid) and destained in destaining solution (40% [v/v] ethanol, 10% [v/v] acetic acid). Subsequently, membranes were cut horizontally to enable immuno-decoration with several antibodies and destained in methanol to remove residual Coomassie brilliant blue. After a wash in TBS/T (20 mM Tris-HCl pH 7.5, 125 mM NaCl, 0.1% [v/v] Tween-20), membranes were blocked in TBS/T containing 5% [w/v] milk powder (TBST-M) or bovine serum albumin (TBST-BSA, for phosphorylation-specific antibodies) and subsequently incubated with primary antibodies diluted in TBST-M or TBST-BSA for several hours at RT or at 4°C overnight. After several washes in TBST-M, membranes were incubated in horseradish-peroxidase coupled secondary antibodies for approximately 45 min and washed again prior to detection by enhanced chemiluminescence (Pierce ECL Plus western blotting substrate) and X-ray films (GE-healthcare) or a CCD camera system (Amersham ImageQuant 680).

5.2.1.4. *BN-PAGE analysis of mitochondrial protein complexes*

BN-PAGE was performed essentially as described (Schägger & von Jagow, 1991; Priesnitz et al, 2020). Mitochondria (50-100 μ g protein per lane) were re-isolated by centrifugation (20,000 x g for 10 min) and resuspended in ice-cold BN-PAGE solubilisation buffer (1% [w/v] digitonin, 20 mM Tris-HCl pH 7.4, 50 mM NaCl, 0.1 mM EDTA, 10% [v/v] glycerol, 1 mM

PMSF) at a concentration of 1 $\mu\text{g}/\mu\text{l}$. After 15 – 30 min, mitochondrial lysates were cleared by centrifugation (20,000 x g for 10 min) and mixed with 10x BN-PAGE loading dye (5% Coomassie brilliant blue G250, 500 mM 6-aminocaproic acid, 100 mM Bis-Tris HCl pH 7.0). Samples were loaded on homemade BN-PAGE gradient gels containing 66.7 mM 6-aminocaproic acid and 50 mM Bis-Tris HCl pH 7.0 and run at 600V, 25 mA in a water-cooled (5°C) Hoefer gel chamber with 4 litres of anode buffer (500 mM Bis-Tris HCl pH 7.0) and cathode buffer (50 mM Tricine-HCl pH 7.0, 15 mM Bis-Tris HCl pH 7.0) containing 0.02% [w/v] Coomassie brilliant blue G250. After samples entered the gel, Coomassie dye was omitted from the cathode buffer and the run was continued until the blue running front reached the end of the gel. For immunoblotting, the gel was soaked in SDS buffer (25 mM Tris, 192 mM glycine, 1% [w/v] SDS) for 5 min prior to transfer to PVDF in a semi-dry blotting chamber as described above.

5.2.1.5. *Molecular Cloning and site-directed mutagenesis*

Standard molecular biology techniques were used for the generation of plasmids. Briefly, open reading frames were amplified from plasmids or yeast genomic DNA by polymerase chain reaction using the Q5 Hot Start polymerase master mix according to manufacturer's recommendations. Yeast genomic DNA was isolated as described in (Löoke et al, 2011). To this end, a yeast colony was suspended in 200 mM lithium acetate and 1% [w/v] SDS and incubated at 70°C for 5 minutes. The DNA was ethanol precipitated and dissolved in 100 μl water, cell debris was pelleted and 1 μl of supernatant was used in a 50 μl PCR reaction. For amplification from plasmids, 1 ng template was used per reaction. Plasmids were assembled by Gibson assembly as published (Gibson et al, 2009) or restriction digest and ligation. Plasmids were verified by Sanger Sequencing (Eurofins Genomics). For site directed mutagenesis, primers were designed using the Quikchange Primer design tool (<https://www.agilent.com/store/primerDesignProgram.jsp>) and PCR reactions were assembled with single primers (Edelheit et al, 2009). After amplification, samples were mixed and annealed by heating to 95°C and gradually lowering the temperature to 37°C, prior to digestion of templates by DpnI and transformation into chemically competent *E. coli*.

5.2.1.6. *Affinity purification of MICOS via Mic60-Protein A*

To analyse MICOS stoichiometry and Mic10 assembly, the yeast MICOS complex was isolated via C-terminally TEV-Protein A-7xHis-tagged Mic60 (Mic60-ProtA) essentially as described (Bohnert et al, 2015). Mitochondria were lysed in lysis buffer (1% [w/v] digitonin, 20 mM Tris-HCl pH 7.4, 50 mM NaCl, 0.1 mM EDTA, 10% [v/v] glycerol, 1 mM PMSF, Roche protease inhibitors) on ice for 45 min, the lysate was clarified by centrifugation and the supernatant was incubated with IgG-sepharose, which was washed with 0.5 M acetate pH 3.4 and equilibrated with lysis buffer lacking digitonin. Proteins were bound to the beads in a

mobicol spin column for 1.5 h, prior to 10 washes with washing buffer (0.3% [w/v] digitonin, 20 mM Tris-HCl pH 7.4, 60 mM NaCl, 0.1 mM EDTA, 10% [v/v] glycerol, 1 mM PMSF). Proteins were eluted by incubation with AcTEV protease for 2.5 h at RT. The TEV protease as well as the protein A tag were removed by incubation with NiNTA resin for 30 min and proteins were eluted by centrifugation. For SDS-PAGE analysis, total and elution fractions were mixed with SDS sample buffer, denatured at 95°C for 5 min, and subjected to SDS-PAGE and immunoblotting as described above. BN-PAGE samples were mixed with BN-PAGE loading dye and processed as described. Membranes were analysed with an anti-Mic10 antibody.

5.2.1.7. *FLAG co-immunoprecipitation*

The mammalian MICOS complex was isolated via MIC10^{FLAG} IP. To this end, mitochondria were lysed in solubilisation buffer (see section 5.2.1.6) for 30 min on ice and incubated with pre-equilibrated Anti-FLAG-M2 affinity gel for 1.5 h at 4°C. Beads were washed 10 times with washing buffer (see section 5.2.1.6) and bound proteins were eluted by addition of 3xFLAG peptide at a final concentration of 100 µg ml⁻¹. Proteins were TCA precipitated, suspended in SDS sample buffer and denatured at 65°C for 15 min for subsequent analysis by SDS-PAGE and immunoblotting.

5.2.1.8. *Chemical crosslinking and affinity purification of crosslinking products*

In organello crosslinking was performed using the amine-reactive crosslinker disuccinimidyl glutarate (DSG) at a concentration of 1 mM for yeast mitochondria, 0.5 mM for ^{FLAG}SAM50 crosslinking and 2 mM for human MIC10 crosslinks. To this end, DSG was dissolved in DMSO and added to isolated mitochondria in SEM buffer (containing 250 mM sucrose for yeast mitochondria and 320 mM sucrose for human mitochondria). After 30 min incubation on ice, the reaction was quenched by addition of 0.1 M Tris pH 7.4, mitochondria were re-isolated by centrifugation and then either directly prepared for SDS-PAGE analysis as described above or subjected to denaturing affinity purification via Mic10^{His} or ^{FLAG}SAM50. Mic10^{His} crosslinks were isolated as described (Bohnert et al, 2015). After lysis in lysis buffer (1% [w/v] SDS, 20 mM Tris-HCl pH 7.4, 50 mM NaCl, 0.1 mM EDTA, 10% [v/v] glycerol, 10 mM imidazole, 1 mM PMSF, Roche protease inhibitors) and incubation at 95°C for 5 min, lysates were centrifuged at RT for 10 min at 20,000 x g and the supernatant was diluted 1:10 with dilution buffer (0.2% [v/v] Triton X-100, 20 mM Tris-HCl pH 7.4, 50 mM NaCl, 0.1 mM EDTA, 10% [v/v] glycerol, 10 mM imidazole, 1 mM PMSF, Roche protease inhibitors) and incubated with pre-equilibrated NiNTA resin at 4°C for 2 h. Beads were washed with washing buffer (0.2% [v/v] Triton X-100, 20 mM Tris-HCl pH 7.4, 50 mM NaCl, 0.1 mM EDTA, 10% [v/v] glycerol, 40 mM imidazole, 1 mM PMSF, Roche protease inhibitors) in mobicol spin

columns at least 5 times and proteins were eluted in elution buffer (0.2% [v/v] Triton X-100, 20 mM Tris-HCl pH 7.4, 50 mM NaCl, 0.1 mM EDTA, 10% [v/v] glycerol, 250 mM imidazole, 1 mM PMSF, Roche protease inhibitors), mixed with SDS sample buffer and analysed by SDS-PAGE and immunoblotting.

^{FLAG}SAM50 crosslinks were purified by FLAG-IP. Mitochondria were lysed in lysis buffer (1% [w/v] SDS, 20 mM Tris-HCl pH 7.4, 50 mM NaCl, 0.1 mM EDTA, 10% [v/v] glycerol, 1 mM PMSF, Roche protease inhibitors), proteins were denatured at 95°C for 5 min, diluted 1:10 with dilution buffer (0.2% [v/v] Triton X-100, 20 mM Tris-HCl pH 7.4, 50 mM NaCl, 0.1 mM EDTA, 10% [v/v] glycerol, 1 mM PMSF, Roche protease inhibitors) and then incubated with pre-equilibrated Anti-FLAG-M2 affinity gel for 1 h at 4°C. Beads were washed 10 x with washing buffer (0.2% [v/v] Triton X-100, 20 mM Tris-HCl pH 7.4, 360 mM NaCl, 0.1 mM EDTA, 10% [v/v] glycerol, 1 mM PMSF, Roche protease inhibitors) and eluted with wash buffer supplemented with 100 µg/ml 3xFLAG peptide. Subsequently, samples were mixed with SDS sample buffer and analysed by SDS-PAGE and immunoblotting.

5.2.1.9. *In vitro* transcription/translation of radiolabelled precursor proteins

Radiolabelled VDAC was produced in rabbit reticulocyte lysate using the TNT SP6 Quick coupled transcription/translation system (Promega). To this end, the VDAC open reading frame was amplified from cDNA and cloned into pGEM4z. This plasmid was then used in a translation reaction with [³⁵S] methionine at 30°C for 90 min, which was stopped by addition of 5 mM cold methionine, 250 mM sucrose and snap-freezing in liquid nitrogen. Lysates were stored at -80°C until further use.

5.2.1.10. *In organello* import and assembly assays

For in organello import and assembly assays, mitochondria were isolated using a mild protocol as described in section 5.2.1.2 and immediately used in an import assay. To this end, 50 µg of isolated mitochondria per reaction were pelleted and resuspended in 100 µl import buffer (250 mM sucrose, 5 mM magnesium acetate, 80 mM potassium acetate, 10 mM sodium succinate, 1 mM DTT, 5 mM ATP, 20 mM HEPES-KOH pH 7.4). After a short incubation at 37°C, the import reaction was started by adding 5% of reticulocyte lysate (see section 5.2.1.9). At the indicated time points, the reaction was stopped by transfer of the samples on ice. Mitochondria were re-isolated by centrifugation (20,000 x g, 5 min), washed with import buffer and prepared for BN-PAGE as described in section 5.2.1.4. After stopping the run, the gel was stained with Coomassie brilliant blue R250 (see section 5.2.1.3) and dried on a Whatman filter paper using a temperature-controlled vacuum drying apparatus. Dried gels were analysed by digital autoradiography using storage phosphor screens and a Typhoon scanner.

5.2.2. Yeast assays

5.2.2.1. Yeast strains and growth conditions

All strains used in this work are derivatives of YPH499 (*MATa ura3-52 lys2-801amber ade2-101ochre trp1-Δ63 his3-Δ200 leu2-Δ1*) and were modified as described in section 5.2.2.2 as well as Table 4. Yeast was typically maintained in YP medium (1% [w/v] bacto-yeast extract, 2% [w/v] bacto-peptone) containing either 2% [w/v] glucose (YPD), 3% [v/v] glycerol (YPG) or 2% [w/v] galactose and 1% [w/v] raffinose (YPGal-Raff). For agar plates, 2.5% bacto-agar was added. Yeast strains containing plasmids with auxotrophic markers were grown in synthetic defined media (0.67% [w/v] YNB without amino acids (BD Difco), amino acid drop-out mix (MP Biomedicals)) supplemented with the desired carbon source. Liquid cultures were grown in conical flasks or 2 ml tubes with Eppendorf LidBacs at 30°C under constant agitation. For long-term storage, yeast was resuspended in 15% [v/v] glycerol and kept at -80°C.

5.2.2.2. Yeast transformations and generation of yeast strains

Yeast was transformed with plasmids (described in Table 4) or purified PCR fragments encoding a deletion or tagging cassette and homology arms, which were either amplified from genomic DNA of respective mutants or tagging plasmids (Longtine et al, 1998) using oligonucleotides designed with the Primers-4-Yeast tool (Yofe & Schuldiner, 2014). For transformation, parental yeast strains were grown to mid-logarithmic phase and pelleted by centrifugation. Cell pellets were washed in lithium acetate mix (0.1 M lithium acetate, 0.1 M Tris-HCl pH 7.6, 1 mM EDTA) and resuspended in 100 μl lithium acetate mix supplemented with 1 mg ml⁻¹ freshly boiled carrier DNA from herring sperm. After addition of 1-5 μg plasmid or PCR product, cells were mixed with 700 μl PEG mix (40% [w/v] PEG4000, 0.1 M lithium acetate, 0.1 M Tris-HCl pH 7.6, 1 mM EDTA) and incubated for at least 30 min at room temperature. After addition of DMSO to a final concentration of 6% [v/v], cells were heat-shocked at 42°C for 15 min, pelleted and then plated on appropriate agar plates for auxotrophic or antibiotic selection. After selection of clones, cells were analysed by SDS-PAGE and immunoblotting and colony PCR when necessary.

5.2.2.3. Semi-automated yeast growth assays

To assess yeast growth in liquid medium in a semi-automated manner, yeast was cultured in 2 ml tubes with air-permeable lids (Eppendorf LidBac) in synthetic defined media containing 2% [w/v] glucose in a benchtop thermo-mixer at 30°C and 1000 rpm to late-logarithmic phase. Two hours before start of the growth assay, fresh media was added to ensure fermentative growth conditions. Subsequently, yeast was diluted to OD₆₀₀ = 0.1 in 500 μl pre-warmed assay medium containing either 0.2% [w/v] glucose or 3% [v/v] glycerol and 0.1% [w/v] glucose in a 48-well plate. Growth was then monitored for 24 hours using a temperature-controlled Tecan

Spark 10M microplate reader set to 30°C. Absorbance at 600 nm was measured every 5 min after shaking the plate for 10 sec in linear mode with an amplitude of 2.5 mm at 630 rpm. Between measurements, the plate was shaken in a double-orbital manner with an amplitude of 1.5 mm at 180 rpm. Optical density measurements were then corrected by subtracting values obtained from a blank well not containing yeast. Mean values obtained from two or three wells were plotted in GraphPad Prism v6.0.

5.2.2.4. *Analysis of yeast cell lysates*

Yeast cells were lysed by adding trichloroacetic acid to a final concentration of 20% [w/v] and subsequently frozen at -20°C to prevent e.g. post-harvesting phosphorylation of Snf1 (Orlova et al, 2008). After thawing the cell suspension on ice, cells were pelleted at 20,000 x g for 15 min, washed with Tris base for neutralisation, resuspended in sample buffer and incubated at 95°C for 5 min. Insoluble material was removed by centrifugation and the supernatant (equivalent to 0.05 OD₆₀₀) was analysed by SDS-PAGE and immunoblotting.

5.2.2.5. *Fluorescence microscopy analysis of mitochondrial morphology*

Yeast were grown in synthetic defined media and resuspended in 5% [w/v] glucose and 10 mM HEPES-KOH pH 7.2, containing 0.5 µg ml⁻¹ DAPI and 175 nM DiOC₆ (3,3'-dihexyloxycarbocyanine iodide). Cells were imaged on a Leica DMI8 fluorescent microscope with a Leica DFC3000 G CCD camera and a 63x/1.40 objective. Z-stacks were deconvolved with Huygens Essential and images were displayed as maximum intensity projections in Fiji. Variations in DiOC₆ uptake were corrected for by adjusting the contrast of individual images.

5.2.2.6. *Fixation of yeast for electron microscopy analysis*

Yeast were grown in synthetic defined media containing glycerol to mid-logarithmic phase, pelleted, washed in 0.1 M citrate buffer pH 4.8 and fixed (4% [w/v] formaldehyde, 0.5% [w/v] glutaraldehyde, 0.1 M citrate pH 4.8) for 3 hours at 30°C. Subsequently, fixed cells were resuspended in citrate buffer and further processed for electron microscopy (by Severine Kunz, MDC Berlin). The cell wall was permeabilised with sodium-metaperiodate and samples were embedded in 10% [w/v] gelatin and 2.3 M sucrose and frozen in liquid nitrogen. After preparation of ultrathin sections and staining with 3% [w/v] tungstosilicic acid hydrate in 2.5% [v/v] polyvinyl alcohol, samples were examined by electron microscopy with a Zeiss EM 910 electron microscope at 80 kV.

5.2.3. Generation and culture of human cell lines

5.2.3.1. Tissue culture and media

The parental HEK293T cell line was obtained from the laboratory of Michael T. Ryan (Melbourne, Australia) (Stroud et al, 2016) and maintained in a humidified incubator at 37°C and 5% CO₂ in Dulbecco's modified Eagle medium (DMEM) containing 4.5 g l⁻¹ glucose, supplemented with 10% FCS and 50 µg ml⁻¹ uridine. To test growth in galactose-containing media, glucose was replaced with 4.5 g l⁻¹ galactose. Cells were detached by trypsin treatment and kept at <90% confluency. For storage, cells were pelleted, resuspended in Bambanker freezing media and stored at -80°C.

5.2.3.2. CRISPR/Cas9-mediated knockout

CRISPR/Cas9 mediated knockout of target genes was performed as described (Ran et al, 2013). sgRNAs (listed in Table 5) were designed using the CHOPCHOP tool (<https://chopchop.rc.fas.harvard.edu>) and oligonucleotides encoding sgRNAs were annealed, phosphorylated with T4 polynucleotide kinase and cloned into the BbsI site of pSpCas9-(BB)-2A-GFP which was transfected into HEK293T cells. 24 hours after transfection, single GFP-positive clones were sorted by fluorescence activated cell sorting (FACS) into 96 well plates. Surviving clonal populations were transferred to 6-well plates and screened by SDS-PAGE and immunoblotting. If possible, successful inactivation of the target gene by indel formation was also verified by Sanger sequencing of sub-cloned amplicons of the targeted region.

5.2.3.3. Retroviral expression

Retroviral expression experiments were performed by Ralf M. Zerbes (University of Freiburg and Monash University, Melbourne) and Alexander von der Malsburg (Saarland University). For stable (re-)expression, open reading frames were amplified from cDNA and cloned into the pBABE-puro vector, which was transfected into HEK293T cells together with pVSV-G and pUMVC-gag-pol. Supernatant, including retroviruses, was harvested 48 h after transfection and used to transduce target cells. Target cells were then treated with puromycin for selection and individual clones or populations were screened by SDS-PAGE and immunoblotting for expression of the target gene.

5.2.3.4. Analysis of cell growth by crystal violet staining and extraction

To assess the growth behaviour of MICOS-mutant HEK293T cell lines, 48 well plates were coated with 0.01% poly-L-lysine prior to seeding 10,000 cells per well. After the indicated time points, media was removed, all wells were washed with PBS and fixed with 4% [w/v] para-formaldehyde in PBS. Fixed plates were stored at 4°C until the end of the growth assay. Subsequently, wells were washed with PBS and stained with 250 µl of a crystal violet solution

(2 mg ml⁻¹ in 10% EtOH) for 30 min. After removal of the staining solution, wells were washed extensively with distilled water to remove unspecific crystal violet staining. After air-drying, the dye was re-extracted with 250 µl 10% [v/v] acetic acid for 1 h and the absorbance at 590 nm was measured using a Tecan Spark 10M microplate reader. Blank-corrected absorbance values were plotted in Graphpad Prism v6.0.

6. Results

6.1. MICOS core subunits are required for efficient metabolic adaptation in yeast

Mitochondrial cristae shape constantly has to adapt to cellular metabolic demands to ensure efficient generation of ATP by oxidative phosphorylation. Cristae shape is determined by several proteinaceous effectors, including the ATP synthase and the dynamin-like GTPase Mgm1/OPA1. While dimeric ATP synthase assemblies appear to be crucial for the formation of tubular cristae and the stabilisation of cristae rims and tips, Mgm1/OPA1 has been implicated in the formation of lamellar cristae by inner membrane fusion as well as the dynamic remodelling of cristae depending on substrate availability. Very little is known about the role of the MICOS complex in the formation and remodelling of cristae. The yeast *Saccharomyces cerevisiae* is a suitable model organism to study these phenomena, since it undergoes a well-defined diauxic shift from glycolysis to respiration, during which it relies on the efficient remodelling of mitochondrial ultrastructure. Preliminary data from our laboratory indicated that alterations in the protein levels of Mic10, a core subunit of MICOS, lead to a delayed adaptation to respiratory metabolism (S. Horvath, pers. communication). To test the hypothesis that MICOS deficiencies lead to an inefficient adaptation to respiratory metabolism, yeast strains lacking or overexpressing Mic10 were grown in synthetic media containing 0.1% glucose as well as 3% of the respiratory carbon source glycerol and the optical density was measured manually to monitor cell proliferation. The resulting growth curve showed a clear diauxic behaviour in wild-type and Mic10 mutant strains (Figure 3a). While no difference could be observed during the first fermentative growth phase, cells lacking or overexpressing Mic10 showed a noticeable lag during the diauxic shift compared to wild-type cells. To further screen a multiple number of mutants, the assay was automated using a microplate reader and 24 or 48 well plates (Figure 3b,c), which allowed for continuous optical density measurements for 24 hours. This semi-automated protocol was then directly compared to manual measurements by measuring the diauxic growth of *mic10* Δ and Mic10 overexpressing cells (Figure 3b). While the absolute absorbance values were not comparable to the manually measured cultures, a clear diauxic growth behaviour could be observed. Importantly, Mic10 mutant cells also showed a delayed diauxic shift. In addition, *mic10* Δ but not Mic10 overexpressing cells showed a reduced respiratory growth rate (Figure 3b). The automated adaptation assay was then used to screen all six yeast MICOS deletion mutants (Figure 3c). Even though deletion of all MICOS subunits, with the exception of Mic26, leads to a noticeable ultrastructural phenotype (von der Malsburg et al, 2011), only deletion of the core subunits Mic10 and Mic60 led to a pronounced adaptation or respiratory growth phenotype of comparable effect size (Figure 3c).

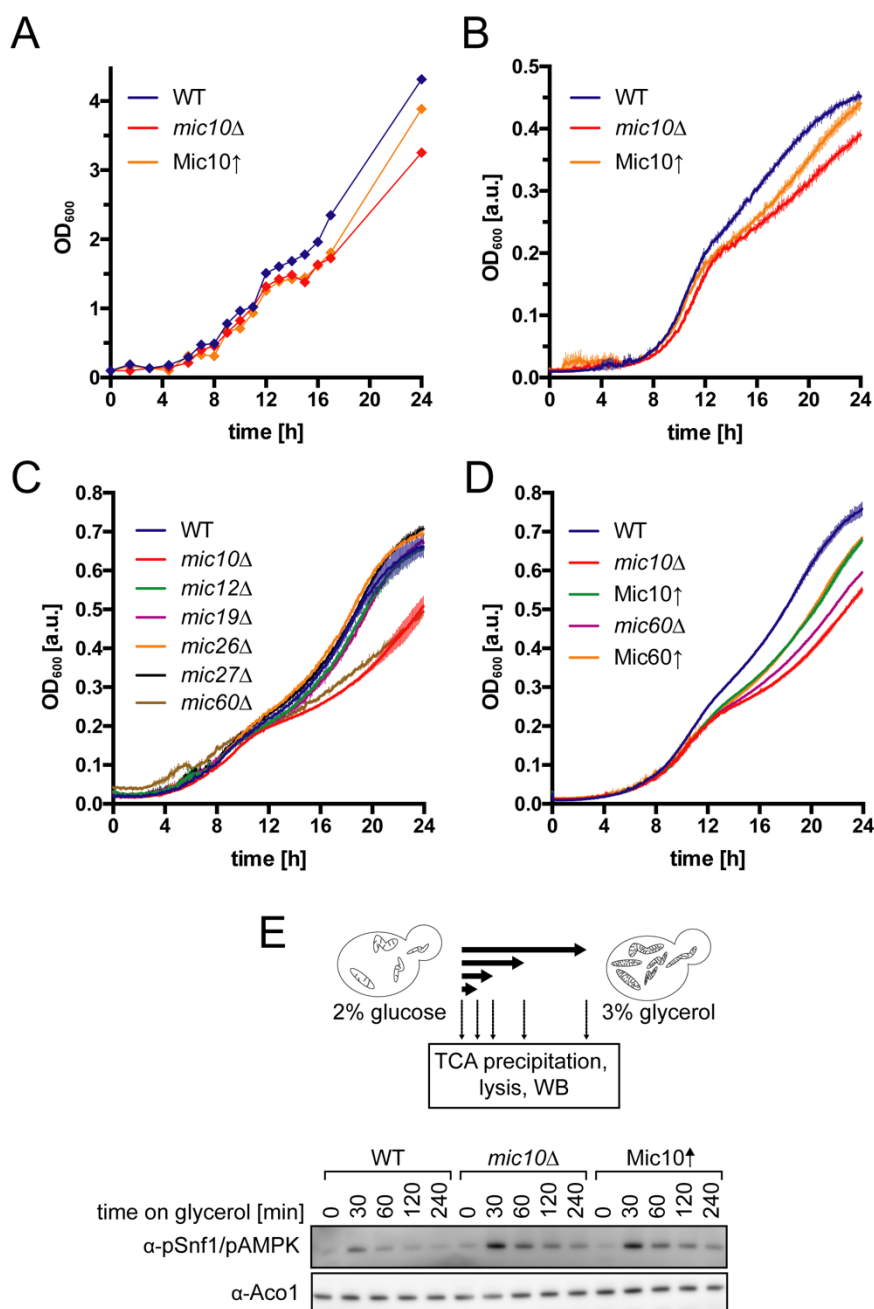


Figure 3 MICOS core subunits are required for efficient adaptation to respiratory metabolism

A. Wild-type, *mic10* Δ and Mic10 overexpressing (Mic10 \uparrow) yeast strains were grown in batch cultures in minimal media containing 0.1% glucose and 3% glycerol for 24 hours at 30°C. At the indicated time points, cellular growth was assessed by manually measuring the optical density at 600 nm (OD₆₀₀). B. Semi-automated growth assay in a 24 well plate. The conditions used in A were adapted to a microplate-reader based assay. Growth in minimal media containing 0.2% glucose was measured for 24 hours (B.-D: representative growth curves, error bars indicate standard deviation from technical replicates). C. Growth assay in 48 well plates using minimal media containing 0.1% glucose and 3% glycerol. The diauxic growth behaviour of all MICOS deletion strains was compared. D. Growth assay comparing the effect of Mic10 and Mic60 deletion and overexpression on diauxic growth using the conditions described in C. E. Analysis of AMPK (Snf1 in yeast) phosphorylation during the switch from glycolytic to respiratory metabolism in Mic10 mutant yeast. Yeast was grown in the presence of 2% glucose before culturing in media containing 3% glycerol. Cultures were stopped at the indicated time points by addition of trichloroacetic acid and phosphorylation of Snf1/AMPK was assessed by immunoblotting analysis of cell lysates.

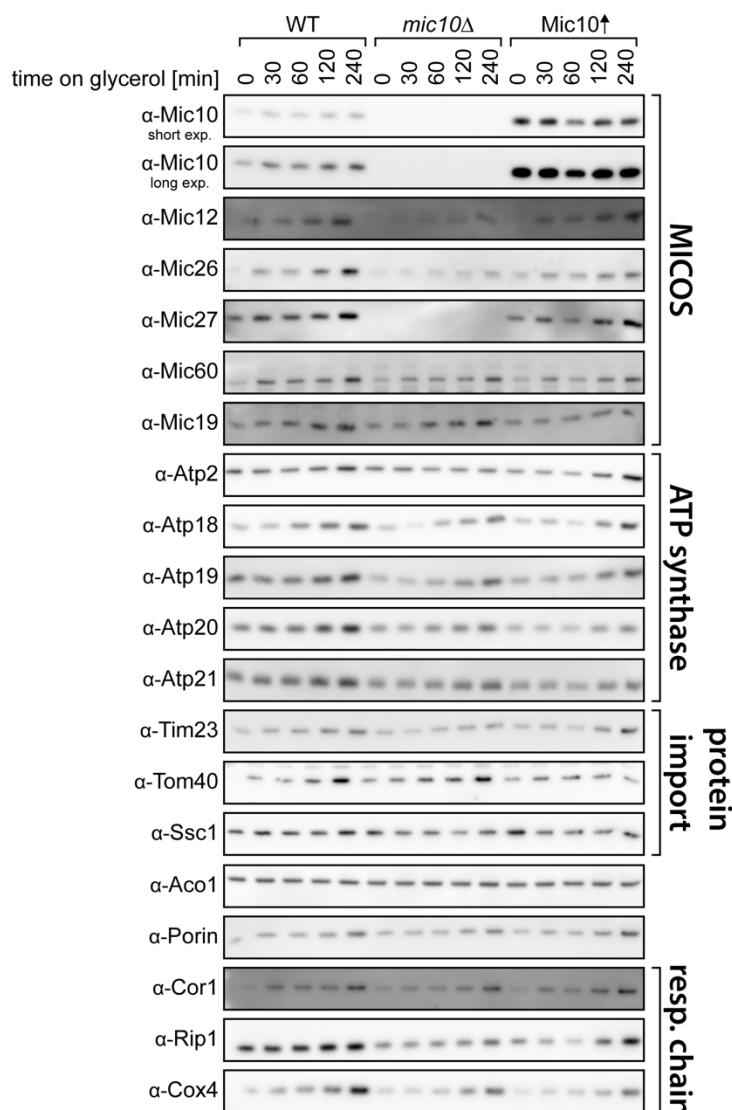


Figure 4 Delayed mitochondrial inner membrane biogenesis in *Mic10* mutant yeast during the diauxic shift

Samples were prepared as in Figure 3e and analysed by immunoblotting with antibodies against various mitochondrial proteins of the inner and outer membrane.

Similarly to *Mic10*, *Mic60* protein levels are crucial for correct mitochondrial architecture, since overexpression leads to increased branching of cristae (Rabl et al, 2009; Bohnert et al, 2015). In metabolic adaptation assays, *Mic10* or *Mic60* overexpression led to a similar phenotype (Figure 3d). To further investigate this phenotype, *Mic10* mutant yeast was grown in glucose-containing media and then switched to glycerol media to mimic a diauxic shift. At various time points, trichloroacetic acid was added and cultures were frozen. Subsequently, the level of phosphorylated AMPK (Snf1 in yeast) was analysed by immunoblotting (Orlova et al, 2008) to assess starvation (Figure 3e). In all cultures, increased pAMPK levels were detected immediately after removal of glucose. This effect was more pronounced in cells lacking or overexpressing *Mic10*, suggesting an impaired adaptation to respiratory metabolism. The same samples were also probed for various mitochondrial proteins (Figure

4). The levels of respiratory chain subunits, such as Cox4, Rip1 and Cor1 as well as ATP synthase subunits increased during the assay, indicating a stimulation of mitochondrial biogenesis. The expression of MICOS subunits showed a very similar behaviour, demonstrating that MICOS expression is important for the adaptation to respiratory metabolism. Interestingly, this increase of mitochondrial inner membrane proteins was slower in *mic10*Δ and Mic10 overexpressing cells, further supporting a delayed metabolic adaptation in these cells.

In summary, overexpression or deletion of MICOS core subunits in yeast leads to a delayed adaptation to respiratory metabolism while the deletion of accessory MICOS subunits had no effect. Mic10 and Mic60 form oligomeric assemblies that either stabilise or induce membrane curvature and their deletion as well as overexpression had an impact on the metabolic flexibility of these cells. Therefore, their levels and activity or assembly is likely spatiotemporally coordinated by regulatory pathways. Since deletion of other MICOS subunits leads to similar ultrastructural phenotypes, but does not affect metabolic adaptation or respiratory growth in a similar manner, MICOS-independent functions of Mic10 and Mic60 might also be involved in the observed phenotypes.

6.2. A *Mic10*-ATP synthase interaction is crucial for metabolic adaptation

While the main function of *Mic10* appears to be the stabilisation of membrane curvature at crista junctions as part of the MICOS complex, recent reports also showed that minor amounts interact directly with the ATP synthase and modulate its oligomeric state by an unknown mechanism (Eydt et al, 2017; Rampelt et al, 2017). Deletion or overexpression of *Mic10* led to a very pronounced effect on the diauxic growth behaviour of yeast, whereas deletion of accessory subunits of the *Mic10* subcomplex had no obvious effect (chapter 6.1). We therefore hypothesised that ATP-synthase bound *Mic10* contributes to the remodelling of mitochondrial ultrastructure during the diauxic shift. To test this hypothesis, *Mic10* was genetically targeted to the ATP synthase by fusing it to the C-terminus of *Atp21* (subunit e of the ATP synthase; construct created and initially characterised by Heike Rampelt, University of Freiburg), which has been shown to be in close proximity to *Mic10* by chemical crosslinking (Eydt et al, 2017; Rampelt et al, 2017). This construct was then expressed in *mic10Δ* yeast harbouring a Protein A tagged allele of *Mic60*, which was used to isolate the MICOS complex. To this end, isolated mitochondria were lysed with the mild non-ionic detergent digitonin and subjected to IgG affinity chromatography (Figure 5a). MICOS subunits could be efficiently co-isolated in the presence of *Mic10*, but not when *Mic10* was deleted (Figure 5a). Furthermore, *mic10Δ* mitochondria contained reduced amounts of *Mic26* and *Mic27*, indicating a destabilisation of the complex (Bohnert et al, 2015). Plasmid-based re-expression of *Mic10* rescued *Mic26* and *Mic27* levels and restored the integrity of MICOS complex after isolation via *Mic60*-ProteinA (Figure 5a). When the elution fractions are analysed on a BN-PAGE, *Mic10* oligomers can be visualised by immunoblotting with antibodies directed against *Mic10* (Bohnert et al, 2015). The *Atp21*-*Mic10* fusion construct could only be co-purified in minor amounts (Figure 5a) and no MICOS-bound oligomers could be detected (Figure 5b). This finding suggests that *Atp21*-*Mic10* is not stably associated with MICOS and does not form MICOS-bound oligomers. Because *Atp21*-*Mic10* did not form MICOS-bound oligomers, which are essential for stabilising crista junctions, we asked whether *Atp21*-*Mic10* would rescue the ultrastructural phenotype observed in *mic10Δ* mitochondria. Since *mic10Δ* mitochondria display no or only a few connections between cristae and the inner boundary membrane, they show a decreased response to hypo-osmotic swelling (von der Malsburg et al, 2011). Outer membrane rupture after swelling can be assessed by analysing protease-accessibility of intermembrane space exposed proteins (Figure 5c). When wild-type mitochondria were treated with hypo-osmotic buffer and proteinase K, proteins of the IMS or proteins with IMS-exposed domains such as *Tim13*, *Tim23* and *Mic60* were efficiently degraded (Figure 5c). This reduction was less pronounced in *mic10Δ* mitochondria but was rescued by plasmid-based expression of *Mic10*. Importantly, the hypoosmotic swelling defect was not rescued by expression of *Atp21*-*Mic10*, which strongly suggests that the *Atp21*-*Mic10* fusion construct does not rescue the function of *Mic10* at the MICOS complex, leading to a collapse of crista

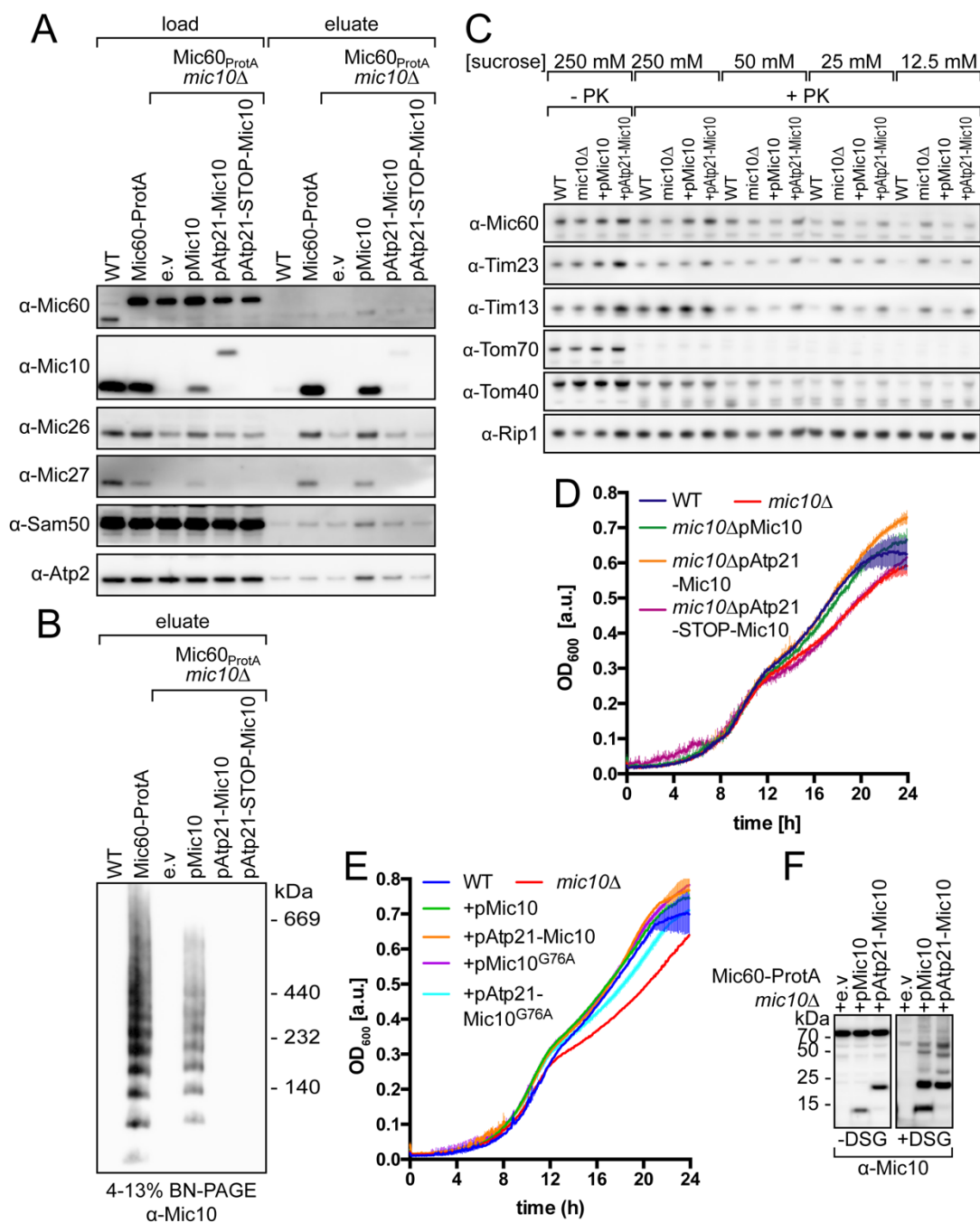


Figure 5 ATP synthase-bound Mic10 is required for efficient adaptation to respiratory metabolism, but does not rescue MICOS activity

A. Mitochondria from the indicated yeast strains were lysed in digitonin and Mic60-ProtA was isolated by IgG affinity chromatography followed by immunoblotting against various MICOS subunits (load: 8% of eluate). B. The eluates obtained in A were directly loaded onto a BN-PAGE and analysed by immunoblotting with antibodies directed against Mic10 to visualize MICOS-bound Mic10 oligomers. C. Mitochondria isolated from the indicated strains were exposed to hypoosmotic swelling conditions using the indicated sucrose concentrations. After 30 min, proteinase K (PK) was added as indicated to assess outer membrane rupture by protease accessibility. Samples were analysed by SDS-PAGE and immunoblotting against various outer and inner membrane proteins. D. Diauxic growth assay (minimal media with 0.2% glucose, see Figure 3) of *mic10*Δ cells complemented with plasmids encoding for Mic10 or Atp21-Mic10. E. Diauxic growth assay in minimal media containing 0.2% glucose with oligomerisation-deficient Mic10 or Atp21-Mic10 variants (D.-E.: Representative growth curves, error bars indicate standard deviation from technical replicates). F. Chemical crosslinking of mitochondria from yeast strains expressing Mic10 or Atp21-Mic10. Mitochondria were treated with disuccinimidyl glutarate (DSG) and analysed by immunoblotting with antibodies against Mic10.

A.-F.: The Atp21-Mic10 fusion construct was cloned and initially characterised by Heike Rampelt, University of Freiburg.

junctions. We next tested whether expression of Atp21-Mic10 could rescue the diauxic shift and respiratory growth phenotypes observed in *mic10* Δ cells. Surprisingly, expression of Atp21-Mic10 fully restored the diauxic growth behaviour of *mic10* Δ cells (Figure 5d). When a stop codon was inserted between the two open reading frames to only allow for plasmid-based expression of Atp21, this rescue was abolished (Figure 5d). It is unclear how Mic10 affects ATP synthase oligomerisation and whether membrane bending activities via homo-oligomerisation at the ATP synthase are required for this function. Expression of an oligomerisation-deficient Mic10 mutant (Mic10^{G76A}) fully rescued the growth phenotype of the *mic10* Δ yeast strain (Figure 5e). In contrast, when the oligomerisation motif of Mic10 was mutated in the Atp21-Mic10 construct (Atp21-Mic10^{G76A}), we observed an intermediate growth phenotype (Figure 5e), suggesting that the Mic10 oligomerisation interface is involved in Mic10-mediated modulation of ATP synthase oligomerisation. To obtain further evidence for oligomerisation of the fusion construct, mitochondria were subjected to chemical crosslinking with disuccinimidyl glutarate (DSG) and subsequent SDS-PAGE and immunoblotting with antibodies directed against Mic10 (Figure 5f). Wild-type Mic10 oligomers could be efficiently captured by crosslinking, since several prominent bands were detected after addition of DSG. Atp21-Mic10 also formed at least three higher molecular weight crosslinking products, which might represent homo-oligomeric assemblies. In conclusion, we observed that genetic targeting of Mic10 to the ATP synthase rescues the diauxic growth defect of *mic10* Δ cells without restoring Mic10 function at the MICOS complex and crista junction architecture. Combined with the observation that the majority of MICOS deletion strains show no obvious diauxic growth phenotype despite a lack of crista junction structures, these data suggest that moonlighting functions of MICOS core subunits are involved in the efficient adaptation of mitochondrial ultrastructure to cellular metabolic demand.

6.3. *Mic10* oligomerisation is regulated by *Mic26-Mic27* antagonism

Some of the data described in this chapter have been published in:

Rampelt H*, **Wollweber F***, Gerke C, de Boer R, van der Klei IJ, Bohnert M, Pfanner N & van der Laan M (2018) Assembly of the mitochondrial cristae organizer *Mic10* is regulated by *Mic26-Mic27* antagonism and cardiolipin. *J. Mol. Biol.* 430: 1883–1890 (*equal contribution)

With the exception of Figure 7d of this thesis, all experiments described here were performed by F.W.

Yeast *Mic10* has been shown to stabilise the membrane curvature at crista junctions by homo-oligomerisation and subsequent formation of a proteinaceous membrane scaffold. Deletion of *Mic10* leads to a collapse of crista junctions and *Mic10* mutants lacking the oligomerisation motif show a phenotype that resembles *mic10Δ* (Bohnert et al, 2015). In contrast, overexpression of *Mic10* leads to an increase of membrane curvature within cristae and enlarged, disorganised crista junctions (Barbot et al, 2015; Bohnert et al, 2015). As shown in chapter 6.1, yeast mutants lacking or overexpressing *Mic10* also fail to efficiently adapt to respiratory metabolism. This can partially be explained by the moonlighting function of *Mic10* at the ATP synthase (see chapter 6.2), which appears to be of crucial importance for the remodelling of mitochondrial ultrastructure in response to altered metabolic conditions. These observations suggest that *Mic10* assembly is spatiotemporally controlled by regulatory mechanisms to prevent excessive membrane bending and to coordinate the membrane organising activities of MICOS as well as the ATP synthase. The *Mic10* subcomplex also contains the accessory subunits *Mic12*, *Mic26* and *Mic27*, which might be important for the assembly of *Mic10* oligomers. A recent study described *Mic12* as a linker between both MICOS subcomplexes (Zerbes et al, 2016). Furthermore, *Mic27* was shown to stabilise *Mic10* oligomers (Zerbes et al, 2016). The role of the *Mic27* paralogue *Mic26* was unknown. *Mic26* is the only known MICOS subunit in yeast that is not strictly required for crista junction maintenance since *mic26Δ* mitochondria show no obvious ultrastructural defects (Harner et al, 2011; Hoppins et al, 2011; von der Malsburg et al, 2011). Importantly, yeast *Mic26* and *Mic27* show a similar membrane topology and share a high degree of sequence similarity as a result of their paralogous relationship (Muñoz-Gómez et al, 2015; Huynen et al, 2016).

To test how *Mic10* oligomerisation is affected by deletion or overexpression of *Mic26* and *Mic27*, mitochondria from yeast cells expressing *Mic60-ProteinA* were lysed with the mild detergent digitonin and subjected to IgG affinity chromatography (Figure 6a). The isolated MICOS complex was then analysed by blue-native electrophoresis and MICOS-bound *Mic10* oligomers were visualised by immunoblotting with an antibody directed against *Mic10* (Figure 6b). As reported previously, deletion of *Mic27* led to an increase of lower molecular weight complexes. In contrast, deletion of *Mic26* resulted in the opposite phenotype (Figure 6b). Most of the *Mic10* signal was found in higher molecular weight complexes. To validate this finding,

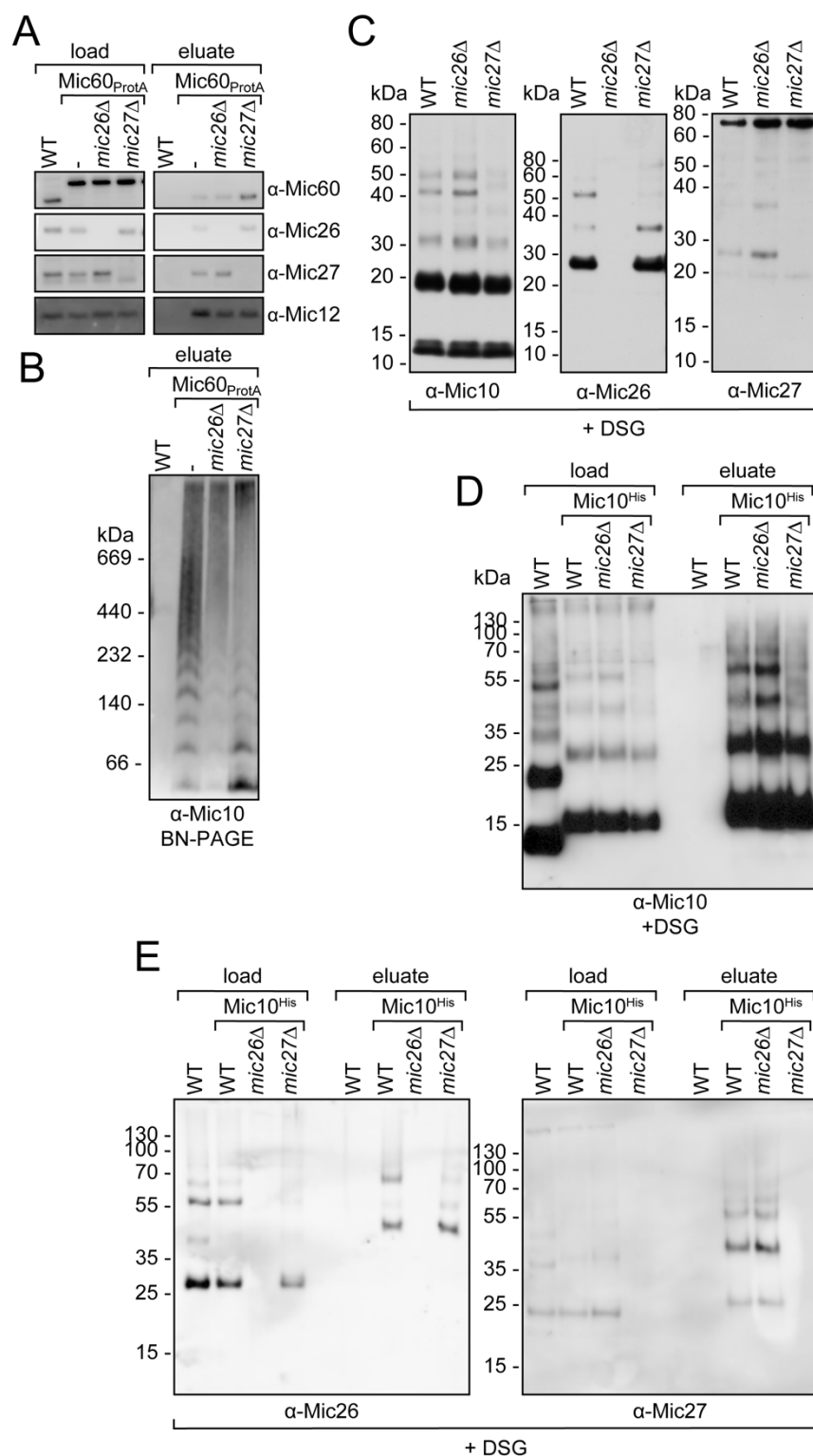


Figure 6 Antagonistic effect of Mic26 and Mic27 on Mic10 oligomerisation.

A. MICOS was purified from mitochondria from cells lacking Mic26 or Mic27 via Mic60-ProtA and eluates were analysed by immunoblotting (load: 8% of eluate). B. Mic10 oligomers were visualised by BN-PAGE and immunoblotting with antibodies directed against Mic10 after isolation of Mic60-ProtA from isolated mitochondria. C. *In organello* DSG crosslinking of mitochondria lacking Mic26 or Mic27. D. Crosslink products were isolated with Mic10^{His} via Ni-NTA chromatography and analysed by immunoblotting with Mic10 antibodies. E. Samples from D were analysed by immunoblotting with antibodies directed against Mic26 or Mic27 (load: 5% of eluate).

mitochondria from cells lacking Mic27 or Mic26 were subjected to chemical crosslinking with DSG and crosslinks were visualised by SDS-PAGE followed by immunoblotting with antibodies directed against Mic10, Mic26 and Mic27 (Figure 6c). Using Mic10 antibodies, several prominent crosslinks could be identified which most likely represent different oligomeric states of the protein. These crosslinks were increased in *mic26* Δ and decreased in *mic27* Δ (Figure 6c), supporting the data obtained with the isolated complex and BN-PAGE. Furthermore, the crosslinking efficiency of Mic26 or Mic27 was increased in the absence of the paralogous subunit. To test whether Mic26 and Mic27 interaction with Mic10 is affected, the experiment was repeated in mitochondria from cells expressing C-terminally deca-histidine tagged Mic10 (Bohnert et al, 2015), which was affinity purified immediately after DSG crosslinking by NiNTA chromatography (Figure 6d). As expected, Mic10^{His} crosslinking products were increased in *mic26* Δ and decreased in *mic27* Δ mitochondria (Figure 6d). Using this strategy, Mic10-Mic26 and Mic10-Mic27 crosslinking products could be isolated in a very efficient manner (Figure 6e), suggesting a close proximity between the two accessory proteins and Mic10. Furthermore, absence of Mic26 led to a slight increase of the Mic27-Mic10 interaction and vice-versa (Figure 6e), supporting an antagonistic influence of Mic26 and Mic27 on Mic10 assembly.

Human Mic27 has been reported to bind cardiolipin *in vitro* (Weber et al, 2013). To test whether a Mic26/27-mediated cardiolipin recruitment is responsible for the effect on Mic10 assembly, we assessed whether deletion of Mic26 or Mic27 globally affects cardiolipin levels or distribution by analysing the stability of cardiolipin-sensitive protein complexes (Pfeiffer et al, 2003; Kutik et al, 2008). To this end, mitochondria were lysed with digitonin and analysed by blue native PAGE followed by immunoblotting with antibodies against the ADP/ATP carrier (AAC) (Figure 7a) and the cytochrome-c-oxidase (respiratory chain complex IV) (Figure 7b). As expected, respiratory chain supercomplexes were destabilised in mitochondria from cells lacking cardiolipin synthase (*Crd1*) (Figure 7b), while no obvious differences could be observed in mitochondria lacking Mic26 or Mic27 (Figure 7b). Furthermore, oligomeric AAC complexes also showed no alteration (Figure 7a), indicating that Mic26 or Mic27 do not globally affect mitochondrial cardiolipin homeostasis. We next tested whether Mic10 oligomerisation is affected in mitochondria from cells lacking cardiolipin synthase by chemical crosslinking (Figure 7c), but did not observe markedly altered levels of Mic10 crosslinking products. We next analysed Mic10 oligomers by BN-PAGE after affinity purification of Mic60-ProtA to test whether high molecular weight complexes of Mic10 oligomers depend on cardiolipin levels. In *crd1* Δ mitochondria we observed reduced amounts of low and high molecular weight Mic10 complexes (Figure 7d). To test whether Mic26 or Mic27 locally affect cardiolipin abundance at the MICOS complex, the *crd1* deletion was combined with deletion of *mic26* and *mic27*. Deletion of *mic26* or *mic27* also caused an up- or downshift of Mic10 oligomers in the absence of *crd1*, respectively, indicating that the effect

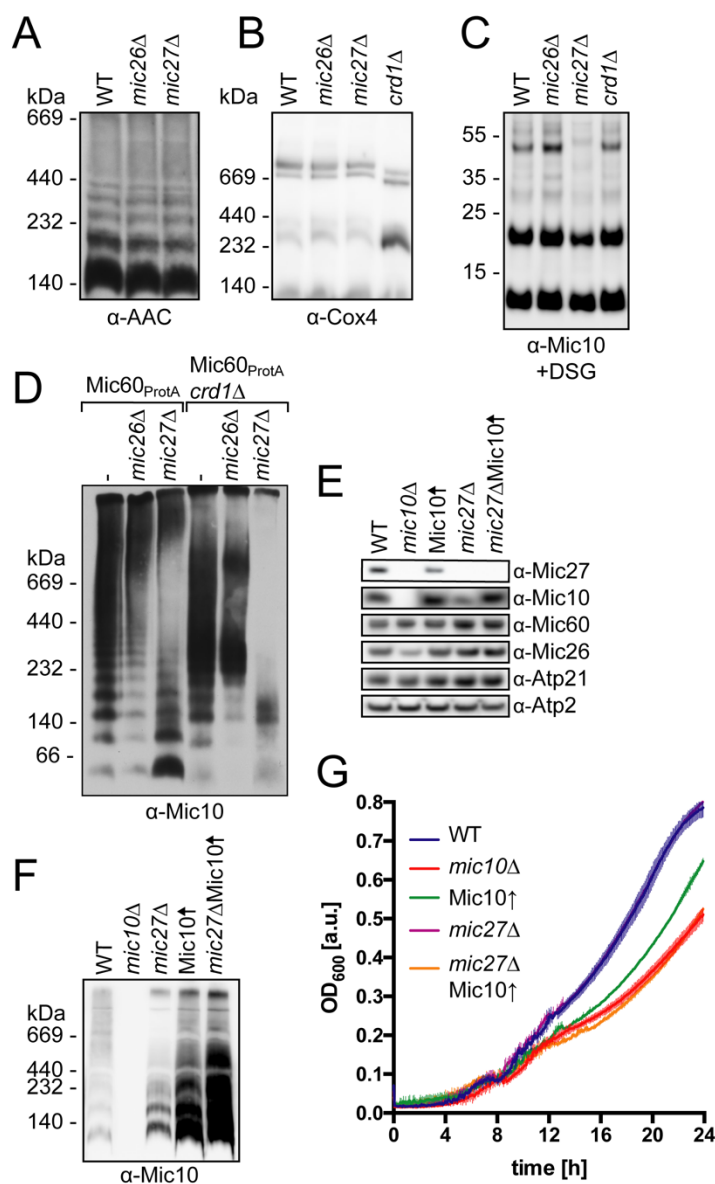


Figure 7 Mic26-Mic27 and cardiolipin independently affect Mic10 assembly.

The cardiolipin sensitive complexes AAC (ATP/ADP carrier) and complex-IV-containing supercomplexes in mitochondria lacking Mic26, Mic27 or Crd1 were analysed by BN-PAGE followed by immunoblotting. C. Mic10 oligomers in mitochondria from cells lacking Mic26, Mic27 or Crd1 were captured by chemical crosslinking with DSG and analysed by immunoblotting. D. MICOS-bound Mic10 oligomers in cells lacking Mic26, Mic27 and/or Crd1 were analysed by native isolation of Mic60-ProtA followed by BN-PAGE and Mic10 immunoblotting. E. SDS-PAGE analysis of MICOS protein levels in *mic27ΔMic10↑* cells. F. Analysis of Mic10 oligomers in *mic27ΔMic10↑* overexpression cells by BN-PAGE of isolated mitochondria. G. Diauxic growth of *mic27Δ* cells overexpressing Mic10 in minimal media containing 0.2% glucose (representative growth curve, error bars indicate standard deviation of technical replicates).

D.: Experiment performed by Heike Rampelt, University of Freiburg

of Mic26 and Mic27 is independent of cardiolipin (Figure 7d). The most pronounced effect was observed in mitochondria lacking Mic27 and cardiolipin.

The physiological relevance of the Mic26-Mic27 regulatory pathway remains elusive, as deletion of these two proteins did not affect the metabolic adaptability of yeast during diauxic

shift experiments (chapter 6.1). Since Mic10 overexpression has a pronounced effect on yeast during the diauxic shift (chapter 6.1), we tested how absence of the stabilising Mic27 proteins affects yeast overexpressing Mic10 (Figure 7e). Mitochondria isolated from the *mic27* Δ Mic10 \uparrow strain showed increased levels of Mic10 oligomers and Mic10-containing high molecular weight complexes compared to wildtype or Mic10 \uparrow (Figure 7f). We next assessed diauxic growth in media containing 0.2% glucose. Interestingly, Mic10 overexpression in *mic27* Δ led to a growth phenotype which was comparable to *mic10* Δ cells and more severe than Mic10 overexpressing strains (Figure 7g). The strong growth phenotype of *mic27* Δ Mic10 \uparrow cells indicates that non-MICOS bound Mic10 negatively affects the ability of yeast to shift to respiratory metabolism and underlines the necessity to regulate the assembly of Mic10.

In summary, oligomeric assemblies of Mic10 are regulated by at least two distinct mechanisms. The two accessory subunits Mic26 and Mic27 directly interact with Mic10 and destabilise or stabilise Mic10 oligomers, respectively. In an independent manner, cardiolipin stabilises MICOS-associated Mic10 oligomers. Consequently, Mic10 assembly is most affected when both stabilising factors, Mic27 and cardiolipin, are absent.

6.4. MICOS organisation is conserved from yeast to man

Some of the data described in this chapter will be communicated in the following manuscript:

Wollweber F, Noll K, Schorr S, Zerbes RM, Ryan MT, Liu F, van der Laan M & von der Malsburg A
MICOS and DNAJC11 spatially coordinate mitochondrial β -barrel protein biogenesis. *In preparation*.

All experiments described in this chapter were performed by F.W.

MICOS composition has mostly been analysed in yeast, due to its excellent genetic tractability and suitability as model organism for mitochondrial research. However, MICOS is highly conserved throughout eukaryotic evolution and MICOS subunits can be found in all known cristae-containing eukaryotes. A major aim of this thesis was to analyse MICOS architecture in a comparative manner in yeast as well as mammalian cells to define conserved and divergent functions of the complex. To analyse MICOS composition in a human cell line, the MICOS core subunit MIC10 was targeted by CRISPR/Cas9 in HEK293T cells, resulting in a MIC10 knock-out (KO) cell line. This cell line was then complemented with a retroviral MIC10^{FLAG} construct, which could be used in co-immunoprecipitations. Mitochondria from the MIC10^{FLAG} cell line and the corresponding parental HEK293T cell line were lysed in the mild detergent digitonin and subjected to FLAG Co-IP. Subsequently, proteins were natively eluted using the FLAG peptide (Figure 8a). All known *bona fide* MICOS subunits (i.e. MIC13, MIC19, MIC25, MIC26, MIC27, MIC60) were co-purified to a similar extent, indicating that the complex remained intact during the purification (Figure 8a). Interestingly, similar amounts of the outer membrane interaction partners SAM50 and DNAJC11 were found in the elution fraction, supporting a model in which MICOS and the SAM machinery form a stable *mitochondrial intermembrane space bridging* (MIB) complex (Ott et al, 2012; Huynen et al, 2016). To investigate whether the subcomplex architecture described in yeast is conserved in mammalian cells, the second core subunit MIC60 was targeted by CRISPR/Cas9. Very minor amounts of MIC60 could still be detected in this cell line (Figure 8b). Sequencing revealed a 108 base pair deletion within the 5' UTR of MIC60, which drastically reduced MIC60 mRNA levels as assessed by RNA-sequencing, while allowing for residual expression (data not shown). Mitochondria from MIC10 and MIC60-deficient HEK293T cell lines were then analysed by SDS-PAGE and immunoblotting (Figure 8b). MIC10 KO led to a loss of MIC13, MIC26 and MIC27, while other MICOS subunits were unaffected. In contrast, MIC60-deficient cells showed decreased levels of all MICOS subunits as well as DNAJC11 and SAM50 (Figure 8b). Next, the same mitochondria were solubilised in digitonin and analysed by BN-Page and immunoblotting with antibodies against all MICOS subunits as well as SAM50 (Figure 8c). All subunits could be detected in several high-molecular-weight protein complexes with a minimum size of approximately 700 kDa. Subunits of the MIC10 subcomplex did not form a detectable complex in the absence of MIC10 or MIC60. In contrast,

complexes also remained intact under these conditions. Triton X-100 solubilised MICOS/MIB complexes migrated faster compared to digitonin controls, also indicating a loss of the MIC10 subcomplex (Figure 8d). The MICOS-SAM connection thus shows a remarkable stability, but it is unknown how both complexes are connected and whether their association can be regulated. Preliminary XL-MS data indicated that MIC19, rather than MIC60, links both complexes (Fan Liu, FMP Berlin, pers. communication). To directly test whether MIC19 or MIC60 connects MICOS and SAM, mitochondria from a ^{FLAG}SAM50 cell line were subjected to chemical crosslinking using DSG. Subsequently, the samples were denatured and SAM50-containing crosslinking products were isolated by affinity purification (Figure 8e). Only a single ca. 100 kDa SAM50 crosslink could be detected. Using a MIC19 antibody, multiple crosslinked bands with a molecular weight of at least 80 kDa were observed, indicating a close proximity between SAM50 and MIC19. In contrast, no specific SAM50-MIC60 crosslinks could be detected.

In summary, MIC60/19/25 and the SAM complex form a stable two-membrane spanning core complex. MIC19 likely links SAM and MICOS. Both subcomplexes can be genetically and biochemically separated, since the Mic10 module, containing MIC10, MIC13, MIC26 and MIC27, is sensitive to harsh detergents and the loss of the MIC60 core complex.

6.5. Human MIC10 affects cristae organising proteins of the inner membrane

Since both MICOS sub-complexes can be easily separated genetically and biochemically (see chapter 6.4), we asked whether their depletion leads to non-overlapping functional defects. In the absence of MIC10, the MIC60 subcomplex remains stable and protein levels of MIC60, MIC19 and MIC25 are similar to wild-type, while MIC60 deletion affected steady-state levels of MIC10 module subunits (chapter 6.4). To understand how the two sub-complexes affect cellular functions, the growth of MIC10 and MIC60 KO HEK293T cells in media containing either glucose or galactose was analysed (Figure 9a). MIC10 and MIC60-deficient cells showed a strongly reduced growth compared to the parental HEK293T cell line. Media containing galactose instead of glucose are known to induce a metabolic shift towards respiratory ATP generation (Marroquin et al, 2007). The growth phenotype of MICOS deficient cell lines was even more pronounced in galactose-containing media (Figure 9a), suggesting that mitochondrial ATP production is compromised. To analyse the effect on mitochondrial ultrastructure, the cells were also analysed by transmission electron microscopy (data by Sibylle Jungbluth, Saarland University). Mitochondria in MIC10-6 and MIC60-22 cells appeared rounded and contained a reduced number of intraorganellar membranes (Figure 9b). Furthermore, no crista junction structures could be detected, indicating that both MICOS core subunits are essential for crista junction maintenance. MIC10 and MIC60-deficient mitochondria appeared to show a similarly disorganised membrane architecture, which might help to explain the similar effect on cellular growth. These observations also suggest that the MIC60 subcomplex, which is stable in MIC10 deficient mitochondria, is not sufficient for maintaining mitochondrial ultrastructure and function in the absence of the MICOS holo-complex. Since the strong growth phenotype of MICOS-deficient cells suggest functional deficiencies in mitochondrial ATP production, we next analysed the stability of respiratory chain supercomplexes which reside in cristae membranes by BN-PAGE analysis (Figure 9c). Despite the strong ultrastructural defects, supercomplexes of complex I, III and IV were still present in MICOS-deficient mitochondria and supercomplex formation was enhanced when cells were shifted to media containing galactose (Figure 9c). In MIC10, but not in MIC60-deficient mitochondria, a slight destabilisation of complex I was observed when cells were cultured in media containing glucose. This phenotype was rescued by culturing cells in galactose-containing media (Figure 9c). Only monomeric species of the ATP synthase were resolved on native PAGE gels using the mild detergent digitonin (Figure 9c). Since yeast Mic10 is involved in the organisation of ATP synthase oligomers (Eydt et al, 2017; Rampelt et al, 2017a; chapter 6.2), we attempted to analyse higher oligomeric states of the human ATP synthase complex. We hypothesised that dimers of the ATP synthase dissociate during the isolation of mitochondrial membranes and therefore repeated the experiment by directly lysing cells in digitonin-containing lysis buffer and analysed the cell lysate by BN-PAGE (Figure 9d). A higher molecular weight complex, most likely representing dimeric

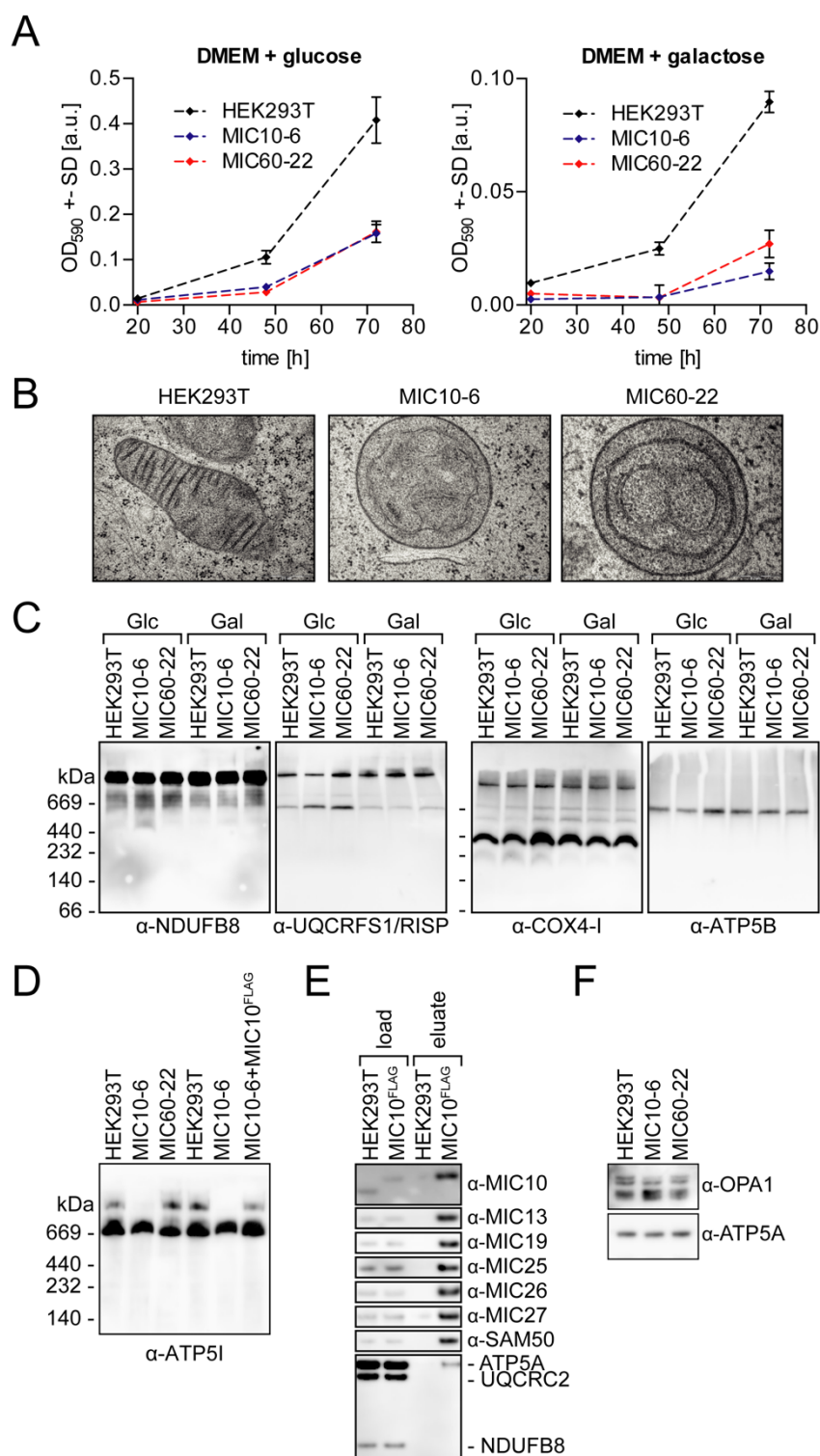


Figure 9 Effect of MIC10 and MIC60 deletion in HEK293T mitochondria

A. Growth of MIC10 and MIC60-deficient HEK293T cell lines in media containing glucose or galactose. Growth was assessed by crystal violet staining followed by extraction of the dye with acetic acid and measurement of the absorbance at 590 nm. Error bars indicate standard deviation from technical replicates B. Representative transmission electron micrographs of MICOS mutant mitochondria. C. Analysis of respiratory chain supercomplexes in mitochondria from MIC10 and MIC60-deficient cells grown in glucose (Glc) or galactose (Gal) containing media. Isolated mitochondria were lysed in digitonin and analysed by BN-PAGE followed by immunoblotting with antibodies against NDUFB8 (complex I), UQCRC1 (complex III), COX4-I (complex IV) or ATP5B (ATP synthase). D. Analysis of ATP synthase assembly by BN-PAGE of cells lysed in digitonin. E. Analysis of Mic10 interacting proteins by isolation of MIC10^{FLAG} followed by SDS-PAGE and immunoblotting (load: 15% of eluate). F. OPA1 processing as assessed by SDS-PAGE and immunoblotting.

B.: Electron microscopy data acquired and analysed by Sibylle Jungbluth (Saarland University). 57

ATP synthase complexes, could be observed in HEK293T cell lysates and lysates from MIC60-deficient cell lines. The higher molecular weight band was, however, absent in lysates from MIC10-deficient cells. Importantly, this phenotype was rescued when MIC10^{FLAG} was re-expressed in MIC10-6 cells (Figure 9d). Yeast Mic10 directly interacts with the ATP synthase to mediate its oligomerisation. To test whether the human protein has a similar influence on the ATP synthase, MIC10^{FLAG} was purified by affinity chromatography after lysis of mitochondria with digitonin and the eluate was analysed using antibodies directed against multiple MICOS subunits as well as respiratory chain subunits (Figure 9e). While components of MICOS were efficiently co-purified, subunits of the respiratory chain (NDUFB8 and UQCRC2) were not detected in the eluate fraction. In contrast, minor amounts of the ATP synthase subunit ATP5A could be detected, indicating that a minor fraction of MIC10^{FLAG} is in proximity to the ATP synthase (Figure 9e). Since MIC10 appears to influence the stability of ATP synthase dimers, which are one of the main cristae organising protein complexes, we also asked whether it influences the second major cristae remodelling protein, OPA1. In total, 8 isoforms of OPA1 exist in human mitochondria, which are further processed by the proteases OMA1 and YME1L (see also chapter 6.8). This results in the formation of longer, membrane-bound OPA1 forms as well as shorter, soluble species and a disturbed balance of these isoforms has been shown to impair the bioenergetic capabilities of mitochondria. To test whether the knockout of MICOS core subunits affects the isoform stoichiometry of OPA1, mitochondria from MIC10 and MIC60-deficient cells were analysed by SDS-PAGE and immunoblotting with an OPA1 antibody. When compared to samples from the parental HEK293T cell line, MIC10 knockout mitochondria showed a decrease of larger isoforms and a pronounced increase of shorter, soluble isoforms (Figure 9f).

In summary, the knockout of MIC10 and MIC60 in HEK293T cells results in a strong growth phenotype, especially when cells use oxidative phosphorylation for the generation of ATP. Both knockout cell lines show severely altered mitochondrial ultrastructure, with a lower number of internal cristae membranes which are not connected to the inner boundary membrane. MIC10, but not MIC60, appears to affect the stability of respiratory chain supercomplexes and dimers of the ATP synthase. Similarly to yeast, minor amounts of ATP synthase subunits can be co-isolated with MIC10. In addition, MIC10 but not MIC60 affects the processing of OPA1. The knockout of MIC10 therefore affects all three major cristae organising systems of the mitochondrial inner membrane.

6.6. Hierarchical organisation of the MIC10 subcomplex

As shown in chapters 6.4 and 6.5, the overall organisation of MICOS is conserved from yeast to humans, since two distinct subcomplexes with partially non-overlapping functions can be defined biochemically or genetically. We next asked to what extent the organisation of the MIC10 subcomplex is conserved in human cell lines. To this end, the accessory subunits of the MIC10 subcomplex, namely MIC13/QIL1, MIC26 and MIC27 were targeted by CRISPR/Cas9. The resulting knockout cell lines were validated by immunoblotting and showed no residual protein expression (Figure 10a). Using antibodies against MICOS subunits, the MICOS composition in MIC10-subcomplex mutants was analysed (Figure 10a). While MIC10 knockout led to a reduction of all MIC10 module subunits, especially MIC13 and MIC26, knockout of the other subunits had only a mild effect on the levels of other subunits, confirming MIC10 as the central core component of the subcomplex. MIC13-deficient mitochondria still showed moderately decreased levels of MIC10 and MIC26, while MIC10 and MIC13 abundance was unaffected by the knockout of MIC26 or MIC27. Importantly, MIC26 and MIC27 protein levels were increased in the absence of the respective paralogous subunit, reminiscent of the antagonistic relationship found in yeast. Next, the stability and composition of the MIB/MICOS complex was analysed by BN-PAGE and immunoblotting with antibodies directed against MICOS subunits and SAM50 (Figure 10b). As described in chapter 6.4, MIC10 knockout leads to a shift of MIC60 and SAM50-containing protein complexes. A similar shift could also be observed in MIC13 deficient mitochondria, which also showed considerably reduced amounts of MIC10 (Figure 10a,b). Importantly, stable complexes containing MIC10 module subunits could neither be detected in MIC10 nor in MIC13 KO mitochondria. In contrast, MIC26 or MIC27 knockout did not affect the migration behaviour and abundance of MIC10 or MIC13 containing complexes (Figure 10b), in agreement with the data obtained by SDS-PAGE analysis (Figure 10a). In yeast, Mic10 was found to form extended oligomers via a conserved GxGxG motif that likely act as a protein scaffold at the crista junction. Since the oligomerisation motif is conserved in the human protein we aimed to detect MIC10 oligomerisation in HEK293T mitochondria. In contrast to yeast, no evidence for oligomerisation was found by BN-PAGE analysis (Figure 10b). To test whether the human protein forms oligomers, isolated mitochondria were chemically crosslinked with DSG and analysed by SDS-PAGE and immunoblotting with antibodies directed against MIC10. Addition of DSG led to the formation of at least three prominent additional bands (marked by an asterisk), with an approximate size of dimeric, trimeric and tetrameric MIC10 (Figure 10c). Importantly, the crosslinking pattern was altered upon deletion of the accessory subunits of the MIC10 subcomplex: MIC13 KO mitochondria showed reduced levels of MIC10 and only monomeric as well as the putative dimeric MIC10 could be detected after crosslinking. MIC26 KO did not alter the overall abundance of MIC10 in mitochondria, but markedly lower levels of trimeric and tetrameric MIC10 were found upon

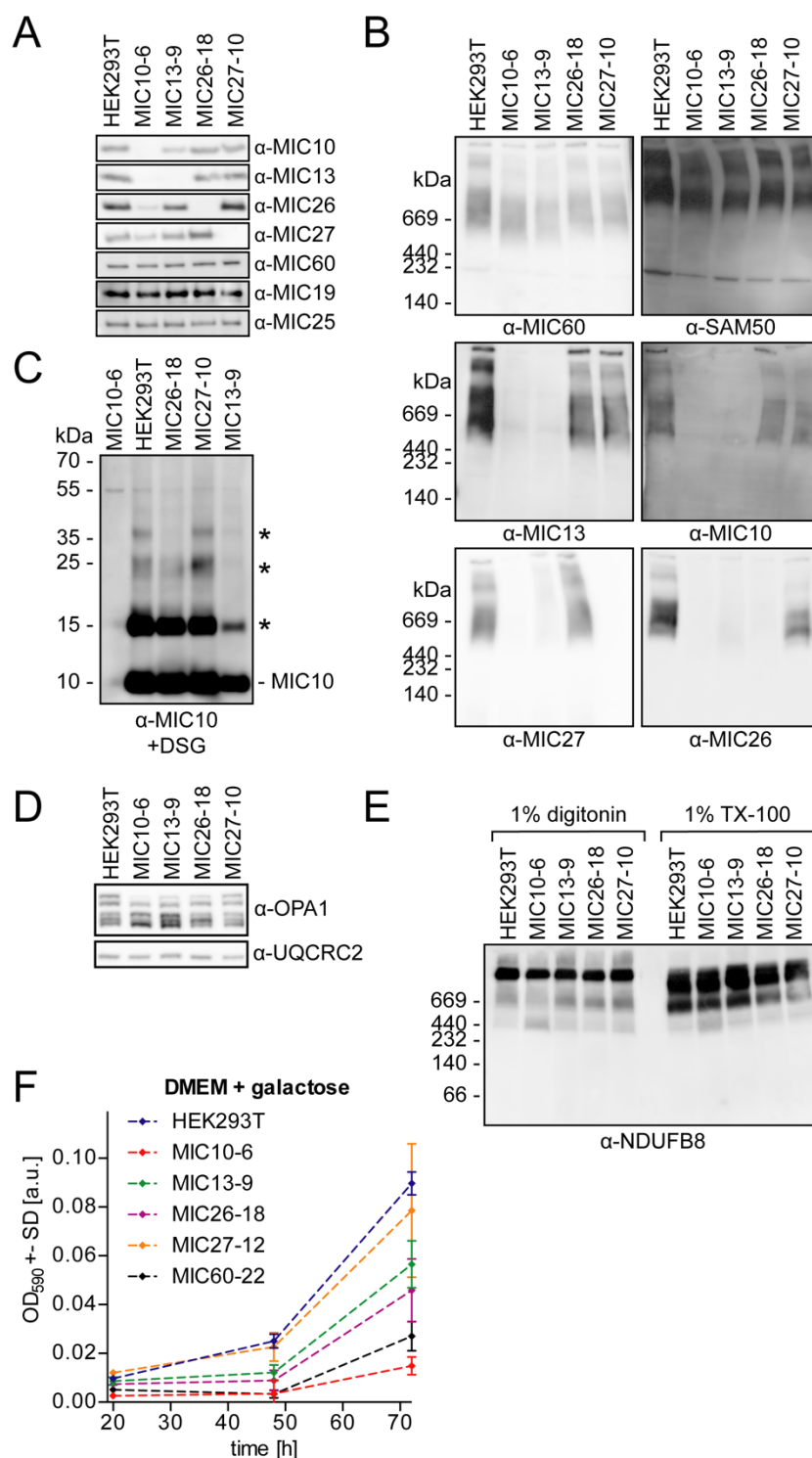


Figure 10 Organisation of the MIC10 subcomplex in human mitochondria

All MIC10-subcomplex subunits were targeted by CRISPR/Cas9 genome editing and mitochondria isolated from the resulting clonal cell lines were analysed by immunoblotting with antibodies directed against MICOS subunits. B. BN-PAGE analysis of the MICOS complex in mitochondria from various MICOS knockout cell lines lysed in digitonin. C. Mitochondria from MIC10 subcomplex knockout cell lines were chemically crosslinked with DSG and analysed by SDS-PAGE and immunoblotting to assess MIC10 oligomerisation. Asterisks indicate putative MIC10 oligomer bands. D. OPA1 processing in MIC10 subcomplex knockout cell lines. E. Complex I supercomplex stability was assessed by BN-PAGE of mitochondria lysed in digitonin or Triton X-100. F. Growth of MICOS knockout cell lines in galactose-containing media as assessed by crystal violet stain, error bars indicate standard deviation from technical replicates.

crosslinking. In contrast, similar or slightly increased amounts of oligomeric MIC10 species could be detected in MIC27-deficient mitochondria. These data further support a hierarchical organisation of the MIC10 sub-complex and show that MIC26 and MIC27, despite not affecting the stability of MIC10/13 complexes (Figure 10b), potentially influence the oligomeric assembly of MIC10 (Figure 10c). We therefore tested how the knockout of MIC13, MIC26 and MIC27 affects OPA1 processing, respiratory chain supercomplex stability as well as cellular growth, which were all found to be impaired by knockout of the MIC10 core subunit (chapter 6.5). As previously described, MIC10 KO led to an increase in short forms and the loss of longer forms of OPA1 (Figure 10d). A similar, albeit weaker effect could be observed in MIC13 KO and MIC26 KO mitochondria, while the OPA1 long/short ratio was not affected in MIC27-deficient mitochondria (Figure 10d). A destabilisation of complex I containing supercomplexes could only be observed in MIC10-deficient mitochondria, while all other knockout cell lines showed unaltered supercomplexes (Figure 10e). In agreement with these observations, the most severe effect on cell growth in galactose containing media was observed in MIC10 KO cells, while MIC13 and MIC26 KO cells showed an intermediary phenotype (Figure 10f). In line with the biochemical data described above, MIC27 KO did not notably influence cell growth.

In summary, human MIC10 forms oligomeric assemblies which are influenced by accessory proteins of the complex. MIC13 is the second most important subunit of the MIC10 module, since its knockout affects MIC10 protein levels and complex stability. MIC26 appears to stabilize MIC10 oligomers and its absence affects respiratory cell growth, while MIC27 knockout does not notably affect the assembly of the MIC10 module.

6.7. The human MICOS/MIB complex and DNAJC11 spatially coordinate β -barrel biogenesis in the outer mitochondrial membrane

Some of the data described in this chapter will be communicated in the following manuscript:

Wollweber F, Noll K, Schorr S, Zerbes RM, Ryan MT, Liu F, van der Laan M & von der Malsburg A
MICOS and DNAJC11 spatially coordinate mitochondrial β -barrel protein biogenesis. *In preparation.*

With the exception of Figure 11b and g of this thesis, all experiments described here were performed by F.W.

As described in chapter 6.4, knockout of MIC60, but not MIC10, leads to a noticeable reduction of SAM50, which is the major subunit of the mitochondrial outer membrane sorting and assembly (SAM) complex that mediates the assembly of β -barrel proteins. Furthermore, SAM50 appears to exclusively co-migrate with MIB complex components on native gels, even upon solubilisation with harsh detergents. To further verify this interaction, mitochondria from HEK293T and MIC10 KO cells were analysed by two-dimensional BN/SDS-PAGE (Figure 11a). SAM50 co-migrated with the MICOS complex subunit MIC13 but formed a stable complex of similar size even in mitochondria lacking the MIC10 subcomplex. On a one-dimensional BN-PAGE, no stable SAM50-containing complex could be detected in mitochondria isolated from cells lacking MIC60 (Figure 11a, chapter 6.4). We hypothesised that the absence of a stable SAM complex and the strong reduction of SAM50 protein levels in MIC60-deficient cells would influence the efficiency of β -barrel import and assembly into the outer membrane. To test this hypothesis, the β -barrel precursor VDAC was synthesised in reticulocyte lysate in the presence of [35 S] methionine and then incubated with mitochondria isolated from HEK293T cell lines lacking MIC10 or MIC60. The import reaction was stopped by transferring samples on ice and the assembly of radiolabelled VDAC was analysed by BN-PAGE followed by autoradiography. VDAC efficiently assembled into 400 kDa protein complexes in HEK293T and MIC10 KO samples in a time-dependent manner, while the assembly was markedly reduced in mitochondria lacking MIC60 (Figure 11b). This import and assembly defect did however not result in reduced levels of β -barrel protein complexes under steady-state conditions (Figure 11c).

We next asked whether the connection between outer membrane protein assembly and crista junction maintenance exists purely as structural necessity, or whether the MIB complex is actively involved in β -barrel assembly. The J-protein DNAJC11 has been described as MICOS interacting protein (Xie et al, 2007) and could be efficiently co-precipitated in MIC10^{FLAG} co-IP experiments (chapter 6.4). To test whether it is a *bona fide* subunit of the MIB complex, mitochondria from MIC10 and MIC60-deficient cell lines as well as the corresponding parental HEK293T cells were analysed by BN-PAGE and immunoblotting with antibodies against DNAJC11, SAM50 and MICOS subunits. DNAJC11 formed several protein complexes, two of which co-migrated with the MIB complex (Figure 11d).

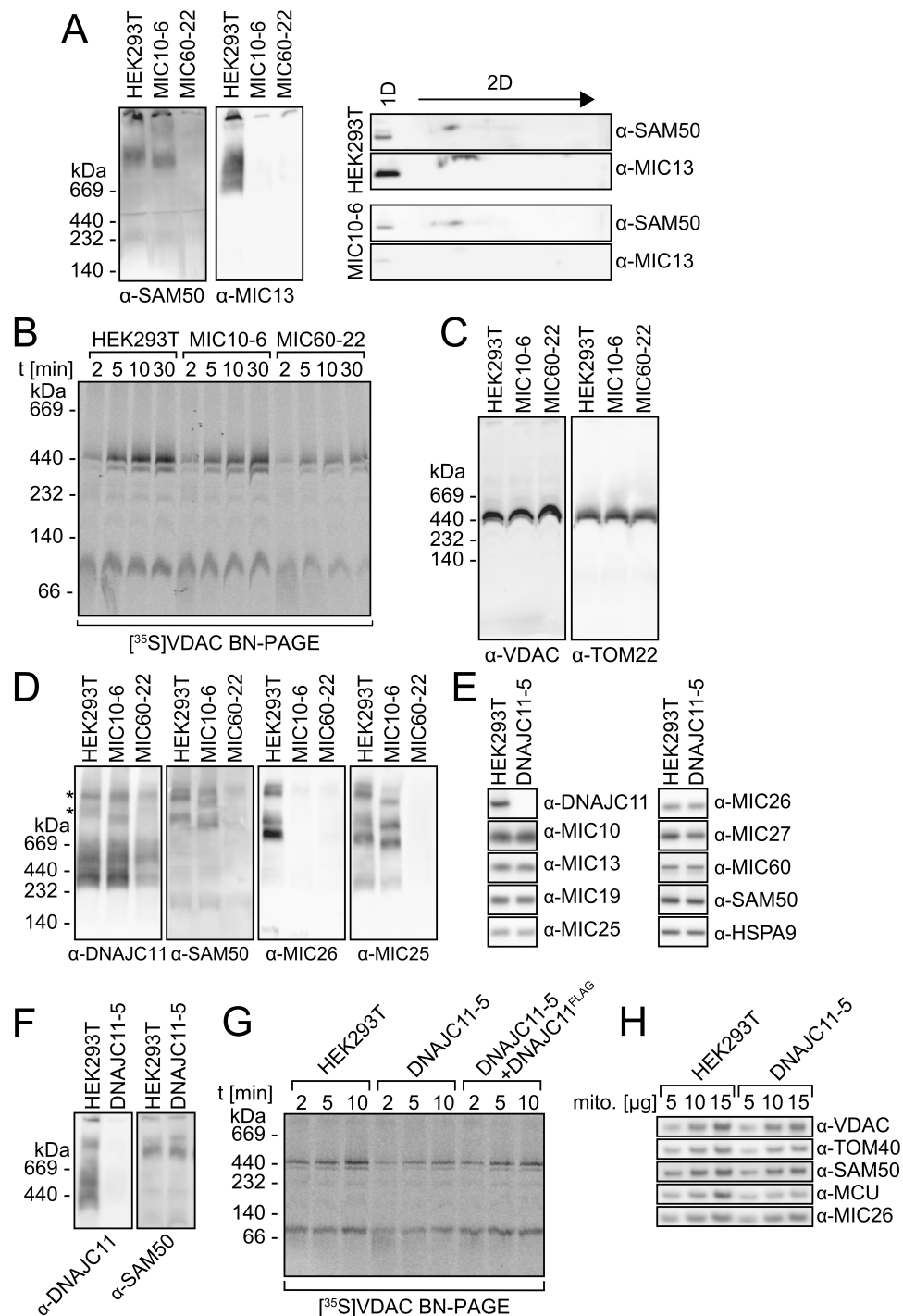


Figure 11 The MIB complex and DNAJC11 spatially coordinate β -barrel biogenesis

A. Two-dimensional BN/SDS-PAGE analysis of SAM50 and MIC13 in HEK293T and MIC10-deficient mitochondria. B. In organello import and assembly assay of radiolabelled VDAC. Mitochondria were incubated with *in vitro* translated [³⁵S]-labelled VDAC for the indicated time points and lysed in digitonin, followed by BN-PAGE and autoradiography. C. BN-PAGE analysis of VDAC and TOM complexes in MIC10 and MIC60-deficient mitochondria. D. BN-PAGE analysis of MIC10 and MIC60-deficient mitochondria using antibodies against MIB complex subunits and DNAJC11. Asterisks show DNAJC11 bands co-migrating with MIB complexes. E. DNAJC11 was targeted by CRISPR/Cas9. The clonal DNAJC11-5 cell line, lacking the DNAJC11 protein, was analysed by SDS-PAGE and immunoblotting of isolated mitochondria. F. SAM complex stability in DNAJC11-deficient cells as assessed by BN-PAGE and immunoblotting. G. In organello assembly of radiolabelled VDAC as described in B using DNAJC11-deficient mitochondria and mitochondria from DNAJC11-5 cells transduced with DNAJC11^{FLAG}. H. Protein levels of β -barrel proteins and the inner membrane carrier protein MCU (mitochondrial calcium uniporter) in mitochondria from HEK293T cells or DNAJC11-5 cells.

B. +G.: import and assembly assays performed together with Katja Noll (Saarland University). 63

These bands migrated faster in mitochondria lacking MIC10, which further supports an association with MICOS/MIB. In addition, several smaller complexes could be detected, which were reduced in MIC60-deficient mitochondria (Figure 11d). We hypothesised that DNAJC11 is involved in β -barrel import since it closely associates with the MIB complex and possesses a J-domain for the interaction with proteins of the Hsp70 family, which are known to chaperone β -barrel precursor proteins in the cytosol (Jores et al, 2018). To test this hypothesis, DNAJC11 was targeted by CRISPR/Cas9 with a single guide RNA and the knock-out was validated by western blotting (Figure 11e). Importantly, the abundance of MICOS subunits and SAM50 were unaffected by DNAJC11 knockout (Figure 11e). In line with this finding, SAM50 complex stability was unaltered, indicating that DNAJC11 does not affect the assembly or stability of the MIB complex (Figure 11f). We next assessed the import and assembly of radiolabelled VDAC into isolated mitochondria. As observed for MIC60-deficient mitochondria, DNAJC11 knockout drastically reduced the efficiency of VDAC assembly and import and this phenotype was partially rescued by retroviral expression of DNAJC11^{FLAG} (Figure 11g). These data suggest that DNAJC11 specifically enhances the efficiency of β -barrel protein biogenesis without affecting the integrity of the MIB complex. To test whether this import and assembly defect affects the amount of β -barrel proteins in mitochondria we analysed mitochondria isolated from DNAJC11 knockout mitochondria by SDS-PAGE and immunoblotting. The steady state protein levels of VDAC and SAM50 were not markedly reduced in mitochondria isolated from DNAJC11 KO cells, while a minor reduction of TOM40 levels could be observed (Figure 11h). The human MICOS complex has recently been found to interact with the TIM22 machinery of the inner membrane, which mediates the assembly of inner membrane carrier proteins. We hypothesised that DNAJC11 is not only involved in outer membrane biogenesis, but also spatially coordinates the entry of hydrophobic inner membrane proteins into mitochondria. Interestingly, we observed a strong reduction of the mitochondrial calcium uniporter (MCU) in DNAJC11 KO mitochondria (Figure 11h), which likely uses the carrier pathway for its assembly. This observation indicates that the substrate spectrum of DNAJC11 might not be limited to β -barrel proteins of the outer membrane, but potentially includes hydrophobic proteins of the inner mitochondrial membrane.

In summary, the MICOS complex forms a stable connection with the outer membrane SAM complex. Stability of SAM depends on an intact MIC60 subcomplex and MIC60 knockout affects SAM functionality. This connection appears to be of functional importance, since MICOS recruits facilitators of mitochondrial protein import, in particular the J-protein DNAJC11, to defined sub-organellar sites, which enhances the efficiency of β -barrel assembly. Preliminary data indicates that MICOS/DNAJC11-mediated spatial coordination of protein biogenesis affects hydrophobic proteins of the outer and the inner mitochondrial membrane.

6.8. Assembly mechanism of the cristae-shaping dymanin-like GTPase

Mgm1

The data described in this chapter have been published in:

Faelber K*, Dietrich L*, Noel JK#, **Wollweber F#**, Pfitzner A-K#, Mühleip A, Sánchez R, Kudryashev M, Chiaruttini N, Lilie H, Schlegel J, Rosenbaum E, Hessenberger M, Matthaeus C, Kunz S, von der Malsburg A, Noé F, Roux A, van der Laan M, Kühlbrandt W & Daumke O (2019) Structure and assembly of the mitochondrial membrane remodelling GTPase Mgm1. *Nature* 571: 429–433

(*# equal contribution)

With the exception of Figure 12a-e and Figure 14c-I of this thesis, all experiments described here were performed by F.W.

The remodelling of mitochondrial ultrastructure in response to cellular metabolic demands or during cell fate decisions such as apoptosis appears to be of pivotal importance for cellular physiology in health and disease, but the molecular basis of these rearrangements is unclear. The two major cristae shaping protein complexes, MICOS and ATP synthase dimers, stabilise the inner membrane at crista junctions and tips, respectively, but their role in the dynamic remodelling of cristae membranes remains elusive. However, many studies implicated the dynamin-like GTPase Mgm1/OPA1 in this process (Meeusen et al, 2006; Patten et al, 2014) and suggested that OPA1 coordinates with other cristae shaping proteins to orchestrate cristae remodelling (Glytsou et al, 2016; Quintana-Cabrera et al, 2018). Proteins of the Mgm1/OPA1 family are required for the fusion of the mitochondrial inner membrane and yeast Mgm1 is essential for the maintenance of the mitochondrial genome (Jones & Fangman, 1992), while human OPA1 has been implicated in the pathogenesis of optical atrophy (Alexander et al, 2000; Delettre et al, 2000). In both species, short soluble and long membrane-bound isoforms can be found in mitochondria, which are formed by proteolytic processing and, in metazoan cells, differential splicing (recently reviewed in Del Dotto et al, 2018). Yeast Mgm1 has been implicated in the biogenesis of lamellar cristae by partial inner membrane fusion (Harner et al, 2016). In mammalian cells, OPA1 assembly was found to be highly dynamic and altered during e.g. apoptotic cristae opening (Frezza et al, 2006) and as a consequence of altered metabolic circumstances (Patten et al, 2014). It is currently unknown how OPA1/Mgm1 assemblies can exert such diverse functions, ranging from inner membrane fusion to the rapid membrane remodelling observed during apoptosis. To elucidate the assembly mechanism, the study summarised in this chapter combined crystal and cryo-electron tomography structures of a fungal Mgm1 protein with *in vivo* data obtained in yeast. This chapter focusses on *in vivo* experiments to validate the structural findings and highlights the most significant findings obtained *in vitro*. All supporting information can be found in Faelber et al, 2019.

The crystal structure of soluble Mgm1 from the thermophilic fungus *Chaetomium thermophilum* (Figure 12a) was solved by Katja Faelber (laboratory of Oliver Daumke, MDC Berlin, Germany). Based on the structure and homology to other dymanin family members,

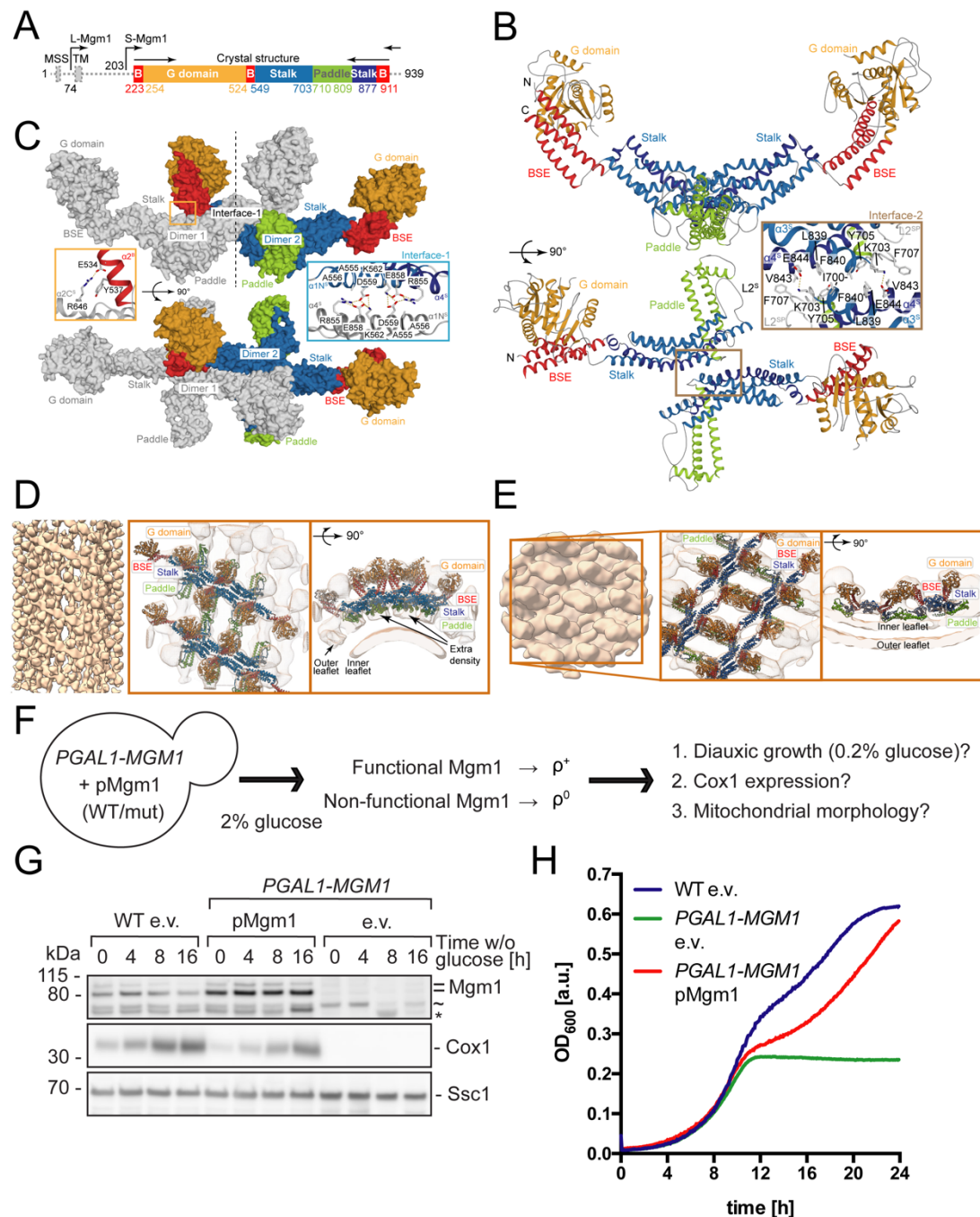


Figure 12 Structure of Mgm1 (as published in Faelber et al., 2019).

Overview of Mgm1 domain architecture from *Chaetomium thermophilus*. The crystallised fragment is displayed in colour. MSS = mitochondrial signal sequence; TM = transmembrane segment; L/S-Mgm1 = long/short isoform. B. Crystal structure of the Mgm1 dimer, domains are coloured as in A. The dimer interface of two opposing stalks is highlighted. C. Structure of the Mgm1 tetramer as seen in the crystal lattice, interface 1 and the BSE-stalk contact are highlighted. D. Cryo-electron tomography analysis of a helical lattice of Mgm1 molecules at the outside of lipid tubules. E. Cryo-ET reconstruction of Mgm1 filaments on the inside of lipid tubules. F. Schematic of a yeast assay to test for Mgm1 loss-of-function mutations. The galactose-inducible/glucose-repressed *GAL1* promoter was inserted upstream of the *MGM1* ORF and mutant Mgm1 was expressed from a plasmid. After growth on glucose, expression of non-functional Mgm1 variants leads to a loss of mitochondrial DNA, which can be assessed by testing diauxic growth, expression of mitochondrially encoded Cox1 and analysis of mitochondrial morphology. G. *PGAL1-MGM1* yeast +/- pMgm1 was cultured on ethanol-containing media for the indicated time points and the expression of plasmid-borne Mgm1, mitochondrially encoded Cox1 and mitochondrial Hsp70 (Ssc1, loading control), was analysed by Western blotting (= l/s Mgm1, ~ unspecific band, * Mgm1 degradation product). H. The ability of *PGAL1-MGM1* +/- pMgm1 for diauxic growth was tested by a growth assay in liquid media containing 0.2% glucose.

A.-C.: Crystal structure solved by Katja Faelber, MDC Berlin; D.-E.: Cryo-ET data acquired by Lea Dietrich, MPI Frankfurt.

four domains could be identified, including a G domain, a bundle signalling element (BSE), a stalk and an Mgm1 specific domain, termed paddle (Figure 12a,b). The paddle domain appeared to be important for membrane binding of the protein and the tubulation of liposomes. The crystal structure also revealed a dimeric arrangement of Mgm1 molecules (Figure 12b). Dimerisation was mediated by an interface formed by a hydrophobic patch of the stalk domains (hereafter termed interface 2), resulting in a V-like shape (Figure 12b). Mutations that disrupt interface 2 not only rendered the protein monomeric, but also led to decreased membrane binding and tubulation of liposomes. Two dimers additionally appeared to form tetramers in the crystal structure via two interfaces, a distinct stalk-stalk contact termed interface 1 as well as a BSE-stalk contact (Figure 12c). In contrast to interface 2 mutants, tetramer interface mutants did not affect membrane binding or tubulation *in vitro*. To further understand the assembly mechanism, the structure of membrane-bound Mgm1 was analysed by cryo-electron tomography and subtomogram averaging (Figure 12d,e; cryo-ET data was acquired by Lea Dietrich in the laboratory of Werner Kühlbrandt, MPI Biophysics, Frankfurt, Germany). Mgm1 deformed liposomes, resulting in the formation of Mgm1-coated membrane tubules, which could be analysed by cryo-ET (Figure 12d). Tetrameric Mgm1 could be fitted into the subtomogram averages, revealing that the paddle domain was in close apposition to the membrane. The Mgm1 coat assembled in a left-handed helical lattice, with contact sites between tetramers formed by interfaces 1 and 2. Interestingly, stable Mgm1 assemblies could also be detected on the inside of lipid tubes (Figure 12e). This arrangement resembles the membrane curvature found in cristae membranes. The subtomogram averages of this regular assembly revealed prominent differences between external and internal Mgm1 lattices. While external assemblies assembled through interface 1 contacts between tetramers, the internal Mgm1 assembly was mediated by contacts in the BSE and stalk regions and a contact by G-domains (Figure 12e). In summary, crystallographic and cryo-ET data suggests that Mgm1 assembly into dimers, tetramers and helical assemblies can occur on the inside and outside of lipid tubes, which possibly helps to explain the diverse array of functions in inner membrane fusion and cristae remodelling.

To test whether the dimer and tetramer interfaces observed in the crystal structure and cryo-ET data affect Mgm1 function *in vivo*, we developed a loss-of-function assay in the yeast *Saccharomyces cerevisiae* which is based on the observation that yeast cells lacking functional Mgm1 rapidly lose the mitochondrial genome (i.e. become ρ^0 ; Figure 12f). To this end, a galactose-inducible and glucose-repressed *GALI* promoter was inserted upstream of the *MGMI* open reading frame in the yeast genome. Subsequently, the strain was transformed with a plasmid containing wild-type Mgm1 or the empty vector and grown on media containing glucose. When glucose was then exchanged for a respiratory carbon source, plasmid-based Mgm1 expression remained constant for several hours, while Mgm1 could not be detected in the strain containing only the empty plasmid (Figure 12g). Importantly, the

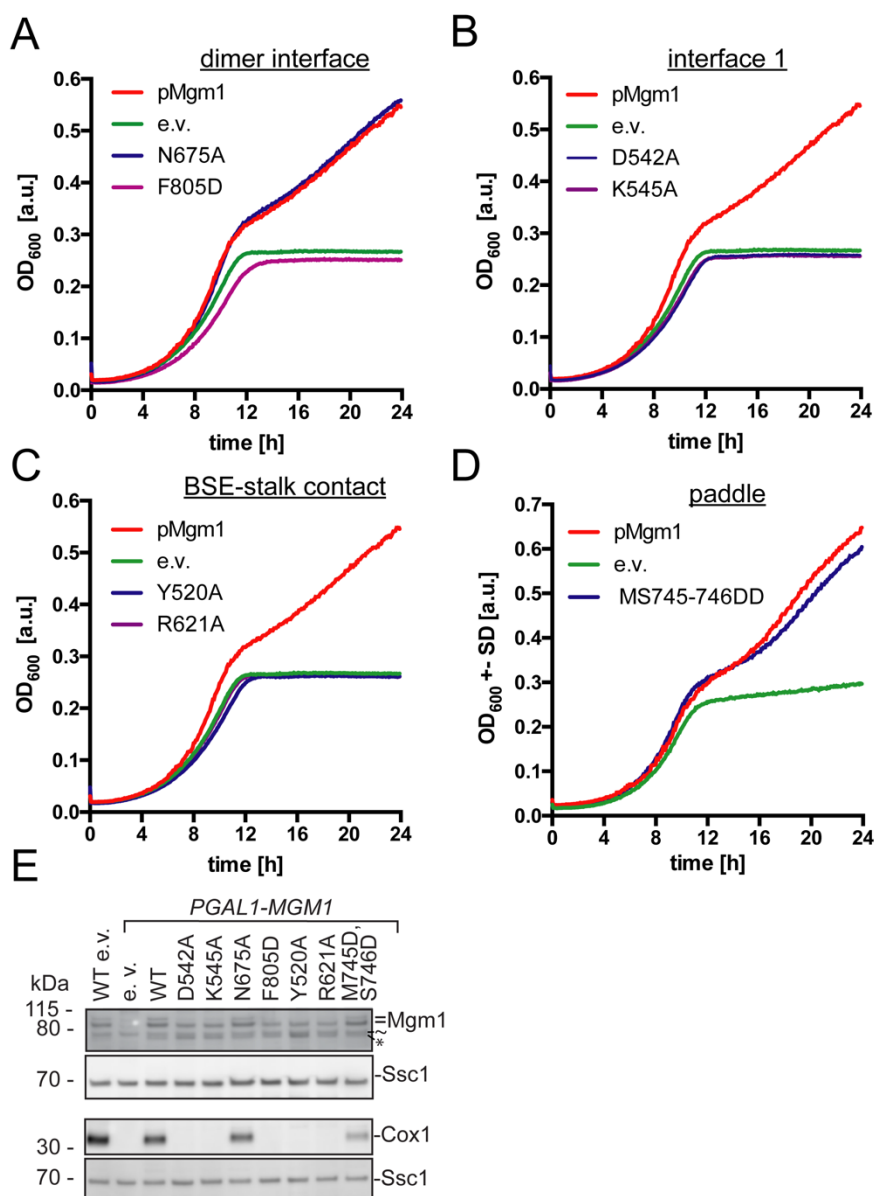


Figure 13 Analysis of Mgm1 dimer and tetramer interface mutants.

A.-D. Selected mutants of Mgm1 were expressed from a plasmid in the *PGAL1-MGM1* yeast strain and then grown in media containing 2% glucose to shut off expression of the chromosomal locus. Their diauxic growth behaviour was then analysed by a growth assay in liquid media containing 0.2% glucose to identify loss-of-function mutations that lead to a loss of respiratory growth competence, indicating loss of mitochondrial DNA (representative growth curves). E. Mitochondria isolated from *PGAL1-MGM1* mutant strains expressing plasmid-borne Mgm1 mutants on glucose-containing media were analysed by Western blotting to detect expression of mutant Mgm1 and assess loss of mitochondrial DNA as indicated by the expression of mtDNA-encoded Cox1.

switch to a respiratory carbon source led to a pronounced increase of mitochondrially encoded Cox1, indicating a stimulation of mitochondrial biogenesis. This could not be observed in the absence of plasmid-borne Mgm1, indicating an irreversible loss of mitochondrial DNA (Figure 12g). In addition, the diauxic growth of *PGAL1-MGM1* strains containing or lacking pMgm1 was compared with a wild-type strain (Figure 12e). While all strains grew similarly during the glycolytic growth phase, no growth could be observed after depletion of glucose in

the shutdown strain transformed with the empty vector (Figure 12e). This apparent loss of mitochondrial function was rescued by transformation with pMgm1. While plasmid-borne expression did not fully restore the growth to wild-type levels, exponential growth under respiratory conditions could be observed (Figure 12e). Next, mutations were introduced into the dimer and tetramer interfaces and yeast mutants were screened for their ability to grow after glucose depletion and the presence of Cox1 in mitochondria after growth on glucose (Figure 13a-e). All mutants were expressed at levels similar to the wild-type protein (Figure 13e). The F805D mutation in the dimer interface led to a complete loss of function, whereas a milder N675A mutation did not affect diauxic growth and only led to mildly reduced levels of Cox1 (Figure 13a, e). All tested mutations in tetramer interfaces resulted in a complete loss of function (Figure 13b, c, e). These data clearly demonstrate that dimer- and tetramerization are required for Mgm1 function *in vivo*. We next analysed the paddle domain, which was observed to affect membrane binding *in vitro* and is in close proximity to the membrane. A double point mutation (M745D,S746D), which abolished membrane binding *in vitro*, did not lead to a loss of respiratory growth competence (Figure 13c). However, Cox1 expression in mitochondria was strongly decreased (Figure 13e), indicating a partial loss of function which results in a reduced number of mitochondrial nucleoids (ρ^- phenotype). While the loss-of-function assay allowed for the direct determination of loss-of-function effects, it does not permit a further investigation of Mgm1 function on membrane morphology. Cells lacking mitochondrial DNA also lack cristae and show a fragmented mitochondrial network, which are two major phenotypes associated with Mgm1/OPA1 dysfunction. We hypothesised that Mgm1 tetramer interface mutants exert dominant-negative phenotypes when expressed in wild-type cells by disturbing the regular assembly of wild-type Mgm1 molecules. To test this hypothesis, wild-type yeast was transformed with plasmids encoding Mgm1 dimer or tetramer interface mutants and respiratory growth competence was assessed by measuring the growth in media containing glycerol. While expression of wild-type Mgm1 or Mgm1 interface 2 (dimer interface) mutants did not affect respiratory growth, all tetramer interface mutants exerted a strong dominant-negative effect (Figure 14a). In particular, Mgm1-Y520A, carrying a mutation in the BSE-stalk contact, almost abolished respiratory growth when expressed in wild-type yeast. These cells, however, retained a significant amount of mtDNA, since only a slight decrease in Cox1 levels could be observed (Figure 14b). This dominant-negative phenotype, which only slightly affects mitochondrial DNA maintenance, enabled a thorough analysis of mitochondrial morphology and ultrastructure. We first analysed mitochondrial network morphology and nucleoid abundance by staining yeast cells grown in respiratory media with the mitochondrial marker DiOC₆ and the DNA-staining agent DAPI. In cells expressing Mgm1-Y520A only a small number of cells retained a tubular mitochondrial network (Figure 14c, d). Furthermore, we frequently observed cells lacking mitochondrial nucleoids. To understand how Mgm1-Y520A affects cristae architecture, yeast cells were analysed by electron

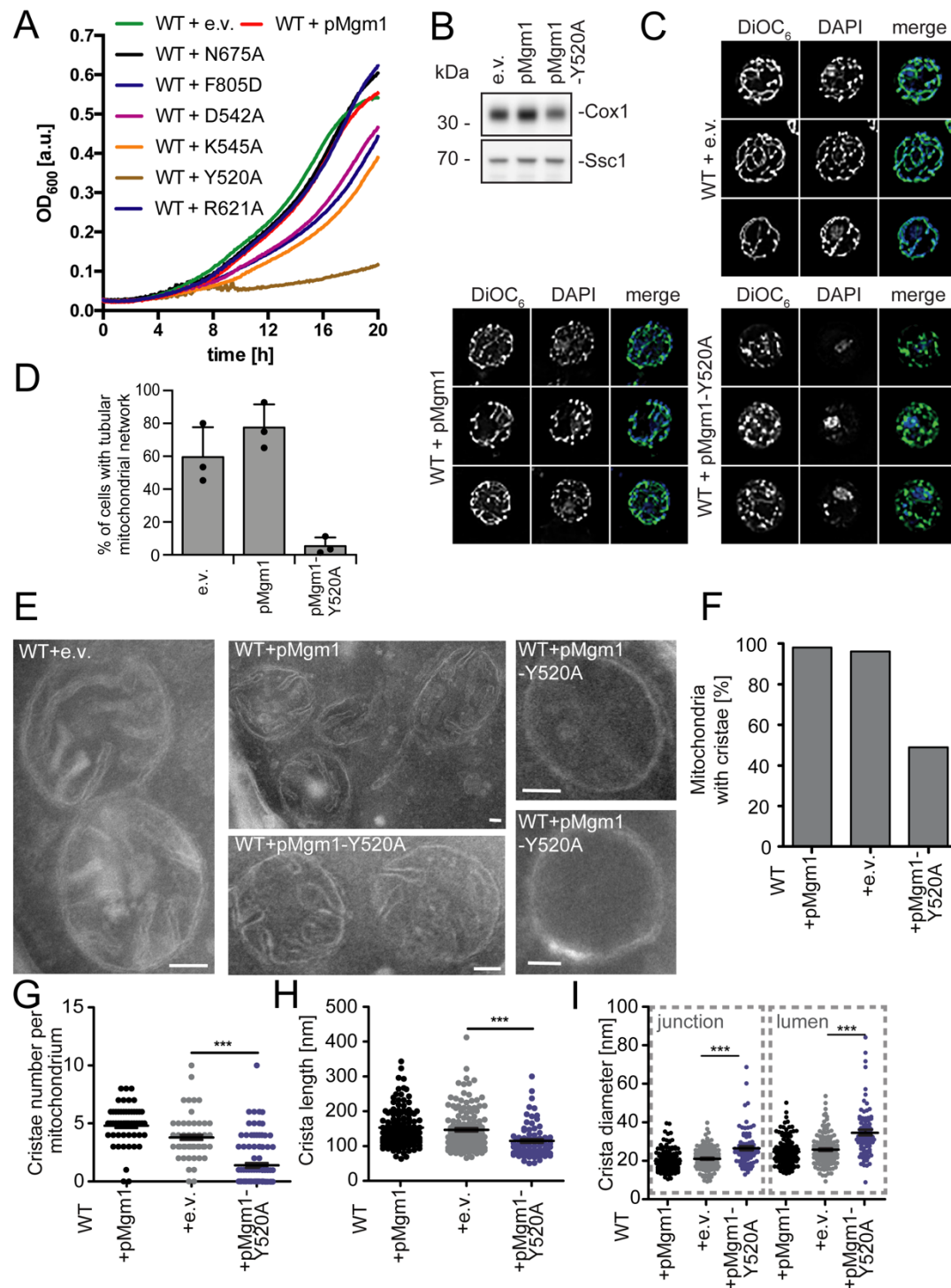


Figure 14 Mgm1 tetramer mutants exert strong dominant-negative phenotypes

A. Mgm1 variants harbouring mutations in the dimer or tetramer interfaces were expressed in wild-type yeast to identify dominant-negative effects. Respiratory growth was analysed in media containing 3% glycerol as carbon source. B. Cox1 expression as a marker for mitochondrial DNA was analysed by immunoblotting of mitochondria from wild-type cells harbouring the empty vector, pMgm1 or pMgm1-Y520A. C. Mitochondrial morphology in the indicated yeast strains was analysed by DiOC₆/DAPI staining of yeast cells and fluorescence microscopy. Image dimension: 7.5x7.5µm. D. Quantification of cells analysed in C with tubular mitochondrial network. E. Representative transmission electron micrographs of yeast strains expressing wild-type Mgm1 or Mgm1-Y520A. Scale bar: 70 nm. F-I: Quantification of cristae morphology parameters in electron micrographs. ***P<0.0001, Mann-Whitney U-test (two-sided, 95% confidence interval).

C.-D.: Microscopy data acquired and analysed by Alexander von der Malsburg, Saarland University; F.-I.: EM data acquired and analysed by Severine Kunz and Claudia Matthaes, MDC Berlin.

microscopy (Figure 14e). In line with a partial loss of mitochondrial DNA, expression of Mgm1-Y520A led to a decreased number of mitochondria containing cristae, which could not be observed after expression of wild-type Mgm1 (Figure 14f). Cristae number (Figure 14g) and cristae length (Figure 14h) was also significantly reduced in Mgm1-Y520A, while the cristae diameter at the crista junction and in the crista lumen was increased (Figure 14i). Importantly, cristae shape was not significantly altered by expression of wild-type Mgm1. These data demonstrate that alterations in the tetrameric assembly of Mgm1 specifically disturb mitochondrial cristae shape, in line with the structural evidence obtained by crystallography and cryo-electron tomography.

In summary, the regular assembly of Mgm1 molecules into dimers, tetramers and helices can occur on the inside and outside of membranes. Mutations in the dimer and tetramer interfaces abolish Mgm1 function *in vivo*. Additionally, Mgm1 alleles that carry mutations in the tetramer interface exert strong dominant-negative phenotypes, which leads to a drastic alteration of cristae structure.

7. Discussion

7.1. MICOS core subunits are required for efficient adaptation to respiratory metabolism in yeast

The MICOS core subunits Mic10 and Mic60 are both required for the maintenance of crista junction structures and both subunits possess membrane-shaping activities, albeit by different mechanisms. Whereas Mic60 influences membrane curvature via lipid binding motifs in its C-terminal domain (Hessenberger et al, 2017; Tarasenko et al, 2017), Mic10 forms an oligomeric protein scaffold within the membrane to stabilise crista junctions (Barbot et al, 2015; Bohnert et al, 2015). Since both core subunits are inducing or stabilising membrane curvature, their activity likely has to be spatiotemporally regulated. A major hypothesis in this thesis was that this requires a close coordination with cellular metabolic demands. This idea is well supported by the observation that not only deletion but also overexpression of Mic10 or Mic60 led to a delayed diauxic shift in yeast (Figure 3). The diauxic shift requires major transcriptional reprogramming (DeRisi et al, 1997), a reorganisation of the mitochondrial proteome (Ohlmeier et al, 2004; Morgenstern et al, 2017; Di Bartolomeo et al, 2020), and an increase in mitochondrial and inner membrane abundance (Egner et al, 2002; Di Bartolomeo et al, 2020). Furthermore, it likely requires signalling via the ER stress pathway (Tran et al, 2019), in a similar manner to the adaptation of mammalian cells to glucose depletion (Balsa et al, 2019). A recent quantitative analysis of the mitochondrial proteome during the diauxic shift (Di Bartolomeo et al, 2020) showed that proteins of the respiratory chain as well as mitochondrial cristae organising proteins, including MICOS and Mgm1, are upregulated during the diauxic shift, in line with the data obtained here. These data demonstrate that respiratory chain expression is coordinated with the formation of mitochondrial cristae.

The defect observed in yeast mutants overexpressing Mic10 or Mic60 during the diauxic shift can possibly be attributed to excessive and unregulated assembly of Mic10 oligomers with a subsequent expansion of crista junctions and deformed cristae membranes (Bohnert et al, 2015), or the generation of membrane curvature within cristae by Mic60 (Rabl et al, 2009). Importantly, overexpression and deletion of Mic10 also caused delayed mitochondrial inner membrane biogenesis as assessed by the protein levels of various cristae proteins (Figure 4). These observations clearly demonstrate that regulatory mechanisms must spatially restrict or stimulate Mic10 and Mic60-mediated membrane bending to ensure efficient cristae biogenesis and maintenance. Interestingly, deletion of accessory MICOS subunits did not cause a pronounced adaptation defect. Since all MICOS deletion mutants with the exception of *mic26Δ* show detached cristae and a drastically reduced number of crista junctions in mitochondria (Harner et al, 2011; Hoppins et al, 2011; von der Malsburg et al, 2011), the observed disturbance of the diauxic growth behaviour in MICOS core subunit mutants cannot be explained by dysfunctional crista junction architecture alone. We also observed that an

oligomerisation deficient mutant of Mic10 (Mic10^{G76A}), which phenocopies the *mic10Δ* crista junction phenotype (Bohnert et al, 2015), does not display a diauxic growth phenotype (Figure 5e). This finding provides additional evidence for the hypothesis that the stability of crista junctions is dispensable for diauxic growth. It is therefore tempting to speculate that Mic10 and Mic60 possess additional functions which are necessary for mitochondrial biogenesis during metabolic adaptation (see also chapter 7.2 and 7.5). It remains to be elucidated, whether deletion and overexpression of Mic10 and Mic60 affects distinct mitochondrial biogenesis pathways. This question could be addressed using a comparative proteomics approach with high temporal resolution during the diauxic shift (Di Bartolomeo et al, 2020) and by analysing the effect of partial loss of function alleles (chapter 7.2).

7.2. The Mic10-ATP synthase interaction is crucial for metabolic adaptation

Since Mic10 and Mic60 are the only MICOS subunits whose absence causes a pronounced growth defect during diauxic shift experiments, they likely possess functions in mitochondrial biogenesis processes which are not related to the stabilisation of crista junction architecture alone. Notably, both subunits have been found to interact with non-MICOS proteins. While Mic60 interacts with various proteins of the outer membrane to facilitate protein biogenesis (Xie et al, 2007; Harner et al, 2011; Hoppins et al, 2011; von der Malsburg et al, 2011; Alkhaja et al, 2012; Bohnert et al, 2012; Ott et al, 2012; Friedman et al, 2015; Tang et al, 2020), Mic10 has been found to interact with the ATP synthase to modulate its assembly into high molecular weight dimer rows (Eydt et al, 2017; Rampelt et al, 2017). These ATP synthase super-assemblies are required for the maintenance of cristae architecture and possibly help to bioenergetically fine-tune cristae compartments by creating local proton sinks (recently reviewed in Kühlbrandt, 2019). To genetically dissect the function of MICOS-bound and ATP-synthase bound Mic10, we directly fused Mic10 to subunit e (Atp21) of the ATP synthase (Figure 5), which mediates its dimerisation (Arnold et al, 1998; Donzeau et al, 2000; Brunner et al, 2002; Everard-Gigot et al, 2005) and can be directly crosslinked to Mic10 in wild-type mitochondria (Eydt et al, 2017; Rampelt et al, 2017). This fusion protein did not form MICOS-bound oligomers and could be co-purified with Mic60 only in very minor amounts, suggesting a loss of function at the MICOS complex. In agreement with this observation, mitochondrial crista junction architecture was disturbed in *mic10Δ* cells expressing the fusion construct as assessed by outer membrane rupture after hypoosmotic swelling. Surprisingly, these cells regained the ability to efficiently adapt during the diauxic shift. This serendipitous finding thus demonstrates that Mic10 at the ATP synthase, rather than its canonical function as a protein scaffold at crista junctions, is essential for the efficient adaptation of mitochondrial ultrastructure during the diauxic shift. This observation confirms that the recently described effect of Mic10 on supra-molecular ATP synthase assembly (Eydt et al, 2017; Rampelt et al, 2017) is physiologically significant. It has been proposed that

MICOS directly interacts with ATP synthase dimers at the crista junctions via Mic10 (Eydt et al, 2017). Our observation that the Atp21-Mic10 fusion construct does not rescue MICOS integrity and crista junction stability but rescues the metabolic adaptability of *mic10Δ* cells rather suggests a MICOS-independent role of Mic10. However, it remains unclear how Mic10 influences ATP synthase oligomerisation. Furthermore, it remains to be elucidated whether this effect is beneficial for the maintenance of mitochondrial cristae shape or whether it can support the biogenesis of cristae, which might be catalysed by ATP synthase-mediated local membrane bending (Harner et al, 2016; Anselmi et al, 2018; Blum et al, 2019). These questions could be addressed by studying the membrane deforming properties of ATP synthase reconstituted together with Mic10 in artificial membrane systems. A similar approach has previously been used to study the influence of OPA1 on ATP synthase assembly (Quintana-Cabrera et al, 2018).

7.3. *Mic10 oligomerisation is regulated by Mic26-27 antagonism and cardiolipin*

Mic10 oligomerisation is one of the central mechanisms to stabilise crista junctions. Using chemical crosslinking we obtained evidence for MIC10 oligomerisation in human cells (Figure 10c), which suggests that this assembly mode is an evolutionarily conserved feature of MICOS. Mic10 has also been found to interact with dimeric species of the F₁F₀-ATP synthase to modulate their oligomerisation into dimer rows (Eydt et al, 2017; Rampelt et al, 2017). Mic10 therefore affects at least two major cristae shaping pathways, leading to the necessity to modulate its activity and control its localisation within the inner mitochondrial membrane. Mic10 is linked to the MIC60 sub-complex by the accessory MICOS subunit Mic12 (QIL1/MIC13 in humans) (Guarani et al, 2015, 2016; Anand et al, 2016; Zerbes et al, 2016). Mic12 deletion leads to a reduction of Mic10 oligomers in yeast (Bohnert et al, 2015; Zerbes et al, 2016) and human cells (chapters 6.6 and 7.4). The Mic10 subcomplex furthermore contains two apolipoproteins, termed Mic26 and Mic27. These paralogues evolved as a consequence of the genome duplication in the *Saccharomycetales* order (Muñoz-Gómez et al, 2015; Huynen et al, 2016). Importantly, an independent duplication occurred during the evolution of vertebrates. In human cells, MIC26 (apolipoprotein O, APOO) can be glycosylated and secreted, while a non-glycosylated isoform is stably associated with MICOS (Weber et al, 2013; Koob et al, 2015; Ott et al, 2015). High levels of mitochondrial MIC26 have been associated with diabetic cardiomyopathy (Turkieh et al, 2014). A second paralogue, termed MIC27 (APOOL), is also associated with MICOS and is able to bind cardiolipin *in vitro* (Weber et al, 2013). In yeast, cardiolipin promotes the formation of stable Mic27 assemblies at crista junctions, especially in the absence of Mic60 (Friedman et al, 2015). Yeast Mic27 was shown to stabilise Mic10 oligomers (Zerbes et al, 2016) and thereby affects the stability of the MICOS complex (Eydt et al, 2017). A Mic27-mediated stabilisation of Mic10

oligomers could be used to locally promote crista junction stability. As a result of this stabilising role, Mic27 deletion results in the collapse of crista junctions and a partial phenocopy of Mic10-deficient cells (Harner et al, 2011; Hoppins et al, 2011; von der Malsburg et al, 2011). In contrast, Mic26 is the only *bona fide* MICOS subunit in yeast that is not absolutely required for the maintenance of crista junction architecture (Harner et al, 2011; Hoppins et al, 2011; von der Malsburg et al, 2011) even though it shares a high degree of sequence similarity with its paralogue.

Using native isolation of the MICOS complex from Mic26 and Mic27-deficient mitochondria followed by blue native PAGE as well as *in organello* crosslinking (Figure 6) we discovered an antagonistic relationship between these two proteins: Mic26 deletion led to a stabilisation of Mic10 oligomers, suggesting a function as “oligomerisation breaker” within the MICOS complex. While Mic27 can locally promote the formation of a proteinaceous crista junction scaffold, Mic26 can thus suppress Mic10 assembly. Both proteins are in close proximity to Mic10 as demonstrated by chemical crosslinking and their protein expression levels as well as Mic10 interaction increases in the absence of the paralogue. In the absence of structural information, it remains unclear how these structurally similar proteins can have opposing effects on Mic10 assembly. It has been hypothesised that Mic26 and Mic27 modulate MICOS assembly by locally altering the lipid environment, since a mammalian orthologue can bind cardiolipin *in vitro* (Weber et al, 2013) and Mic27 assembly is affected by the presence of cardiolipin in yeast (Friedman et al, 2015). While this hypothesis provides an appealing link between protein-mediated stabilisation of membrane curvature and the distribution of non-bilayer forming phospholipids at crista junctions, a number of observations described here suggest that it cannot explain the effect of Mic26 and Mic27 on Mic10 assembly (Figure 7). Mic26 or Mic27 deletion did not globally affect cardiolipin-sensitive protein complexes of the inner membrane such as the ADP-ATP carrier (Kutik et al, 2008) and respiratory chain supercomplexes (Pfeiffer et al, 2003). More importantly, effects on Mic10 oligomerisation could be observed even in the absence of the cardiolipin synthase Crd1. Cardiolipin deficiency also led to a destabilisation of Mic10 oligomers, but this effect was independent of MICOS apolipoproteins. Importantly, cardiolipin did not affect Mic10 oligomers analysed in chemical crosslinking experiments, but rather altered large Mic10 assemblies observed during native PAGE experiments. Several lines of evidence therefore strongly suggest that Mic26 and Mic27 directly influence Mic10 assembly in an antagonistic manner and cardiolipin independently stabilises the Mic10 protein scaffold by a distinct mechanism. This regulatory mechanism might be partially conserved during opisthokont evolution, since we found that the knockout of MIC26 in human cell lines phenocopied the effect of *mic27Δ* in yeast with respect to Mic10 oligomer formation. In agreement with these findings, we observed a growth phenotype of MIC26 knockout cells. In contrast, MIC27 knockout did not markedly affect MICOS assembly or cellular growth under respiratory conditions (Figure 10a,c,f).

The regulation of Mic10 assembly and disassembly might help to coordinate Mic10 function at the MICOS complex and the ATP synthase. In agreement with this hypothesis, *mic27* deletion has been found to affect ATP synthase oligomerisation, while Mic10 association with the ATP synthase was unaffected (Eydt et al, 2017). The strong diauxic growth phenotype observed in *mic27*ΔMic10↑ cells further supports this hypothesis. Since neither *mic26*Δ nor *mic27*Δ cells show a noticeable growth defect, their regulatory role likely finetunes Mic10 function, which might not be required in defined laboratory conditions. It is therefore still unclear during which cellular circumstances this novel regulatory pathway becomes relevant, especially considering the very weak phenotypes of Mic26-deficient yeast and MIC27 knockout HEK293T cells. However, the observation that multiple paralogous apolipoprotein-O like subunits can be found in MICOS complexes of divergent organisms indicates that an antagonistic regulation of MICOS assembly provides an evolutionary benefit. A possible scenario where an antagonistic regulation of crista junction architecture might be beneficial is the yeast metabolic cycle, a single-cell oscillatory metabolic reprogramming which temporally separates various pathways (Tu et al, 2005). MICOS subunit RNA levels fluctuate considerably during the different stages of the cycle, reflecting the importance of mitochondrial ultrastructure for the cellular metabolic signature (Tu et al, 2005). Surprisingly, Mic26, i.e. the Mic10 oligomerisation breaking MICOS subunit, appears to follow a different transcriptomic programme (Tu et al, 2005). Studying Mic26/Mic27 mutants under non-standard laboratory conditions such as the yeast metabolic cycle might thus reveal how these proteins help to coordinate mitochondrial ultrastructure with metabolic demands. The complex metabolic transitions during developmental and differentiation processes in metazoans (Zhang et al, 2018) might also serve as a model system to address similar questions.

7.4. MICOS organisation is conserved from yeast to man

A major aim of this thesis was to compare MICOS organisation in yeast and human cells to identify conserved functions of individual MICOS subunits and compare the overall architecture of the complex. A better understanding of MICOS in human cells is of crucial importance since MICOS subunits are also implicated in the pathogenesis of multiple diseases (reviewed in Eramo et al, 2020). For instance, MIC13 deficiency leads to hepatocerebralopathy (Guarani et al, 2016; Zeharia et al, 2016) and MIC60 has been implicated in the development of Parkinson's disease (Van Laar et al, 2019), while elevated MIC26 levels have been found in diabetic cardiomyopathy (Turkieh et al, 2014).

Using CRISPR/Cas9 genome editing with single guide RNAs we have been able to generate knockout HEK293T cell lines for all MIC10 subcomplex subunits (MIC10, MIC13, MIC26 and MIC27) and obtained a MIC60-deficient cell line, which expresses very low levels of the protein. Importantly, several attempts to target MIC19 failed, while its paralogue MIC25 was successfully knocked out (data not shown). Previous studies used RNAi-mediated knockdown

of individual MICOS subunits to demonstrate that the MIC60-19-SAM module is essential for the maintenance of crista architecture, while the accessory subunits MIC13, MIC25, MIC26 and MIC27 are dispensable (Ott et al, 2015). This hierarchical organisation of MICOS subunits is well supported by the data described in this thesis. A recent study suggested that MIC19 and MIC60 also localised to the crista lumen and MIC19 was shown to interact with respiratory complex IV (Sastri et al, 2017). Similarly to MIC10 (Eydt et al, 2017; Rampelt et al, 2017), it might therefore possess an additional function outside of the MICOS complex, which could explain its essential role in the maintenance of cellular fitness. Interestingly, MIC60 and MIC19 might not be essential in all cell lines (Kondadi et al, 2020; Tang et al, 2020), which might indicate tissue-specific roles of the proteins.

By comparing MIC10 and MIC60-deficient cells we obtained novel evidence for the existence of two MICOS modules in human cells, since knockout of MIC10 only affected MIC10 subcomplex subunits, whereas MIC60 knockout resulted in a loss or drastic reduction of all MICOS subunits (Figure 8b,c), which is well supported by previous studies that used knockout or knockdown cell lines (Ott et al, 2012, 2015; Guarani et al, 2015; Anand et al, 2016; Li et al, 2016; Kondadi et al, 2020; Tang et al, 2020). An important novel finding described here is that the SAM-MIC19-MIC25-MIC60 complex was more stable than the association between MICOS subcomplexes as assessed by BN-PAGE analysis after solubilisation with different detergents (Figure 8d). The contact site formed by SAM and the MIC60 subcomplex appears to be surprisingly stable. Crosslinking experiments suggest that the MICOS-SAM connection is mostly mediated by MIC19, rather than MIC60 (Figure 8e). In agreement with this hypothesis, N-terminal myristoylation of MIC19 is required for its interaction with SAM50, but not MIC60 (Darshi et al, 2011). Interestingly, *in vitro* experiments indicated that SAM50 can also interact with MIC60 and MIC25 (Ding et al, 2015). However, MIC19 is required for the stable connection between MICOS and SAM in cells (Darshi et al, 2011; Tang et al, 2020), while MIC25 is dispensable (Ding et al, 2015; Tang et al, 2020). MIC19 was recently described to be a substrate of the stress-induced protease OMA1, which might enable a regulated disassembly of the stable two-membrane spanning MIB complex under certain stress situations (Tang et al, 2020). Importantly, the biochemical characterisation of the human MICOS complex described here also offers novel experimental opportunities: since a very stable MIB “core” complex, consisting of at least MIC60, MIC19, MIC25 and SAM50 can be purified from mitochondria in a relatively simple manner, single particle cryo-electron microscopy (Kühlbrandt, 2014) might soon offer first insights into the structure of the MICOS complex.

We also compared the functional consequences of MIC10 and MIC60-deficiency (Figure 9). As expected, both knockout cell lines showed a strong alteration of mitochondrial ultrastructure and a strongly reduced growth rate. This effect on cell growth has not always been observed (Callegari et al, 2019) and might therefore depend on the cellular background.

Surprisingly, only minor alterations of respiratory chain supercomplexes could be observed in MIC10 knockout cells, while we did not observe defects in MIC60-deficient cells. Contrary to a previous study (Callegari et al, 2019), we also observed a destabilisation of high molecular weight ATP synthase complexes in MIC10-deficient cells. The human MIC10 protein might thus influence the assembly of other cristae organising proteins, similarly to yeast Mic10 (chapter 7.2). This hypothesis is supported by the observation that minor amounts of ATP synthase could be co-precipitated in MIC10^{FLAG} IPs. Interestingly, a previously published crosslinking study found an interaction of MIC27 with the ATP synthase (Schweppe et al, 2017). The influence of MIC10 on ATP synthase assembly might therefore be conserved throughout opisthokont evolution.

The analysis of a complete set of MIC10 subcomplex knockout cell lines described here revealed a hierarchical organisation of subunits within the complex (Figure 10). In agreement with previous studies (Guarani et al, 2015, 2016; Anand et al, 2016), MIC13 knockout had a strong effect on the stability of the MIC10 subcomplex and MIC10 protein levels. MIC26 and MIC27 were found to be dispensable for the overall stability of the subcomplex. However, MIC26 stabilised MIC10 oligomers, reminiscent of the situation in yeast, where Mic27 stabilises MIC10 oligomers (see also chapter 7.3). MIC27 knockout only mildly affected MIC10 oligomerisation and did not cause a growth phenotype. Future work will have to clarify, whether its association with the ATP synthase (Schweppe et al, 2017) helps to spatially coordinate MIC10 function. MIC10 deficiency also led to a decrease of long OPA1 isoforms. There is currently no evidence for a direct association of MIC10 and OPA1. In contrast, multiple studies described an interaction between MIC60 and OPA1 (Barrera et al, 2016; Glytsou et al, 2016; Schweppe et al, 2017). The effect of MIC10 on OPA1 processing might therefore be an indirect adaptation to e.g. oxidative stress (Lee et al, 2020). Importantly, knockout of MIC10 subcomplex subunits also led to a similar phenotype, and the severity of the phenotype correlated with the effect on MIC10 oligomerisation. A relative increase of short OPA1 isoforms could be observed in cells lacking MIC10, MIC13 and MIC26, but not in cells lacking MIC27. Future studies could overexpress OPA1 isoforms in MICOS knockout cell lines to dissect the functions of these two cristae organising systems. Interestingly, the MIC60-deficient cell line described here did not show altered processing of OPA1. In addition, the stability of the ATP synthase and the respiratory chain was unaffected, clearly indicating non-overlapping functions of MICOS core subunits. Unbiased multi-omic approaches might help to elucidate the specific functions of both subcomplexes.

7.5. The MIB complex and DNAJC11 spatially coordinate mitochondrial protein biogenesis

The detailed biochemical analysis of the human MICOS complex described in chapter 7.4 revealed that the MIC60 subcomplex forms a surprisingly stable contact with the SAM

machinery of the outer mitochondrial membrane. The interaction of SAM and MICOS in human cells has been identified by many groups (Xie et al, 2007; Darshi et al, 2011; Alkhaja et al, 2012; Ott et al, 2012; Ding et al, 2015; Huynen et al, 2016) and the contact site was termed mitochondrial intermembrane space bridging (MIB) complex (Ott et al, 2012; Huynen et al, 2016). SAM50 depletion leads to a pronounced alteration of mitochondrial cristae architecture (Ott et al, 2012). After depleting MIC60 by CRISPR/Cas9 to very low levels we observed a strong reduction of SAM50 protein levels in mitochondria, similarly to what has been observed after siRNA-mediated MIC60 knockdown (Ding et al, 2015; Ott et al, 2015). More importantly, we found SAM to exclusively co-migrate with MIC60-containing protein complexes in blue native PAGE experiments and were unable to identify SAM50-containing protein complexes in MIC60 depleted cells. In addition, the SAM50/MIC60 containing complexes were stable even after treatment with the harsh detergent Triton X100 and after genetic depletion of the MIC10 subcomplex (Figure 8, Figure 11a,b). Multiple lines of evidence thus support the significance of the MIC60-SAM connection in membrane-bridging. Several hypotheses might explain why MIC60 and SAM form such a stable membrane contact site: i. The evolution of both proteins can be traced back to bacterial ancestors of mitochondria. Since a MIC60-SAM interaction has been identified across the eukaryotic lineage (Muñoz-Gómez et al, 2015; Kaurov et al, 2018), it might have evolved in the endosymbiotic ancestor of mitochondria, just like the membrane-shaping function of MIC60 (Tarasenko et al, 2017). ii. Properties of β -barrel proteins, such as their long half-life (Christiano et al, 2014), might be beneficial for the formation of stable membrane-contact sites. This hypothesis is strongly supported by the observation that all mitochondrial β -barrel proteins have been implicated in the formation of intra- or interorganellar contact sites (Pfanner et al, 2019). iii. Since SAM substrates (such as TOM40 and the VDAC complex) mediate the exchange of proteins and metabolites, respectively, a localized biogenesis of these protein machineries at crista junctions might be beneficial. Furthermore, the biogenesis of β -barrel proteins requires the cooperation of TOM and SAM in the outer membrane. Since TOM is much more abundant than SAM (Morgenstern et al, 2017), it might be beneficial to channel the biogenesis of β -barrel proteins at distinct sites of the outer membrane, such as crista junction sites. These hypotheses are not mutually exclusive and none of them can currently be rejected. However, their validity can be experimentally addressed: By studying the MICOS complex in more organisms outside of the opisthokont supergroup (as has been done for *Trypanosoma brucei* (Kaurov et al, 2018)) one could identify the evolutionarily most significant connections between protein biogenesis and cristae shaping machineries. Furthermore, studying the interactome of MIC60 orthologues in alphaproteobacteria, which are the closest modern relatives of mitochondria, will reveal which interactions evolved in pre-eukaryotic times and thereby clarify the evolutionary relationship between MICOS and the SAM complex. By genetically distinguishing protein import and membrane-bridging functions of this contact site

one might also be able to address whether the protein biogenesis – MICOS connection is a by-product of the essential membrane bridging component of the MIB complex or essential for eukaryotic life. A similar approach has been used in yeast, revealing that Mic60-mediated outer-inner membrane tethering is necessary, but not sufficient for maintaining crista junction architecture (Zerbes et al, 2012).

We hypothesised that the remarkably stable MIB-mediated contact site between both mitochondrial membranes is not only structurally important but also plays a direct role in protein biogenesis. Depletion of MIC60 and subsequent loss of SAM50 led to a reduced assembly rate of β -barrel precursor proteins in *in organello* import assays (Figure 11b). Protein biogenesis and the MICOS complex seem to be coupled in every organism studied so far: the yeast MICOS complex is linked to the TOM and SAM machinery of the outer membrane as well as the intermembrane-space MIA machinery (von der Malsburg et al, 2011; Bohnert et al, 2012; Varabyova et al, 2013), the human MICOS complex interacts with SAM as well as TIM22 (Xie et al, 2007; Ott et al, 2012; Callegari et al, 2019) and a potential MIA40 orthologue was recently identified to be a subunit of the MICOS machinery in the highly divergent excavate *Trypanosoma brucei* (Kaurov et al, 2018). These results, supported by the findings described here, demonstrate that a close connection between membrane structure and protein biogenesis in the highly organized mitochondrion is beneficial and likely essential for efficient mitochondrial biogenesis.

The identification of DNAJC11 as *bona fide* subunit of the MIB complex of mammalian cells (Figure 11d-f) further supports the hypothesis that MICOS serves as a central hub for biogenesis of hydrophobic mitochondrial proteins. Data described in chapters 6.4 and 6.7 and previous studies showed that DNAJC11 associates with the MIC60/SAM module in the outer mitochondrial membrane (Xie et al, 2007; Ioakeimidis et al, 2014; Huynen et al, 2016). DNAJC11 possesses a conserved J-domain that possibly stimulates the Hsp70 reaction cycle and a recently published interactome of DNAJC11 indeed revealed an interaction with cytosolic Hsp70 chaperones in cultured cells as well as intact brain tissue (Violitzi et al, 2019). We therefore hypothesised that it could recruit chaperone-bound mitochondrial precursor proteins (Jores et al, 2018) in the cytosol to mitochondrial subdomains. Its interaction with the MICOS machinery would enable efficient substrate channelling of hydrophobic mitochondrial precursors. In agreement with this hypothesis, HEK293T cells lacking DNAJC11 showed a slower biogenesis of β -barrel proteins as assessed by *in organello* import and assembly assays with radiolabelled β -barrel precursors (Figure 11g). Importantly, MICOS and SAM integrity was unaffected in cells lacking DNAJC11 and the β -barrel import defect was rescued after re-expression of DNAJC11^{FLAG}, clearly showing that DNAJC11 directly affects the biogenesis of outer membrane proteins. We hypothesised that the substrate spectrum of DNAJC11 is not limited to β -barrel proteins of the outer membrane, since MICOS also interacts with the carrier translocase (Callegari et al, 2019). Consistent with this idea, DNJAC11 knockout led to

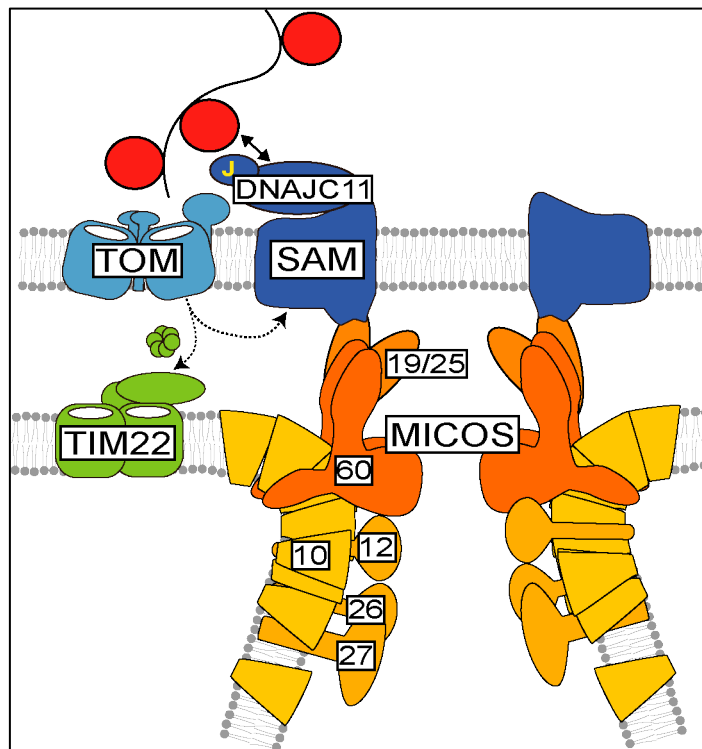


Figure 15 Hypothetical model of MICOS/DNAJC11 mediated spatial coordination of protein import

MICOS bridges both mitochondrial membranes by forming a very stable contact site with the SAM complex (termed MIB complex). The direct contact between MICOS and SAM is likely mediated by MIC19. MICOS deficiency can lead to impaired β -barrel biogenesis. The J-protein DNAJC11 also affects the efficiency of β -barrel import, presumably by recruiting Hsp70-bound precursor proteins to import sites. Since MICOS also interacts with the carrier translocase of the inner membrane (TIM22) complex, and TIM22 substrate proteins (such as MCU) are reduced in DNAJC11-deficient mitochondria, DNAJC11-mediated coordination of protein import at the MIB complex might affect the biogenesis of hydrophobic proteins in both mitochondrial membranes.

chaperones, termed Xdj1 and Djp1, connect TOM receptors with chaperone-bound substrates of the TOM channel (Opaliński et al, 2018), reminiscent of the proposed role of DNAJC11 in human mitochondria. Future studies will have to characterise additional substrates of DNAJC11 using *in organello* import assays. Furthermore, a global analysis of the mitochondrial proteome after DNAJC11 depletion could help to define the substrate spectrum. It will also be interesting to characterise the functional consequences of DNAJC11 impairment, since mice lacking DNAJC11 showed severe neuromuscular deficits (Ioakeimidis et al, 2014) and DNAJC11 knockout cells show strongly reduced growth rates (Alexander von der Malsburg, pers. communication). The inefficient import of mitochondrial proteins in DNAJC11-deficient cells might lead to increased levels of hydrophobic and aggregation-prone mitochondrial proteins in the cytosol, which could sequester cytosolic chaperones, potentially resulting in global proteotoxicity. To evaluate this hypothesis, one could test whether

decreased protein levels of the mitochondrial calcium uniporter, which is an inner membrane protein of the carrier family.

The localisation of DNAJC11 in the outer membrane (Ioakeimidis et al, 2014), its interaction with cytosolic chaperones (Violitzi et al, 2019) and the β -barrel biogenesis phenotype described here all support a role of the protein in substrate channelling of hydrophobic mitochondrial precursor proteins to the correct sub-organellar location. Interestingly, J-protein dependent targeting of mitochondrial precursor proteins might be an evolutionarily conserved phenomenon. A recent study in yeast found that two cytosolic

expression of aggregation-prone poly-glutamine-repeat constructs (see e.g. Itakura et al, 2016) leads to altered solubility of hydrophobic mitochondrial proteins in DNAJC11 knockout cells. In summary, DNAJC11 at the MIB complex likely recruits chaperone-bound hydrophobic mitochondrial precursor proteins in the cytosol to defined biogenesis sites. This spatial coordination of the import process by DNAJC11 at the MIB complex enables an efficient assembly of mitochondrial precursor proteins, since MICOS interacts with protein translocases of both mitochondrial membranes.

7.6. Helical arrays of Mgm1 tetramers shape the inner mitochondrial membrane

This thesis mostly focussed on the MICOS complex in yeast and human cells and its role in e.g. the metabolic adaptation to respiratory metabolism. While MICOS is essential for the maintenance of crista junction structures, it remains unclear whether it is directly involved in the dynamic adaptation of crista to altered metabolic conditions. Very recent evidence has implicated MICOS in the fusion of cristae (Kondadi et al, 2020), but there is currently no data supporting a dynamic reorganisation of MICOS during metabolic transitions. Its core subunits appear to promote mitochondrial biogenesis during e.g. the diauxic shift, but this could possibly be attributed to additional functions (chapter 7.1). In contrast, a plethora of studies have shown that the dynamin-like GTPase OPA1/Mgm1 dynamically alters cristae shape to finetune the bioenergetic properties of mitochondrial ultrastructure. Proteins of the Mgm1/OPA1 family are major determinants of mitochondrial ultrastructure and fulfil at least two roles in mediating inner membrane fusion and the dynamic remodelling of cristae architecture. The fusion activity might also be linked to a role in the formation of cristae by partial inner membrane fusion (Harner et al, 2016). Importantly, OPA1 is able to directly respond to altered metabolic circumstances (Patten et al, 2014). In the absence of high-resolution structural information it remained unclear how Mgm1/OPA1 can mediate such a diverse set of membrane remodelling activities. We therefore attempted to further elucidate the assembly mechanism of Mgm1 by combining structural studies with *in vivo* data.

The crystal structure of the Mgm1 tetramer (Figure 12a-c) revealed that Mgm1 possesses an architecture similar to other dynamin-like GTPases with a conserved domain organisation. In contrast to dynamin, a unique paddle domain mediates membrane contact. In addition, the macro-molecular assembly of Mgm1 into dimers and tetramers differs from dynamin (Faelber et al, 2011; Ford et al, 2011). Mgm1 dimers form a V-shape, which assemble into an elongated tetramer via interface-1. Cryo-ET analysis of membrane-bound Mgm1 (Figure 12d-e) showed that it can assemble into helical filaments, similarly to other dynamin-like GTPases (Faelber et al, 2011; Ford et al, 2011; Kalia et al, 2018; Kong et al, 2018). Importantly, helical filaments were observed on positively and negatively curved membranes. This unique feature could help to explain its role in the maintenance and remodelling of cristae membranes.

To determine whether the dimer and tetramer interfaces are physiologically relevant we employed a loss-of-function screen, which made use of the observation that Mgm1 dysfunction in yeast results in a rapid loss of mitochondrial DNA (Jones & Fangman, 1992) and allowed for an unbiased assessment of the effect of Mgm1 mutations. To this end, an inducible promoter was inserted upstream of the genomic Mgm1 open reading frame and mutant Mgm1 alleles were expressed from plasmids (Figure 12f-h, Figure 13). An important advantage of this method is the absence of compensatory mutations and possibly a reduced occurrence of spontaneous mitochondrial DNA loss acquired during traditional mutagenesis studies, such as plasmid shuffling, which is prevented by the expression of wildtype Mgm1 from the genomic locus prior to the assay. This theoretically reduces the occurrence of false-positive results. In agreement with the data obtained from the crystal structure, mutations in the dimer or tetramer interfaces caused a complete loss of function, as assessed by the ability to grow on respiratory carbon sources and the expression of mitochondrially encoded Cox1. This finding provides strong support for the role of these interfaces for Mgm1 function *in vivo*. Importantly, this data also shows that the interfaces observed in the *Chaetomium thermophilum* construct are conserved in budding yeast.

A major disadvantage of this loss-of-function screen is that subtle defects of Mgm1 function are unlikely to cause a pronounced phenotype, resulting in false negative results. Mutations of the paddle region, which appears to mediate membrane binding, resulted in an intermediate phenotype with a partial loss of mitochondrial DNA and an altered mitochondrial network morphology, but did not cause a complete loss of respiratory growth. A complete loss of function results in a loss of mitochondrial DNA, which is known to cause mitochondrial fragmentation and a strong reduction of mitochondrial cristae. Mgm1 function can thus not be assessed in further molecular detail. To circumvent these effects, one could either downregulate mitochondrial fission, for example by expressing dominant-negative alleles of the fission-mediating dynamin Dnm1 (Zick et al, 2009), or take advantage of the assembly mode of Mgm1 itself: We hypothesised that expression of tetramerisation-deficient Mgm1 alleles would cause strong dominant-negative effects and indeed observed strong respiratory growth phenotypes when we expressed tetramer-interface mutants in wild-type cells (Figure 14). In particular, we found that Mgm1-Y520A can suppress Mgm1 function in wild-type without causing a loss of the mitochondrial genome. This allowed us to analyse the cristae morphology defects caused by Mgm1 tetramer dissociation. We not only found fewer cristae, but also a significant widening of the cristae lumen. This finding strongly suggests that Mgm1 assembly into tetramers and helical filaments is important for the determination of mitochondrial cristae width. In addition, the serendipitous discovery of dominant-negative Mgm1 alleles will help to decipher cristae remodelling in higher molecular detail in future studies.

This study also suggested a possible model of Mgm1-mediated cristae remodelling based on cryo-electron tomography evidence (Figure 12d-e). *C. thermophilum* Mgm1 assembled on the outside of lipid tubules in helical filaments of tetramers, which were arranged in a similar manner as observed in the crystal structure. At the same time, an inside decoration was observed in some tubules. This assembly on a negatively curved membrane is unique among members of the dynamin family. Importantly, it resembles a putative assembly mode on the inside of cristae membranes and might explain the tightening of cristae observed after OPA1 overexpression (Frezza et al, 2006). Combined with the finding that the expression of tetramerisation-deficient Mgm1 leads to a widening of cristae it appears very likely that helical filaments of Mgm1 on the inside of cristae membranes determine the shape of cristae. An important remaining question is whether and how the GTPase activity of Mgm1 influences its assembly. Multiple lines of evidence favour a model in which a GTPase-dependent power stroke could pull filaments against each other even though the subtomogram averages of nucleotide-free and GTP γ S-bound Mgm1 assemblies on negatively curved membranes did not show any noticeable differences, possibly due to the limited resolution of 20.6 Å and 18.8 Å, respectively. Importantly, the crystal structure revealed that the G and BSE domains of Mgm1 and dynamin show a very similar structure. The GTPase activity of OPA1 is required for its cristae remodelling activity (Frezza et al, 2006) and previously reported temperature sensitive mutations of Mgm1 are localised in GTP binding loops as well as interface 1 and the G/BSE domain interface (Meeusen et al, 2006). In further agreement with this hypothesis, GTP addition in tube pulling assays resulted in a measurable force (Faelber et al, 2019). A power stroke in a left-handed helical assembly of Mgm1 on the inside of a membrane tube would result in a constriction, while it would expand the diameter of the tube in a right-handed assembly. Both activities are possibly required for the physiological function of the protein (Frezza et al, 2006). A very recent study provided further evidence for a GTP-dependent remodelling of cristae (Zhang et al, 2020). The authors imaged s-OPA1 assemblies on lipid tubules in an arrangement very similar to CtMgm1. Addition of GTP γ S resulted in a conformational change of the left-handed helical assembly and an expansion of the lipid tube, in agreement with the data presented here. This study not only provides support for the hypothesis that a GTP-dependent power stroke in Mgm1 filaments can remodel cristae membranes, but also demonstrates that Mgm1/OPA1 assembly is largely conserved.

Another very recent study reported a trimeric structure of *S. cerevisiae* Mgm1 (Yan et al, 2020). These trimers are arranged in a head-to-tail manner, but the trimer interfaces are not conserved in *C. thermophilum*. The concave trimer might associate with the membrane and create a curved tip that could possibly trigger fusion events between two opposing membranes. This trimeric assembly of s-Mgm1 could be anchored to the membrane by transmembrane-domain containing l-Mgm1, which is required for fusion (Zick et al, 2009; Ge et al, 2020). Local membrane bending, which is a requirement for Mgm1-mediated inner membrane fusion

(Rujiviphat et al, 2015) could also be created by the tetramer-based helical filaments observed in our study. The trimeric structure observed by Yan et al. and the tetrameric assembly found in our study are not mutually exclusive but could help to explain the two distinct functions of Mgm1 in membrane fusion and cristae remodelling. Future studies will have to image a mix of short and long Mgm1 isoforms assembled on model membranes using e.g. cryo-electron tomography to further define the mechanism of Mgm1-mediated membrane fusion. Importantly, cristae stabilisation requires only the short OPA1 isoforms (Del Dotto et al, 2017; Lee et al, 2017) and can therefore be explained by the model presented here.

7.7. Conclusion

The dynamic reorganisation of cristae is enabled by an interplay of multiple protein machineries. MICOS forms stable contacts to the outer membrane and thereby anchors crista junctions at specific sites. It also forms the proteinaceous backbone of crista junctions to stabilise the membrane curvature. OPA1/Mgm1 dynamically remodels cristae membranes in response to the metabolic state of the cell. Due to its function in inner membrane fusion it might also be involved in the biogenesis of cristae. Finally, dimer rows of the ATP synthase shape cristae membranes to create a bioenergetically optimised compartment for oxidative phosphorylation. Work described in this thesis shed light on the assembly of these cristae shaping machineries and their interplay.

A biochemical analysis of human MICOS knockout cell lines revealed that MICOS organisation into two subcomplexes is conserved from yeast to man (chapters 6.4, 6.6). Since only MICOS core subunits are required for efficient adaptation to respiratory metabolism in yeast (chapter 6.1), they possibly possess underappreciated moonlighting functions which are important for mitochondrial biogenesis. The interaction of Mic10 with the ATP synthase, which is likely conserved throughout evolution (chapter 6.6), is of particular importance (chapter 6.2). We therefore hypothesised that Mic10 assembly has to be spatially regulated and found that it is influenced by the accessory subunits Mic26 and Mic27 in an antagonistic manner and independently by cardiolipin (chapter 6.3, Rampelt et al, 2018). Future studies will have to elucidate which upstream signalling pathways can control this novel pathway and during which cellular circumstances Mic26/27-dependent regulation plays a role. While Mic10 influences the assembly of inner membrane cristae organising proteins, the second subunit Mic60 forms contacts with the outer membrane (chapter 6.4). Our analyses of the human MICOS complex, which closely associates with the SAM complex, revealed that this membrane bridging function of the Mic60 module is important for the efficient biogenesis of outer membrane β -barrel proteins (chapter 6.7). We furthermore found that the J-protein DNAJC11 is a genuine subunit of the MIB complex and possibly recruits mitochondrial precursor proteins in the cytosol to import sites (chapter 6.7). MICOS thus forms a central biogenesis hub at specific sites in mitochondria. Unbiased multi-omics analyses of MICOS

knockout cell lines could reveal additional functions. Importantly, only very little is known about tissue-specific roles of MICOS subunits in metazoans. A comprehensive characterisation of mouse models and patient samples might therefore offer unexpected insights into the role of MICOS in mitochondrial function. Clearly, its impact on mitochondrial biogenesis is only beginning to emerge.

Future studies will have to determine the structure of the MICOS complex to better understand its various roles. This thesis also described a possible assembly mechanism of OPA1/Mgm1 based on the crystal structure of the Mgm1 tetramer, cryo-ET data of Mgm1 filaments on the inside and outside of lipid tubules and *in vivo* data in yeast that provides evidence for a role of these tetrameric assemblies in shaping cristae membranes (chapter 6.8, Faelber et al, 2019). This structural insight into Mgm1-mediated membrane remodelling represents a major advance in the understanding of cristae remodelling. Future studies will have to image combinations of multiple Mgm1/OPA1 isoforms to also elucidate inner membrane fusion.

Work described in this thesis and many other studies revealed extensive crosstalk between cristae shaping proteins. These machineries are thus not separate entities, but their assembly and activity is mutually influenced. The dynamic remodelling of cristae membranes cannot be fully elucidated by biochemical means alone. When combined with e.g. recent advances in live cell super-resolution microscopy they can help to unravel how MICOS, OPA1/Mgm1, the ATP synthase and possible novel cristae shaping proteins cooperate in generating and remodelling cristae membranes in response to the metabolic demands of the cell.

8. References

- [1] Aaltonen MJ, Friedman JR, Osman C, Salin B, di Rago J-P, Nunnari J, Langer T, Tatsuta T (2016) MICOS and phospholipid transfer by Ups2–Mdm35 organize membrane lipid synthesis in mitochondria. *J. Cell Biol.* 213: 525–534
- [2] Abrams AJ, Hufnagel RB, Rebelo A, Zanna C, Patel N, Gonzalez MA, Campeanu IJ, Griffin LB, Groenewald S, Strickland A V., Tao F, Speziani F, Abreu L, Schüle R, Caporali L, La Morgia C, Maresca A, Liguori R, Lodi R, Ahmed ZM, et al (2015) Mutations in SLC25A46, encoding a UGO1-like protein, cause an optic atrophy spectrum disorder. *Nat. Genet.* 47: 926–932
- [3] Abrisch RG, Gumbin SC, Wisniewski BT, Lackner LL, Voeltz GK (2020) Fission and fusion machineries converge at ER contact sites to regulate mitochondrial morphology. *J. Cell Biol.* 219: e201911122
- [4] Acehan D, Malhotra A, Xu Y, Ren M, Stokes DL, Schlame M (2011) Cardiolipin Affects the Supramolecular Organization of ATP Synthase in Mitochondria. *Biophys. J.* 100: 2184–2192
- [5] Acín-Pérez R, Fernández-Silva P, Peleato ML, Pérez-Martos A, Enriquez JA (2008) Respiratory Active Mitochondrial Supercomplexes. *Mol. Cell* 32: 529–539
- [6] Alexander C, Votruba M, Pesch UEA, Thiselton DL, Mayer S, Moore A, Rodriguez M, Kellner U, Leo-Kottler B, Auburger G, Bhattacharya SS, Wissinger B (2000) OPA1, encoding a dynamin-related GTPase, is mutated in autosomal dominant optic atrophy linked to chromosome 3q28. *Nat. Genet.* 26: 211–215
- [7] Alkhaja AK, Jans DC, Nikolov M, Vukotic M, Lytovchenko O, Ludewig F, Schliebs W, Riedel D, Urlaub H, Jakobs S, Deckers M (2012) MINOS1 is a conserved component of mitofilin complexes and required for mitochondrial function and cristae organization. *Mol. Biol. Cell* 23: 247–257
- [8] Allen RD, Schroeder CC, Fok AK (1989) An investigation of mitochondrial inner membranes by rapid-freeze deep-etch techniques. *J. Cell Biol.* 108: 2233–2240
- [9] Anand R, Strecker V, Urbach J, Wittig I, Reichert AS (2016) Mic13 is essential for formation of crista junctions in mammalian cells. *PLoS One* 11: e0160258
- [10] Anselmi C, Davies KM, Faraldo-Gómez JD (2018) --Mitochondrial ATP synthase dimers spontaneously associate due to a long-range membrane-induced force-. *J. Gen. Physiol.* 150: 763–770
- [11] Arnold I, Pfeiffer K, Neupert W, Stuart RA, Schägger H (1998) Yeast mitochondrial F1F0-ATP synthase exists as a dimer: identification of three dimer-specific subunits. *EMBO J.* 17: 7170–8
- [12] Arselin G, Giraud M-F, Dautant A, Vaillier J, Brethes D, Couлары-Salin B, Schaeffer J, Velours J (2003) The GxxxG motif of the transmembrane domain of subunit e is involved in the dimerization/oligomerization of the yeast ATP synthase complex in the mitochondrial membrane. *Eur. J. Biochem.* 270: 1875–1884
- [13] Arselin G, Vaillier J, Salin B, Schaeffer J, Giraud MF, Dautant A, Brèthes D, Velours J (2004) The modulation in subunits e and g amounts of yeast ATP synthase modifies mitochondrial cristae morphology. *J. Biol. Chem.* 279: 40392–40399

- [14] Balsa E, Soustek MS, Thomas A, Cogliati S, García-Poyatos C, Martín-García E, Jedrychowski M, Gygi SP, Enriquez JA, Puigserver P (2019) ER and Nutrient Stress Promote Assembly of Respiratory Chain Supercomplexes through the PERK-eIF2 α Axis. *Mol. Cell* 74: 877–890
- [15] Ban T, Ishihara T, Kohno H, Saita S, Ichimura A, Maenaka K, Oka T, Mihara K, Ishihara N (2017) Molecular basis of selective mitochondrial fusion by heterotypic action between OPA1 and cardiolipin. *Nat. Cell Biol.* 19: 856–863
- [16] Barbot M, Jans DC, Schulz C, Denkert N, Kroppen B, Hoppert M, Jakobs S, Meinecke M (2015) Mic10 Oligomerizes to Bend Mitochondrial Inner Membranes at Cristae Junctions. *Cell Metab.* 21: 756–763
- [17] Barrera M, Koob S, Dikov D, Vogel F, Reichert AS (2016) OPA1 functionally interacts with MIC60 but is dispensable for crista junction formation. *FEBS Lett.* 590: 3309–3322
- [18] Di Bartolomeo F, Malina C, Campbell K, Mormino M, Fuchs J, Vorontsov E, Gustafsson CM, Nielsen J (2020) Absolute yeast mitochondrial proteome quantification reveals trade-off between biosynthesis and energy generation during diauxic shift. *Proc. Natl. Acad. Sci.* 117: 7524–7535
- [19] Bazán S, Mileykovskaya E, Mallampalli VKPS, Heacock P, Sparagna GC, Dowhan W (2013) Cardiolipin-dependent reconstitution of respiratory supercomplexes from purified *Saccharomyces cerevisiae* complexes III and IV. *J. Biol. Chem.* 288: 401–411
- [20] Becker T, Song J, Pfanner N (2019) Versatility of Preprotein Transfer from the Cytosol to Mitochondria. *Trends Cell Biol.* 29: 534–548
- [21] Benador IY, Veliova M, Mahdaviani K, Petcherski A, Wikstrom JD, Assali EA, Acín-Pérez R, Shum M, Oliveira MF, Cinti S, Sztalryd C, Barshop WD, Wohlschlegel JA, Corkey BE, Liesa M, Shirihai OS (2018) Mitochondria Bound to Lipid Droplets Have Unique Bioenergetics, Composition, and Dynamics that Support Lipid Droplet Expansion. *Cell Metab.* 27: 869–885
- [22] Blaza JN, Serreli R, Jones AJY, Mohammed K, Hirst J (2014) Kinetic evidence against partitioning of the ubiquinone pool and the catalytic relevance of respiratory-chain supercomplexes. *Proc. Natl. Acad. Sci.* 111: 15735–40
- [23] Blum TB, Hahn A, Meier T, Davies KM, Kühlbrandt W (2019) Dimers of mitochondrial ATP synthase induce membrane curvature and self-assemble into rows. *Proc. Natl. Acad. Sci.* 116: 4250–4255
- [24] Bohnert M, Wenz L-S, Zerbes RM, Horvath SE, Stroud DA, von der Malsburg K, Müller JM, Oeljeklaus S, Perschil I, Warscheid B, Chacinska A, Veenhuis M, van der Klei IJ, Daum G, Wiedemann N, Becker T, Pfanner N, van der Laan M (2012) Role of mitochondrial inner membrane organizing system in protein biogenesis of the mitochondrial outer membrane. *Mol. Biol. Cell* 23: 3948–3956
- [25] Bohnert M, Zerbes RM, Davies KM, Mühleip AW, Rampelt H, Horvath SE, Boenke T, Kram A, Perschil I, Veenhuis M, Kühlbrandt W, van der Klei IJ, Pfanner N, van der Laan M (2015) Central Role of Mic10 in the Mitochondrial Contact Site and Cristae Organizing System. *Cell Metab.* 21: 747–755
- [26] Bornhövd C, Vogel F, Neupert W, Reichert AS (2006) Mitochondrial Membrane Potential Is Dependent on the Oligomeric State of F₁F₀-ATP Synthase Supracomplexes. *J. Biol. Chem.* 281: 13990–13998

- [27] Böttinger L, Horvath SE, Kleinschroth T, Hunte C, Daum G, Pfanner N, Becker T (2012) Phosphatidylethanolamine and Cardiolipin Differentially Affect the Stability of Mitochondrial Respiratory Chain Supercomplexes. *J. Mol. Biol.* 423: 677–686
- [28] Brandt T, Mourier A, Tain LS, Partridge L, Larsson N-G, Kühlbrandt W (2017) Changes of mitochondrial ultrastructure and function during ageing in mice and *Drosophila*. *Elife* 6: e24662
- [29] Brunner S, Everard-Gigot V, Stuart R a. (2002) Structure of the Yeast F₁F_o-ATP Synthase Forms Homodimers. *J. Biol. Chem.* 277: 48484–48489
- [30] Busch KB (2020) Inner mitochondrial membrane compartmentalization: Dynamics across scales. *Int. J. Biochem. Cell Biol.* 120: 105694
- [31] Busch KB, Deckers-Hebestreit G, Hanke GT, Mulikidjanian AY (2013) Dynamics of bioenergetic microcompartments. *Biol. Chem.* 394: 163–188
- [32] Bustos DM, Velours J (2005) The Modification of the Conserved GXXXG Motif of the Membrane-spanning Segment of Subunit g Destabilizes the Supramolecular Species of Yeast ATP Synthase. *J. Biol. Chem.* 280: 29004–29010
- [33] Buzhynskyy N, Sens P, Prima V, Sturgis JN, Scheuring S (2007) Rows of ATP Synthase Dimers in Native Mitochondrial Inner Membranes. *Biophys. J.* 93: 2870–2876
- [34] Callegari S, Müller T, Schulz C, Lenz C, Jans DC, Wissel M, Opazo F, Rizzoli SO, Jakobs S, Urlaub H, Rehling P, Deckers M (2019) A MICOS-TIM22 Association Promotes Carrier Import into Human Mitochondria. *J. Mol. Biol.* 431: 2835–2851
- [35] Christiano R, Nagaraj N, Fröhlich F, Walther TC (2014) Global Proteome Turnover Analyses of the Yeasts *S.cerevisiae* and *S.pombe*. *Cell Rep.* 9: 1959–1965
- [36] Cipolat S, de Brito OM, Dal Zilio B, Scorrano L (2004) OPA1 requires mitofusin 1 to promote mitochondrial fusion. *Proc. Natl. Acad. Sci.* 101: 15927–15932
- [37] Civileto G, Varanita T, Cerutti R, Gorletta T, Barbaro S, Marchet S, Lamperti C, Viscomi C, Scorrano L, Zeviani M (2015) Opa1 overexpression ameliorates the phenotype of two mitochondrial disease mouse models. *Cell Metab.* 21: 845–854
- [38] Cogliati S, Frezza C, Soriano ME, Varanita T, Quintana-Cabrera R, Corrado M, Cipolat S, Costa V, Casarin A, Gomes LC, Perales-Clemente E, Salviati L, Fernandez-Silva P, Enriquez JA, Scorrano L (2013) Mitochondrial cristae shape determines respiratory chain supercomplexes assembly and respiratory efficiency. *Cell* 155: 160–171
- [39] Cruciat CM, Brunner S, Baumann F, Neupert W, Stuart RA (2000) The cytochrome bc₁ and cytochrome c oxidase complexes associate to form a single supracomplex in yeast mitochondria. *J. Biol. Chem.* 275: 18093–18098
- [40] Darshi M, Mendiola VL, Mackey MR, Murphy AN, Koller A, Perkins G a., Ellisman MH, Taylor SS (2011) ChChd3, an inner mitochondrial membrane protein, is essential for maintaining Crista integrity and mitochondrial function. *J. Biol. Chem.* 286: 2918–2932
- [41] Daum B, Walter A, Horst A, Osiewacz HD, Kuhlbrandt W (2013) Age-dependent dissociation of ATP synthase dimers and loss of inner-membrane cristae in mitochondria. *Proc. Natl. Acad. Sci.* 110: 15301–15306
- [42] Davies KM, Anselmi C, Wittig I, Faraldo-Gomez JD, Kuhlbrandt W (2012) Structure of the yeast F₁F_o-ATP synthase dimer and its role in shaping the mitochondrial cristae. *Proc. Natl. Acad. Sci.* 109: 13602–13607

- [43] Davies KM, Blum TB, Kühlbrandt W (2018) Conserved in situ arrangement of complex I and III2 in mitochondrial respiratory chain supercomplexes of mammals, yeast, and plants. *Proc. Natl. Acad. Sci.* 115: 3024–3029
- [44] Dekker PJT, Martin F, Maarse AC, Bömer U, Müller H, Guiard B, Meijer M, Rassow J, Pfanner N (1997) The Tim core complex defines the number of mitochondrial translocation contact sites and can hold arrested preproteins in the absence of matrix Hsp70-Tim44. *EMBO J.* 16: 5408–5419
- [45] Delettre C, Lenaers G, Griffoin J-M, Gigarel N, Lorenzo C, Belenguer P, Pelloquin L, Grosgeorge J, Turc-Carel C, Perret E, Astarie-Dequeker C, Lasquelléc L, Arnaud B, Ducommun B, Kaplan J, Hamel CP (2000) Nuclear gene OPA1, encoding a mitochondrial dynamin-related protein, is mutated in dominant optic atrophy. *Nat. Genet.* 26: 207–210
- [46] DeRisi JL, Iyer VR, Brown PO (1997) Exploring the Metabolic and Genetic Control of Gene Expression on a Genomic Scale. *Science* 278: 680–686
- [47] DeVay RM, Dominguez-Ramirez L, Lackner LL, Hoppins S, Stahlberg H, Nunnari J (2009) Coassembly of Mgm1 isoforms requires cardiolipin and mediates mitochondrial inner membrane fusion. *J. Cell Biol.* 186: 793–803
- [48] Diaz F, Fukui H, Garcia S, Moraes CT (2006) Cytochrome c oxidase is required for the assembly/stability of respiratory complex I in mouse fibroblasts. *Mol. Cell. Biol.* 26: 4872–4881
- [49] Ding C, Wu Z, Huang L, Wang Y, Xue J, Chen S, Deng Z, Wang L, Song Z, Chen S (2015) Mitofilin and CHCHD6 physically interact with Sam50 to sustain cristae structure. *Sci. Rep.* 5: 16064
- [50] Dolezal P, Likic V, Tachezy J, Lithgow T (2006) Evolution of the molecular machines for protein import into mitochondria. *Science* 313: 314–318
- [51] Donzeau M, Káldi K, Adam A, Paschen S, Wanner G, Guiard B, Bauer MF, Neupert W, Brunner M (2000) Tim23 Links the Inner and Outer Mitochondrial Membranes. *Cell* 101: 401–412
- [52] Del Dotto V, Fogazza M, Carelli V, Rugolo M, Zanna C (2018a) Eight human OPA1 isoforms, long and short: What are they for? *Biochim. Biophys. Acta - Bioenerg.* 1859: 263–269
- [53] Del Dotto V, Fogazza M, Lenaers G, Rugolo M, Carelli V, Zanna C (2018b) OPA1: How much do we know to approach therapy? *Pharmacol. Res.* 131: 199–210
- [54] Del Dotto V, Mishra P, Vidoni S, Fogazza M, Maresca A, Caporali L, McCaffery JM, Cappelletti M, Baruffini E, Lenaers G, Chan D, Rugolo M, Carelli V, Zanna C (2017) OPA1 Isoforms in the Hierarchical Organization of Mitochondrial Functions. *Cell Rep.* 19: 2557–2571
- [55] Dudkina N V., Heinemeyer J, Keegstra W, Boekema EJ, Braun H-P (2005) Structure of dimeric ATP synthase from mitochondria: An angular association of monomers induces the strong curvature of the inner membrane. *FEBS Lett.* 579: 5769–5772
- [56] Edelheit O, Hanukoglu A, Hanukoglu I (2009) Simple and efficient site-directed mutagenesis using two single-primer reactions in parallel to generate mutants for protein structure-function studies. *BMC Biotechnol.* 9: 61
- [57] Egner A, Jakobs S, Hell SW (2002) Fast 100-nm resolution three-dimensional microscope reveals structural plasticity of mitochondria in live yeast. *Proc. Natl. Acad. Sci.* 99: 3370–3375
- [58] Eisenberg-Bord M, Shai N, Schuldiner M, Bohnert M (2016) A Tether Is a Tether Is a Tether: Tethering at Membrane Contact Sites. *Dev. Cell* 39: 395–409

- [59] Eramo MJ, Lisnyak V, Formosa LE, Ryan MT (2020) The ‘mitochondrial contact site and cristae organising system’ (MICOS) in health and human disease. *J. Biochem.* 167: 243–255
- [60] Everard-Gigot V, Dunn CD, Dolan BM, Brunner S, Jensen RE, Stuart RA (2005) Functional Analysis of Subunit e of the F₁F_o-ATP Synthase of the Yeast *Saccharomyces cerevisiae*: Importance of the N-Terminal Membrane Anchor Region. *Eukaryot. Cell* 4: 346–355
- [61] Eydt K, Davis KM, Behrendt C, Wittig I, Reichert AS (2017) Cristae architecture is determined by an interplay of the MICOS complex and the F₁F_o ATP synthase via Mic27 and Mic10. *Microb. Cell* 4: 259–272
- [62] Faccenda D, Tan CH, Seraphim A, Duchon MR, Campanella M (2013) IF1 limits the apoptotic-signalling cascade by preventing mitochondrial remodelling. *Cell Death Differ.* 20: 686–97
- [63] Faelber K, Dietrich L, Noel JK, Wollweber F, Pfitzner A-K, Mühleip A, Sánchez R, Kudryashev M, Chiaruttini N, Lilie H, Schlegel J, Rosenbaum E, Hessenberger M, Matthaeus C, Kunz S, von der Malsburg A, Noé F, Roux A, van der Laan M, Kühlbrandt W, et al (2019) Structure and assembly of the mitochondrial membrane remodelling GTPase Mgm1. *Nature* 571: 429–433
- [64] Faelber K, Posor Y, Gao S, Held M, Roske Y, Schulze D, Haucke V, Noé F, Daumke O (2011) Crystal structure of nucleotide-free dynamin. *Nature* 477: 556–60
- [65] Ford MGJ, Jenni S, Nunnari J (2011) The crystal structure of dynamin. *Nature* 477: 561–566
- [66] Frey TG, Mannella CA (2000) The internal structure of mitochondria. *Trends Biochem. Sci.* 25: 319–324
- [67] Frezza C, Cipolat S, Martins de Brito O, Micaroni M, Beznoussenko G V., Rudka T, Bartoli D, Polishuck RS, Danial NN, De Strooper B, Scorrano L (2006) OPA1 Controls Apoptotic Cristae Remodeling Independently from Mitochondrial Fusion. *Cell* 126: 177–189
- [68] Friedman JR, Mourier A, Yamada J, McCaffery JM, Nunnari J (2015) MICOS coordinates with respiratory complexes and lipids to establish mitochondrial inner membrane architecture. *Elife* 4: e07739
- [69] Ge Y, Shi X, Boopathy S, McDonald J, Smith AW, Chao LH (2020) Two forms of opa1 cooperate to complete fusion of the mitochondrial inner-membrane. *Elife* 9: e50973
- [70] Gebert M, Schrempp SG, Mehnert CS, Heißwolf AK, Oeljeklaus S, Ieva R, Bohnert M, von der Malsburg K, Wiese S, Kleinschroth T, Hunte C, Meyer HE, Haferkamp I, Guiard B, Warscheid B, Pfanner N, van der Laan M, Heisswolf AK, Oeljeklaus S, Ieva R, et al (2012) Mgr2 promotes coupling of the mitochondrial presequence translocase to partner complexes. *J. Cell Biol.* 197: 595–604
- [71] Giacomello M, Pyakurel A, Glytsou C, Scorrano L (2020) The cell biology of mitochondrial membrane dynamics. *Nat. Rev. Mol. Cell Biol.* 1: 95–109
- [72] Gibson DG, Young L, Chuang RY, Venter JC, Hutchison CA, Smith HO (2009) Enzymatic assembly of DNA molecules up to several hundred kilobases. *Nat. Methods* 6: 343–345
- [73] Gilkerson RW, Selker JML, Capaldi RA (2003) The cristal membrane of mitochondria is the principal site of oxidative phosphorylation. *FEBS Lett.* 546: 355–358
- [74] Glytsou C, Calvo E, Cogliati S, Mehrotra A, Anastasia I, Rigoni G, Raimondi A, Shintani N, Loureiro M, Vazquez J, Pellegrini L, Enriquez JA, Scorrano L, Soriano ME (2016) Optic Atrophy 1 Is Epistatic to the Core MICOS Component MIC60 in Mitochondrial Cristae Shape Control. *Cell Rep.* 17: 3024–3034

- [75] Gold VAM, Ieva R, Walter A, Pfanner N, van der Laan M, Kühlbrandt W, Huang H, Frohman M a (2014) Visualizing active membrane protein complexes by electron cryotomography. *Nat. Commun.* 5: 4129
- [76] Gomkale R, Cruz-Zaragoza LD, Suppanz I, Guiard B, Montoya J, Callegari S, Pacheu-Grau D, Warscheid B, Rehling P (2020) Defining the Substrate Spectrum of the TIM22 Complex Identifies Pyruvate Carrier Subunits as Unconventional Cargos. *Curr. Biol.* 30: 1119-1127.e5
- [77] Gottschalk B, Klec C, Leitinger G, Bernhart E, Rost R, Bischof H, Madreiter-Sokolowski CT, Radulović S, Eroglu E, Sattler W, Waldeck-Weiermair M, Malli R, Graier WF (2019) MICU1 controls cristae junction and spatially anchors mitochondrial Ca²⁺ uniporter complex. *Nat. Commun.* 10: 3732
- [78] Guarani V, Jardel C, Chrétien D, Lombès A, Bénit P, Labasse C, Lacène E, Bourillon A, Imbard A, Benoist J-F, Dorboz I, Gilleron M, Goetzman ES, Gaignard P, Slama A, Elmaleh-Bergès M, Romero NB, Rustin P, Ogier de Baulny H, Paulo JA, et al (2016) QIL1 mutation causes MICOS disassembly and early onset fatal mitochondrial encephalopathy with liver disease. *Elife* 5: e17163
- [79] Guarani V, McNeill EM, Paulo J a, Huttlin EL, Fröhlich F, Gygi SP, Vactor D Van, Wade Harper J (2015) QIL1 is a novel mitochondrial protein required for MICOS complex stability and cristae morphology. *Elife* 4: e06265
- [80] Guo H, Bueler SA, Rubinstein JL (2017) Atomic model for the dimeric FO region of mitochondrial ATP synthase. *Science* 358: 936–940
- [81] Hackenbrock CR (1966) Ultrastructural bases for metabolically linked mechanical activity in mitochondria. I. Reversible ultrastructural changes with change in metabolic steady state in isolated liver mitochondria. *J. Cell Biol.* 30: 269–297
- [82] Hackenbrock CR (1968) Ultrastructural bases for metabolically linked mechanical activity in mitochondria. II. Electron transport-linked ultrastructural transformations in mitochondria. *J. Cell Biol.* 37: 345–369
- [83] Hahn A, Parey K, Bublitz M, Mills DJ, Zickermann V, Vonck J, Kühlbrandt W, Meier T (2016) Structure of a Complete ATP Synthase Dimer Reveals the Molecular Basis of Inner Mitochondrial Membrane Morphology. *Mol. Cell* 63: 445–456
- [84] Hansen KG, Aviram N, Laborenz J, Bibi C, Meyer M, Spang A, Schuldiner M, Herrmann JM (2018) An ER surface retrieval pathway safeguards the import of mitochondrial membrane proteins in yeast. *Science* 361: 1118–1122
- [85] Hansen KG, Herrmann JM (2019) Transport of Proteins into Mitochondria. *Protein J.* 38: 330–342
- [86] Harner ME, Unger AK, Geerts WJ, Mari M, Izawa T, Stenger M, Geimer S, Reggiori F, Westermann B, Neupert W (2016) An evidence based hypothesis on the existence of two pathways of mitochondrial crista formation. *Elife* 5: e18853
- [87] Harner M, Körner C, Walther D, Mokranjac D, Kaesmacher J, Welsch U, Griffith J, Mann M, Reggiori F, Neupert W (2011) The mitochondrial contact site complex, a determinant of mitochondrial architecture. *EMBO J.* 30: 4356–4370
- [88] Hashimi H (2019) A parasite’s take on the evolutionary cell biology of MICOS. *PLOS Pathog.* 15: e1008166

- [89] Herlan M, Vogel F, Bornhövd C, Neupert W, Reichert AS (2003) Processing of Mgm1 by the Rhomboid-type Protease Pcp1 Is Required for Maintenance of Mitochondrial Morphology and of Mitochondrial DNA. *J. Biol. Chem.* 278: 27781–27788
- [90] Hessenberger M, Zerbes RM, Rampelt H, Kunz S, Xavier AH, Purfürst B, Lilie H, Pfanner N, van der Laan M, Daumke O (2017) Regulated membrane remodeling by Mic60 controls formation of mitochondrial crista junctions. *Nat. Commun.* 8: 15258
- [91] Hoppins S, Collins SR, Cassidy-Stone A, Hummel E, DeVay RM, Lackner LL, Westermann B, Schuldiner M, Weissman JS, Nunnari J (2011) A mitochondrial-focused genetic interaction map reveals a scaffold-like complex required for inner membrane organization in mitochondria. *J. Cell Biol.* 195: 323–340
- [92] Horvath SE, Rampelt H, Oeljeklaus S, Warscheid B, van der Laan M, Pfanner N (2015) Role of membrane contact sites in protein import into mitochondria. *Protein Sci.* 24: 277–297
- [93] Huynen MA, Mühlmeister M, Gotthardt K, Guerrero-Castillo S, Brandt U (2016) Evolution and structural organization of the mitochondrial contact site (MICOS) complex and the mitochondrial intermembrane space bridging (MIB) complex. *Biochim. Biophys. Acta* 1863: 91–101
- [94] Ieva R, Schrempp SG, Opaliński Ł, Wollweber F, Höß P, Heißwolf AK, Gebert M, Zhang Y, Guiard B, Rospert S, Becker T, Chacinska A, Pfanner N, van der Laan M (2014) Mgr2 Functions as Lateral Gatekeeper for Preprotein Sorting in the Mitochondrial Inner Membrane. *Mol. Cell* 56: 641–652
- [95] Ikon N, Ryan RO (2017) Cardiolipin and mitochondrial cristae organization. *Biochim. Biophys. Acta - Biomembr.* 1859: 1156–1163
- [96] Ioakeimidis F, Ott C, Kozjak-Pavlovic V, Violitzi F, Rinotas V, Makrinou E, Eliopoulos E, Fasseas C, Kollias G, Douni E (2014) A Splicing Mutation in the Novel Mitochondrial Protein DNAJC11 Causes Motor Neuron Pathology Associated with Cristae Disorganization, and Lymphoid Abnormalities in Mice. *PLoS One* 9: e104237
- [97] Itakura E, Zavodszky E, Shao S, Wohlever ML, Keenan RJ, Hegde RS (2016) Ubiquilins Chaperone and Triage Mitochondrial Membrane Proteins for Degradation. *Mol. Cell* 63: 21–33
- [98] Janer A, Prudent J, Paupe V, Fahiminiya S, Majewski J, Sgarioto N, Des Rosiers C, Forest A, Lin Z, Gingras A, Mitchell G, McBride HM, Shoubridge EA (2016) SLC25A46 is required for mitochondrial lipid homeostasis and cristae maintenance and is responsible for Leigh syndrome. *EMBO Mol. Med.* 8: 1019–1038
- [99] Jans DC, Wurm CA, Riedel D, Wenzel D, Stagge F, Deckers M, Rehling P, Jakobs S (2013) STED super-resolution microscopy reveals an array of MINOS clusters along human mitochondria. *Proc. Natl. Acad. Sci.* 110: 8936–8941
- [100] Jiko C, Davies KM, Shinzawa-Itoh K, Tani K, Maeda S, Mills DJ, Tsukihara T, Fujiyoshi Y, Kühlbrandt W, Gerle C (2015) Bovine F1Fo ATP synthase monomers bend the lipid bilayer in 2D membrane crystals. *Elife* 4: e06119
- [101] Jimenez L, Laporte D, Duvezin-Caubet S, Courtout F, Sagot I (2014) Mitochondrial ATP synthases cluster as discrete domains that reorganize with the cellular demand for oxidative phosphorylation. *J. Cell Sci.* 127: 719–26

- [102] John GB, Shang Y, Li L, Renken C, Mannella CA, Selker JML, Rangell L, Bennett MJ, Zha J (2005) The mitochondrial inner membrane protein mitofilin controls cristae morphology. *Mol. Biol. Cell* 16: 1543–1554
- [103] Johnston AJ, Hoogenraad J, Dougan DA, Truscott KN, Yano M, Mori M, Hoogenraad NJ, Ryan MT (2002) Insertion and assembly of human Tom7 into the preprotein translocase complex of the outer mitochondrial membrane. *J. Biol. Chem.* 277: 42197–42204
- [104] Jones BA, Fangman WL (1992) Mitochondrial DNA maintenance in yeast requires a protein containing a region related to the GTP-binding domain of dynamin. *Genes Dev.* 6: 380–389
- [105] Jores T, Lawatscheck J, Beke V, Franz-Wachtel M, Yunoki K, Fitzgerald JC, Macek B, Endo T, Kalbacher H, Buchner J, Rapaport D (2018) Cytosolic Hsp70 and Hsp40 chaperones enable the biogenesis of mitochondrial β -barrel proteins. *J. Cell Biol.* 217: 3091–3108
- [106] Kalia R, Wang RY-R, Yusuf A, Thomas P V., Agard DA, Shaw JM, Frost A (2018) Structural basis of mitochondrial receptor binding and constriction by DRP1. *Nature* 558: 401–405
- [107] Kaurov I, Vancová M, Schimanski B, Cadena LR, Heller J, Bílý T, Potěšil D, Eichenberger C, Bruce H, Oeljeklaus S, Warscheid B, Zdráhal Z, Schneider A, Lukeš J, Hashimi H (2018) The Diverged Trypanosome MICOS Complex as a Hub for Mitochondrial Cristae Shaping and Protein Import. *Curr. Biol.* 28: 3393-3407.e5
- [108] Khalifat N, Puff N, Bonneau S, Fournier J-B, Angelova MI (2008) Membrane Deformation under Local pH Gradient: Mimicking Mitochondrial Cristae Dynamics. *Biophys. J.* 95: 4924–4933
- [109] Kondadi AK, Anand R, Hänsch S, Urbach J, Zobel T, Wolf DM, Segawa M, Liesa M, Shirihai OS, Weidtkamp-Peters S, Reichert AS (2020) Cristae undergo continuous cycles of membrane remodelling in a MICOS-dependent manner. *EMBO Rep.* 21: 654541
- [110] Kong L, Sochacki KA, Wang H, Fang S, Canagarajah B, Kehr AD, Rice WJ, Strub M-P, Taraska JW, Hinshaw JE (2018) Cryo-EM of the dynamin polymer assembled on lipid membrane. *Nature* 560: 258–262
- [111] Koob S, Barrera M, Anand R, Reichert AS (2015) The non-glycosylated isoform of MIC26 is a constituent of the mammalian MICOS complex and promotes formation of crista junctions. *Biochim. Biophys. Acta - Mol. Cell Res.* 1853: 1551–1563
- [112] Korner C, Barrera M, Dukanovic J, Eydt K, Harner M, Rabl R, Vogel F, Rapaport D, Neupert W, Reichert AS (2012) The C-terminal domain of Fcjl is required for formation of crista junctions and interacts with the TOB/SAM complex in mitochondria. *Mol. Biol. Cell* 23: 2143–2155
- [113] Kühlbrandt W (2014) The Resolution Revolution. *Science* 343: 1443–1444
- [114] Kühlbrandt W (2019) Structure and Mechanisms of F-Type ATP Synthases. *Annu. Rev. Biochem.* 88: 515–549
- [115] Kutik S, Rissler M, Guan XL, Guiard B, Shui G, Gebert N, Heacock PN, Rehling P, Dowhan W, Wenk MR, Pfanner N, Wiedemann N (2008) The translocator maintenance protein Tam41 is required for mitochondrial cardiolipin biosynthesis. *J. Cell Biol.* 183: 1213–21
- [116] van der Laan M, Wiedemann N, Mick DU, Guiard B, Rehling P, Pfanner N (2006) A Role for Tim21 in Membrane-Potential-Dependent Preprotein Sorting in Mitochondria. *Curr. Biol.* 16: 2271–2276

- [117] Van Laar VS, Anthony Otero P, Hastings TG, Berman SB (2019) Potential role of MIC60/mitofilin in Parkinson's disease. *Front. Neurosci.* 12: 898
- [118] Laemmli UK (1970) Cleavage of structural proteins during the assembly of the head of bacteriophage T4. *Nature* 227: 680–685
- [119] Lapuente-Brun E, Moreno-Loshuertos R, Acín-Pérez R, Latorre-Pellicer A, Colás C, Balsa E, Perales-Clemente E, Quirós PM, Calvo E, Rodríguez-Hernández M a, Navas P, Cruz R, Carracedo Á, López-Otín C, Pérez-Martos A, Fernández-Silva P, Fernández-Vizarra E, Enríquez JA (2013) Supercomplex Assembly Determines Electron Flux in the Mitochondrial Electron Transport Chain. *Science* 340: 1567–1570
- [120] Lee H, Smith SB, Sheu S-S, Yoon Y (2020) The short variant of optic atrophy 1 (OPA1) improves cell survival under oxidative stress. *J. Biol. Chem.* 295: 6543–6560
- [121] Lee H, Smith SB, Yoon Y (2017) The short variant of the mitochondrial dynamin OPA1 maintains mitochondrial energetics and cristae structure. *J. Biol. Chem.* 292: 7115–7130
- [122] Lewis SC, Uchiyama LF, Nunnari J (2016) ER-mitochondria contacts couple mtDNA synthesis with mitochondrial division in human cells. *Science* 353: aaf5549
- [123] Li H, Ruan Y, Zhang K, Jian F, Hu C, Miao L, Gong L, Sun L, Zhang X, Chen S, Chen H, Liu D, Song Z (2016) Mic60/Mitofilin determines MICOS assembly essential for mitochondrial dynamics and mtDNA nucleoid organization. *Cell Death Differ.* 23: 380–392
- [124] Longtine MS, Mckenzie III A, Demarini DJ, Shah NG, Wach A, Brachat A, Philippsen P, Pringle JR (1998) Additional modules for versatile and economical PCR-based gene deletion and modification in *Saccharomyces cerevisiae*. *Yeast* 14: 953–961
- [125] Lööke M, Kristjuhan K, Kristjuhan A (2011) Extraction of Genomic Dna From Yeasts for PCR-Based Applications. *Biotechniques* 50: 325–328
- [126] von der Malsburg K, Müller JM, Bohnert M, Oeljeklaus S, Kwiatkowska P, Becker T, Loniewska-Lwowska A, Wiese S, Rao S, Milenkovic D, Hutu DP, Zerbes RM, Schulze-Specking A, Meyer HE, Martinou J-C, Rospert S, Rehling P, Meisinger C, Veenhuis M, Warscheid B, et al (2011) Dual Role of Mitofilin in Mitochondrial Membrane Organization and Protein Biogenesis. *Dev. Cell* 21: 694–707
- [127] Mannella CA (2006) Structure and dynamics of the mitochondrial inner membrane cristae. *Biochim. Biophys. Acta - Mol. Cell Res.* 1763: 542–548
- [128] Maranzana E, Barbero G, Falasca AI, Lenaz G, Genova ML (2013) Mitochondrial respiratory supercomplex association limits production of reactive oxygen species from complex I. *Antioxid. Redox Signal.* 19: 1469–80
- [129] Marroquin LD, Hynes J, Dykens JA, Jamieson JD, Will Y (2007) Circumventing the Crabtree Effect: Replacing Media Glucose with Galactose Increases Susceptibility of HepG2 Cells to Mitochondrial Toxicants. *Toxicol. Sci.* 97: 539–547
- [130] McBride HM, Neuspiel M, Wasiak S (2006) Mitochondria: More Than Just a Powerhouse. *Curr. Biol.* 16: 551–560
- [131] McQuibban GA, Saurya S, Freeman M (2003) Mitochondrial membrane remodelling regulated by a conserved rhomboid protease. *Nature* 423: 537–541

- [132] Meeusen S, DeVay R, Block J, Cassidy-Stone A, Wayson S, McCaffery JM, Nunnari J (2006) Mitochondrial Inner-Membrane Fusion and Crista Maintenance Requires the Dynamin-Related GTPase Mgm1. *Cell* 127: 383–395
- [133] Mehnert CS, Rampelt H, Gebert M, Oeljeklaus S, Schrempp SG, Kochbeck L, Guiard B, Warscheid B, van der Laan M (2014) The Mitochondrial ADP/ATP Carrier Associates with the Inner Membrane Presequence Translocase in a Stoichiometric Manner. *J. Biol. Chem.* 289: 27352–27362
- [134] Meisinger C, Pfanner N, Truscott KN (2006) Isolation of yeast mitochondria. *Methods Mol. Biol.* 313: 33–39
- [135] Merkwirth C, Dargazanli S, Tatsuta T, Geimer S, Löwer B, Wunderlich FT, von Kleist-Retzow J-CC, Waisman A, Westermann B, Langer T (2008) Prohibitins control cell proliferation and apoptosis by regulating OPA1-dependent cristae morphogenesis in mitochondria. *Genes Dev.* 22: 476–488
- [136] Michaud M, Gros V, Tardif M, Brugière S, Ferro M, Prinz WA, Toulmay A, Mathur J, Wozny M, Falconet D, Maréchal E, Block MA, Jouhet J (2016) AtMic60 Is Involved in Plant Mitochondria Lipid Trafficking and Is Part of a Large Complex. *Curr. Biol.* 26: 627–639
- [137] Milenkovic D, Blaza JN, Larsson NG, Hirst J (2017) The Enigma of the Respiratory Chain Supercomplex. *Cell Metab.* 25: 765–776
- [138] Mishra P, Carelli V, Manfredi G, Chan DC (2014) Proteolytic cleavage of Opa1 stimulates mitochondrial inner membrane fusion and couples fusion to oxidative phosphorylation. *Cell Metab.* 19: 630–641
- [139] Morgenstern M, Stiller SB, Lübbert P, Peikert CD, Dannenmaier S, Drepper F, Weill U, Höß P, Feuerstein R, Gebert M, Bohnert M, van der Laan M, Schuldiner M, Schütze C, Oeljeklaus S, Pfanner N, Wiedemann N, Warscheid B (2017) Definition of a High-Confidence Mitochondrial Proteome at Quantitative Scale. *Cell Rep.* 19: 2836–2852
- [140] Mottis A, Herzig S, Auwerx J (2019) Mitocellular communication: Shaping health and disease. *Science* 366: 827–832
- [141] Muñoz-Gómez SA, Slamovits CH, Dacks JB, Baier KA, Spencer KD, Wideman JG (2015) Ancient Homology of the Mitochondrial Contact Site and Cristae Organizing System Points to an Endosymbiotic Origin of Mitochondrial Cristae. *Curr. Biol.* 25: 1489–1495
- [142] Muñoz-Gómez SA, Wideman JG, Roger AJ, Slamovits CH, Agashe D (2017) The origin of mitochondrial cristae from alphaproteobacteria. *Mol. Biol. Evol.* 34: 943–956
- [143] Murley A, Lackner LL, Osman C, West M, Voeltz GK, Walter P, Nunnari J (2013) ER-associated mitochondrial division links the distribution of mitochondria and mitochondrial DNA in yeast. *Elife* 2: e00422
- [144] Murley A, Nunnari J (2016) The Emerging Network of Mitochondria-Organelle Contacts. *Mol. Cell* 61: 648–653
- [145] Nagashima S, Tábara L-C, Tilokani L, Paupe V, Anand H, Pogson JH, Zunino R, McBride HM, Prudent J (2020) Golgi-derived PI(4)P-containing vesicles drive late steps of mitochondrial division. *Science* 367: 1366–1371

- [146] Nakamura S, Matsui A, Akabane S, Tamura Y, Hatano A, Miyano Y, Omote H, Kajikawa M, Maenaka K, Moriyama Y, Endo T, Oka T (2020) The mitochondrial inner membrane protein LETM1 modulates cristae organization through its LETM domain. *Commun. Biol.* 3: 99
- [147] Ohlmeier S, Kastaniotis AJ, Hiltunen JK, Bergmann U (2004) The Yeast Mitochondrial Proteome, a Study of Fermentative and Respiratory Growth. *J. Biol. Chem.* 279: 3956–3979
- [148] Olichon A, ElAchouri G, Baricault L, Delettre C, Belenguer P, Lenaers G (2007) OPA1 alternate splicing uncouples an evolutionary conserved function in mitochondrial fusion from a vertebrate restricted function in apoptosis. *Cell Death Differ.* 14: 682–692
- [149] Olichon A, Emorine LJ, Descoins E, Pelloquin L, Brichese L, Gas N, Guillou E, Delettre C, Valette A, Hamel CP, Ducommun B, Lenaers G, Belenguer P (2002) The human dynamin-related protein OPA1 is anchored to the mitochondrial inner membrane facing the intermembrane space. *FEBS Lett.* 523: 171–176
- [150] Opaliński Ł, Song J, Priesnitz C, Wenz L-S, Oeljeklaus S, Warscheid B, Pfanner N, Becker T (2018) Recruitment of Cytosolic J-Proteins by TOM Receptors Promotes Mitochondrial Protein Biogenesis. *Cell Rep.* 25: 2036–2043
- [151] Orlova M, Barrett L, Kuchin S (2008) Detection of endogenous Snf1 and its activation state: application to *Saccharomyces* and *Candida* species. *Yeast* 25: 745–754
- [152] Osman C, Merkwirth C, Langer T (2009) Prohibitins and the functional compartmentalization of mitochondrial membranes. *J. Cell Sci.* 122: 3823–3830
- [153] Ott C, Ross K, Straub S, Thiede B, Gotz M, Goosmann C, Krischke M, Mueller MJ, Krohne G, Rudel T, Kozjak-Pavlovic V (2012) Sam50 Functions in Mitochondrial Intermembrane Space Bridging and Biogenesis of Respiratory Complexes. *Mol. Cell. Biol.* 32: 1173–1188
- [154] Ott C, Dorsch E, Fraunholz M, Straub S, Kozjak-Pavlovic V (2015) Detailed Analysis of the Human Mitochondrial Contact Site Complex Indicate a Hierarchy of Subunits. *PLoS One* 10: e0120213
- [155] Pánek T, Eliáš M, Vancová M, Lukeš J, Hashimi H (2020) Returning to the Fold for Lessons in Mitochondrial Crista Diversity and Evolution. *Curr. Biol.* 30: R575–R588
- [156] Patten DA, Wong J, Khacho M, Soubannier V, Mailloux RJ, Pilon-Larose K, MacLaurin JG, Park DS, McBride HM, Trinkle-Mulcahy L, Harper M, Germain M, Slack RS (2014) OPA1-dependent cristae modulation is essential for cellular adaptation to metabolic demand. *EMBO J.* 33: 2676–2691
- [157] Paumard P, Vaillier J, Couлары B, Schaeffer J, Soubannier V, Mueller DM, Brèthes D, Di Rago JP, Velours J (2002) The ATP synthase is involved in generating mitochondrial cristae morphology. *EMBO J.* 21: 221–230
- [158] Pfanner N, Hartl FU, Guiard B, Neupert W (1987) Mitochondrial precursor proteins are imported through a hydrophilic membrane environment. *Eur. J. Biochem.* 169: 289–293
- [159] Pfanner N, van der Laan M, Amati P, Capaldi RA, Caudy AA, Chacinska A, Darshi M, Deckers M, Hoppins S, Icho T, Jakobs S, Ji J, Kozjak-Pavlovic V, Meisinger C, Odgren PR, Park SK, Rehling P, Reichert AS, Sheikh MS, Taylor SS, et al (2014) Uniform nomenclature for the mitochondrial contact site and cristae organizing system. *J. Cell Biol.* 204: 1083–1086
- [160] Pfanner N, Warscheid B, Wiedemann N (2019) Mitochondrial proteins: from biogenesis to functional networks. *Nat. Rev. Mol. Cell Biol.* 20: 267–284

- [161] Pfeiffer K, Gohil V, Stuart RA, Hunte C, Brandt U, Greenberg ML, Schägger H (2003) Cardiolipin Stabilizes Respiratory Chain Supercomplexes. *J. Biol. Chem.* 278: 52873–52880
- [162] Picard M, McManus MJ, Csordás G, Várnai P, Dorn II GW, Williams D, Hajnóczky G, Wallace DC (2015) Trans-mitochondrial coordination of cristae at regulated membrane junctions. *Nat. Commun.* 6: 6259
- [163] Plecítá-Hlavatá L, Engstová H, Alán LM, Špaček T, Dlasková A, Smolková K, Špačková J, Tauber J, Strádalová V, Malínský J, Lessard M, Bewersdorf J, Ježek P (2016) Hypoxic HepG2 cell adaptation decreases ATP synthase dimers and ATP production in inflated cristae by mitofilin down-regulation concomitant to MICOS clustering. *FASEB J.* 30: 1941–1957
- [164] Priesnitz C, Pfanner N, Becker T (2020) Studying protein import into mitochondria. In *Membrane Protein Transport* pp 45–79. Elsevier Inc.
- [165] Qiu J, Wenz L-S, Zerbes RM, Oeljeklaus S, Bohnert M, Stroud DA, Wirth C, Ellenrieder L, Thornton N, Kutik S, Wiese S, Schulze-Specking A, Zufall N, Chacinska A, Guiard B, Hunte C, Warscheid B, van der Laan M, Pfanner N, Wiedemann N, et al (2013) Coupling of Mitochondrial Import and Export Translocases by Receptor-Mediated Supercomplex Formation. *Cell* 154: 596–608
- [166] Quintana-Cabrera R, Quirin C, Glytsou C, Corrado M, Urbani A, Pellattiero A, Calvo E, Vázquez J, Enríquez JA, Gerle C, Soriano ME, Bernardi P, Scorrano L (2018) The cristae modulator Optic atrophy 1 requires mitochondrial ATP synthase oligomers to safeguard mitochondrial function. *Nat. Commun.* 9: 3399
- [167] Rabl R, Soubannier V, Scholz R, Vogel F, Mendl N, Vasiljev-Neumeyer A, Körner C, Jagasia R, Keil T, Baumeister W, Cyrklaff M, Neupert W, Reichert AS (2009) Formation of cristae and crista junctions in mitochondria depends on antagonism between Fcj1 and Su e / g. *J. Cell Biol.* 185: 1047–1063
- [168] Rampelt H, Bohnert M, Zerbes RM, Horvath SE, Warscheid B, Pfanner N, van der Laan M (2017) Mic10, a Core Subunit of the Mitochondrial Contact Site and Cristae Organizing System, Interacts with the Dimeric F1Fo -ATP Synthase. *J. Mol. Biol.* 429: 1162–1170
- [169] Rampelt H, Sucec I, Bersch B, Horten P, Perschil I, Martinou J-C, van der Laan M, Wiedemann N, Schanda P, Pfanner N (2020) The mitochondrial carrier pathway transports non-canonical substrates with an odd number of transmembrane segments. *BMC Biol.* 18: 2
- [170] Rampelt H, Wollweber F, Gerke C, de Boer R, van der Klei IJ, Bohnert M, Pfanner N, van der Laan M (2018) Assembly of the Mitochondrial Cristae Organizer Mic10 Is Regulated by Mic26–Mic27 Antagonism and Cardiolipin. *J. Mol. Biol.* 430: 1883–1890
- [171] Ran FA, Hsu PD, Wright J, Agarwala V, Scott DA, Zhang F (2013) Genome engineering using the CRISPR-Cas9 system. *Nat. Protoc.* 8: 2281–2308
- [172] Reichert AS, Neupert W (2002) Contact sites between the outer and inner membrane of mitochondria-role in protein transport. *Biochim. Biophys. Acta* 1592: 41–49
- [173] Renken C, Siragusa G, Perkins G, Washington L, Nulton J, Salamon P, Frey TG (2002) A thermodynamic model describing the nature of the crista junction: A structural motif in the mitochondrion. *J. Struct. Biol.* 138: 137–144
- [174] Rieger B, Junge W, Busch KB (2014) Lateral pH gradient between OXPHOS complex IV and F0F1 ATP-synthase in folded mitochondrial membranes. *Nat. Commun.* 5: 3103

- [175] Roger AJ, Muñoz-Gómez SA, Kamikawa R (2017) The Origin and Diversification of Mitochondria. *Curr. Biol.* 27: R1177–R1192
- [176] Rujiviphat J, Wong MK, Won A, Shih YL, Yip CM, McQuibban GA (2015) Mitochondrial Genome Maintenance 1 (Mgm1) Protein Alters Membrane Topology and Promotes Local Membrane Bending. *J. Mol. Biol.* 427: 2599–2609
- [177] Russ WP, Engelman DM (2000) The GxxxG motif: A framework for transmembrane helix-helix association. *J. Mol. Biol.* 296: 911–919
- [178] Sakowska P, Jans DC, Mohanraj K, Riedel D, Jakobs S, Chacinska A (2015) The Oxidation Status of Mic19 Regulates MICOS Assembly. *Mol. Cell. Biol.* 35: 4222–4237
- [179] Salewskij K, Rieger B, Hager F, Arroum T, Duwe P, Villalta J, Colgiati S, Richter CP, Psathaki OE, Enriquez JA, Dellmann T, Busch KB (2020) The spatio-temporal organization of mitochondrial FIFO ATP synthase in cristae depends on its activity mode. *Biochim. Biophys. Acta - Bioenerg.* 1861: 148091
- [180] Sastri M, Darshi M, Mackey M, Ramachandra R, Ju S, Phan S, Adams S, Stein K, Douglas CR, Kim JJ, Ellisman MH, Taylor SS, Perkins GA (2017) Sub-mitochondrial localization of the genetic-tagged mitochondrial intermembrane space-bridging components Mic19, Mic60 and Sam50. *J. Cell Sci.* 130: 3248–3260
- [181] Schäfer E, Seelert H, Reifschneider NH, Krause F, Dencher NA, Vonck J (2006) Architecture of Active Mammalian Respiratory Chain Supercomplexes. *J. Biol. Chem.* 281: 15370–15375
- [182] Schägger H, Pfeiffer K (2000) Supercomplexes in the respiratory chains of yeast and mammalian mitochondria. *EMBO J.* 19: 1777–1783
- [183] Schägger H, De Coo R, Bauer MF, Hofmann S, Godino C, Brandt U (2004) Significance of respirasomes for the assembly/stability of human respiratory chain complex I. *J. Biol. Chem.* 279: 36349–36353
- [184] Schägger H, von Jagow G (1991) Blue native electrophoresis for isolation of membrane protein complexes in enzymatically active form. *Anal. Biochem.* 199: 223–231
- [185] Schindelin J, Arganda-Carreras I, Frise E, Kaynig V, Longair M, Pietzsch T, Preibisch S, Rueden C, Saalfeld S, Schmid B, Tinevez J-Y, White DJ, Hartenstein V, Eliceiri K, Tomancak P, Cardona A (2012) Fiji: an open-source platform for biological-image analysis. *Nat. Methods* 9: 676–682
- [186] Schleyer M, Neupert W (1985) Transport of proteins into mitochondria: translocational intermediates spanning contact sites between outer and inner membranes. *Cell* 43: 339–350
- [187] Schweppe DK, Chavez JD, Lee CF, Caudal A, Kruse SE, Stuppard R, Marcinek DJ, Shadel GS, Tian R, Bruce JE (2017) Mitochondrial protein interactome elucidated by chemical cross-linking mass spectrometry. *Proc. Natl. Acad. Sci.* 114: 1732–1737
- [188] Scorrano L, Ashiya M, Buttle K, Weiler S, Oakes SA, Mannella CA, Korsmeyer SJ (2002) A Distinct Pathway Remodels Mitochondrial Cristae and Mobilizes Cytochrome c during Apoptosis. *Dev. Cell* 2: 55–67
- [189] Shiota T, Mabuchi H, Tanaka-Yamano S, Yamano K, Endo T (2011) In vivo protein-interaction mapping of a mitochondrial translocator protein Tom22 at work. *Proc. Natl. Acad. Sci.* 108: 15179–15183

- [190] Sickmann A, Reinders J, Wagner Y, Joppich C, Zahedi R, Meyer HE, Schonfisch B, Perschil I, Chacinska A, Guiard B, Rehling P, Pfanner N, Meisinger C (2003) The proteome of *Saccharomyces cerevisiae* mitochondria. *Proc. Natl. Acad. Sci.* 100: 13207–13212
- [191] Sikorski RS, Hieter P (1989) A system of shuttle vectors and yeast host strains designed for efficient manipulation of DNA in *Saccharomyces cerevisiae*. *Genetics* 122: 19–27
- [192] Song Z, Chen H, Fiket M, Alexander C, Chan DC (2007) OPA1 processing controls mitochondrial fusion and is regulated by mRNA splicing, membrane potential, and Yme1L. *J. Cell Biol.* 178: 749–755
- [193] Steffen J, Vashisht AA, Wan J, Jen JC, Claypool SM, James A, Wohlschlegel JA, Koehler CM (2017) Rapid degradation of mutant SLC25A46 by the ubiquitin-proteasome system results in MFN1/2-mediated hyperfusion of mitochondria. *Mol. Biol. Cell* 28: 600–612
- [194] Stephan T, Roesch A, Riedel D, Jakobs S (2019) Live-cell STED nanoscopy of mitochondrial cristae. *Sci. Rep.* 9: 12419
- [195] Stoldt S, Stephan T, Jans DC, Brüser C, Lange F, Keller-Findeisen J, Riedel D, Hell SW, Jakobs S (2019) Mic60 exhibits a coordinated clustered distribution along and across yeast and mammalian mitochondria. *Proc. Natl. Acad. Sci.* 116: 9853–9858
- [196] Stoldt S, Wenzel D, Kehrein K, Riedel D, Ott M, Jakobs S (2018) Spatial orchestration of mitochondrial translation and OXPHOS complex assembly. *Nat. Cell Biol.* 20: 528–534
- [197] Strauss M, Hofhaus G, Schröder RR, Kühlbrandt W (2008) Dimer ribbons of ATP synthase shape the inner mitochondrial membrane. *EMBO J.* 27: 1154–1160
- [198] Stroud DA, Surgenor EE, Formosa LE, Reljic B, Frazier AE, Dibley MG, Osellame LD, Stait T, Beilharz TH, Thorburn DR, Salim A, Ryan MT (2016) Accessory subunits are integral for assembly and function of human mitochondrial complex I. *Nature* 538: 123–126
- [199] Tamura Y, Harada Y, Yamano K, Watanabe K, Ishikawa D, Ohshima C, Nishikawa S, Yamamoto H, Endo T (2006) Identification of Tam41 maintaining integrity of the TIM23 protein translocator complex in mitochondria. *J. Cell Biol.* 174: 631–637
- [200] Tang J, Zhang K, Dong J, Yan C, Hu C, Ji H, Chen L, Chen S, Zhao H, Song Z (2020) Sam50–Mic19–Mic60 axis determines mitochondrial cristae architecture by mediating mitochondrial outer and inner membrane contact. *Cell Death Differ.* 27: 146–160
- [201] Tarasenko D, Barbot M, Jans DC, Kroppen B, Sadowski B, Heim G, Möbius W, Jakobs S, Meinecke M (2017) The MICOS component Mic60 displays a conserved membrane-bending activity that is necessary for normal cristae morphology. *J. Cell Biol.* 216: 889–899
- [202] Teixeira FK, Sanchez CG, Hurd TR, Seifert JRK, Czech B, Preall JB, Hannon GJ, Lehmann R (2015) ATP synthase promotes germ cell differentiation independent of oxidative phosphorylation. *Nat. Cell Biol.* 17: 689–696
- [203] Toth A, Meyrat A, Stoldt S, Santiago R, Wenzel D, Jakobs S, von Ballmoos C, Ott M (2020) Kinetic coupling of the respiratory chain with ATP synthase, but not proton gradients, drives ATP production in cristae membranes. *Proc. Natl. Acad. Sci.* 117: 2412–2421
- [204] Tran DM, Ishiwata-Kimata Y, Mai TC, Kubo M, Kimata Y (2019) The unfolded protein response alongside the diauxic shift of yeast cells and its involvement in mitochondria enlargement. *Sci. Rep.* 9: 12780

- [205] Trouillard M, Meunier B, Rappaport F (2011) Questioning the functional relevance of mitochondrial supercomplexes by time-resolved analysis of the respiratory chain. *Proc. Natl. Acad. Sci.* 108: E1027–E1034
- [206] Tu BP, Kudlicki A, Rowicka M, McKnight SL (2005) Logic of the yeast metabolic cycle: Temporal compartmentalization of cellular processes. *Science* 310: 1152–1158
- [207] Turkieh A, Caubère C, Barutaut M, Desmoulin F, Harmancey R, Galinier M, Berry M, Dambrin C, Polidori C, Casteilla L, Koukoui F, Rouet P, Smih F (2014) Apolipoprotein O is mitochondrial and promotes lipotoxicity in heart. *J. Clin. Invest.* 124: 2277–2286
- [208] Vafai SB, Mootha VK (2012) Mitochondrial disorders as windows into an ancient organelle. *Nature* 491: 374–83
- [209] Varabyova A, Topf U, Kwiatkowska P, Wrobel L, Kaus-Drobek M, Chacinska A (2013) Mia40 and MINOS act in parallel with Ccs1 in the biogenesis of mitochondrial Sod1. *FEBS J.* 280: 4943–4959
- [210] Varanita T, Soriano ME, Romanello V, Zaglia T, Quintana-Cabrera R, Semenzato M, Menabò R, Costa V, Civiletto G, Pesce P, Viscomi C, Zeviani M, Di Lisa F, Mongillo M, Sandri M, Scorrano L (2015) The Opa1-Dependent Mitochondrial Cristae Remodeling Pathway Controls Atrophic, Apoptotic, and Ischemic Tissue Damage. *Cell Metab.* 21: 834–844
- [211] Vempati UD, Han X, Moraes CT (2009) Lack of Cytochrome c in Mouse Fibroblasts Disrupts Assembly/Stability of Respiratory Complexes I and IV. *J. Biol. Chem.* 284: 4383–4391
- [212] Vincent AE, Ng YS, White K, Davey T, Mannella C, Falkous G, Feeney C, Schaefer AM, McFarland R, Gorman GS, Taylor RW, Turnbull DM, Picard M (2016) The Spectrum of Mitochondrial Ultrastructural Defects in Mitochondrial Myopathy. *Sci. Rep.* 6: 30610
- [213] Violitzi F, Perivolidi V-I, Thireou T, Grivas I, Haralambous S, Samiotaki M, Panayotou G, Douni E (2019) Mapping Interactome Networks of DNAJC11, a Novel Mitochondrial Protein Causing Neuromuscular Pathology in Mice. *J. Proteome Res.* 18: 3896–3912
- [214] Vogel F, Bornhövd C, Neupert W, Reichert AS (2006) Dynamic subcompartmentalization of the mitochondrial inner membrane. *J. Cell Biol.* 175: 237–247
- [215] Waegemann K, Popov-Čeleketić D, Neupert W, Azem A, Mokranjac D (2014) Cooperation of TOM and TIM23 Complexes during Translocation of Proteins into Mitochondria. *J. Mol. Biol.* 1075–1084
- [216] Walker JE (2013) The ATP synthase: The understood, the uncertain and the unknown. *Biochem. Soc. Trans.* 41: 1–16
- [217] Wang C, Taki M, Sato Y, Tamura Y, Yaginuma H, Okada Y, Yamaguchi S (2019a) A photostable fluorescent marker for the superresolution live imaging of the dynamic structure of the mitochondrial cristae. *Proc. Natl. Acad. Sci.* 116: 15817–15822
- [218] Wang L, Yan Z, Vihinen H, Eriksson O, Wang W, Soliymani R, Lu Y, Xue Y, Jokitalo E, Li J, Zhao H (2019b) FAM92A1 is a BAR domain protein required for mitochondrial ultrastructure and function. *J. Cell Biol.* 218: 97–111
- [219] Weber TA, Koob S, Heide H, Wittig I, Head B, van der Blik A, Brandt U, Mittelbronn M, Reichert AS (2013) APOOL Is a Cardiolipin-Binding Constituent of the Mitofilin/MINOS Protein Complex Determining Cristae Morphology in Mammalian Mitochondria. *PLoS One* 8: e63683

- [220] Weinhäupl K, Lindau C, Hessel A, Wang Y, Schütze C, Jores T, Melchionda L, Schönfisch B, Kalbacher H, Bersch B, Rapaport D, Brennich M, Lindorff-Larsen K, Wiedemann N, Schanda P (2018) Structural Basis of Membrane Protein Chaperoning through the Mitochondrial Intermembrane Space. *Cell* 175: 1365-1379.e25
- [221] Wiedemann N, Pfanner N (2017) Mitochondrial Machineries for Protein Import and Assembly. *Annu. Rev. Biochem.* 86: 685–714
- [222] Wolf DM, Segawa M, Kondadi AK, Anand R, Bailey ST, Reichert AS, Blik AM, Shackelford DB, Liesa M, Shirihai OS (2019) Individual cristae within the same mitochondrion display different membrane potentials and are functionally independent. *EMBO J.* 38: e101056
- [223] Wollweber F, von der Malsburg K, van der Laan M (2017) Mitochondrial contact site and cristae organizing system: A central player in membrane shaping and crosstalk. *Biochim. Biophys. Acta - Mol. Cell Res.* 1864: 1481–1489
- [224] Wong ED, Wagner JA, Scott S V., Okreglak V, Holewinski TJ, Cassidy-Stone A, Nunnari J (2003) The intramitochondrial dynamin-related GTPase, Mgm1p, is a component of a protein complex that mediates mitochondrial fusion. *J. Cell Biol.* 160: 303–311
- [225] Wu H, Carvalho P, Voeltz GK (2018) Here, there, and everywhere: The importance of ER membrane contact sites. *Science* 361: ean5835
- [226] Wurm CA, Jakobs S (2006) Differential protein distributions define two sub-compartments of the mitochondrial inner membrane in yeast. *FEBS Lett.* 580: 5628–5634
- [227] Xie J, Marusich MF, Souda P, Whitelegge J, Capaldi RA (2007) The mitochondrial inner membrane protein Mitofilin exists as a complex with SAM50, metaxins 1 and 2, coiled-coil-helix coiled-coil-helix domain-containing protein 3 and 6 and DnaJC11. *FEBS Lett.* 581: 3545–3549
- [228] Yan L, Qi Y, Ricketson D, Li L, Subramanian K, Zhao J, Yu C, Wu L, Sarsam R, Wong M, Lou Z, Rao Z, Nunnari J, Hu J (2020) Structural analysis of a trimeric assembly of the mitochondrial dynamin-like GTPase Mgm1. *Proc. Natl. Acad. Sci.* 117: 4061–4070
- [229] Yofe I, Schuldiner M (2014) Primers-4-Yeast: a comprehensive web tool for planning primers for *Saccharomyces cerevisiae*. *Yeast* 31: 77–80
- [230] Yotsuyanagi Y (1962) Études sur le chondriome de la levure. *J. Ultrastruct. Res.* 7: 141–158
- [231] Zeharia A, Friedman JR, Tobar A, Saada A, Konen O, Fellig Y, Shaag A, Nunnari J, Elpeleg O (2016) Mitochondrial hepato-encephalopathy due to deficiency of QIL1/MIC13 (C19orf70), a MICOS complex subunit. *Eur. J. Hum. Genet.* 24: 1778–1782
- [232] Zerbes RM, Bohnert M, Stroud DA, von der Malsburg K, Kram A, Oeljeklaus S, Warscheid B, Becker T, Wiedemann N, Veenhuis M, van der Klei IJ, Pfanner N, van der Laan M (2012) Role of MINOS in Mitochondrial Membrane Architecture: Cristae Morphology and Outer Membrane Interactions Differentially Depend on Mitofilin Domains. *J. Mol. Biol.* 422: 183–191
- [233] Zerbes RM, Höß P, Pfanner N, van der Laan M, Bohnert M (2016) Distinct roles of Mic12 and Mic27 in the mitochondrial contact site and cristae organizing system. *J. Mol. Biol.* 428: 1485–1492
- [234] Zhang D, Zhang Y, Ma J, Zhu C, Niu T, Chen W, Pang X, Zhai Y, Sun F (2020) Cryo-EM structures of S-OPA1 reveal its interactions with membrane and changes upon nucleotide binding. *Elife* 9: e50294

- [235] Zhang H, Menzies KJ, Auwerx J (2018) The role of mitochondria in stem cell fate and aging. *Development* 145: dev143420
- [236] Zhang M, Mileykovskaya E, Dowhan W (2002) Gluing the respiratory chain together: Cardiolipin is required for supercomplex formation in the inner mitochondrial membrane. *J. Biol. Chem.* 277: 43553–43556
- [237] Zick M, Duvezin-Caubet S, Schäfer A, Vogel F, Neupert W, Reichert AS (2009) Distinct roles of the two isoforms of the dynamin-like GTPase Mgm1 in mitochondrial fusion. *FEBS Lett.* 583: 2237–2243

9. Abbreviations

Å	Ångstrom
a.u.	arbitrary units
AAC	ATP/ADP carrier
ATP	adenosine triphosphate
BN-PAGE	blue native polyacrylamide gel electrophoresis
BSE	Bundle signalling element
Cas9	CRISPR-associated protein 9
CJ	crista junction
cl.	clone
CM	cristae membrane
CRISPR	clustered regularly interspaced short palindromic repeats
cryo-ET	cryo-electron tomography
DNA	deoxyribonucleic acid
DSG	disuccinimidyl glutarate (chemical crosslinker)
ECL	enhanced chemiluminescence
ERMES	ER-mitochondria encounter structure
F ₁	F1 fraction of mitochondrial ATP synthase
FLAG	Octapeptide (DYKDDDDK) protein tag for affinity purifications
F ₀	oligomycin-sensitive fraction of mitochondrial ATP synthase
GFP	green fluorescent protein
GTP	guanosine triphosphate
h	hours
HEK	human embryonic kidney cells
HRP	horseradish peroxidase
Hsp	heat shock protein
IBM	inner boundary membrane
IMM	inner mitochondrial membrane
IMS	intermembrane space
kDa	kilo-Dalton
KO	knockout
M	moles per liter
mA	milliampere
mg	milligram
Mgm1	mitochondrial genome maintenance 1 protein
MIA	mitochondrial intermembrane space import and assembly pathway
MIB	mitochondrial intermembrane space bridging complex

MICOS	mitochondrial contact site and cristae organising system
MicX	subunit of the MICOS complex, X = molecular weight in kDa
min	minutes
mM	millimoles per liter
mtDNA	mitochondrial DNA
NiNTA	Nickel-nitrilotriacetic acid beads
nm	nanometer
OD ₆₀₀	optical density at 600 nm
OMM	outer mitochondrial membrane
OPA1	optical atrophy 1 protein
ORF	open reading frame
OXPHOS	oxidative phosphorylation
PBS	Phosphate-buffered saline
PK	proteinase K
ProtA	Protein A (C-terminal protein tag for affinity purifications, also contains TEV cleavage site and hepta-histidine tag)
RNA	ribonucleic acid
RNAi	RNA interference
ROS	reactive oxygen species
rpm	revolutions per minute
SAM	sorting and assembly machinery
SDS-PAGE	sodium dodecyl sulphate polyacrylamide gel electrophoresis
sgRNA	single guide RNA
TBS	Tris-buffered saline
TCA cycle	tricarboxylic acid cycle
TEV	Tobacco Etch Virus
TIM22	carrier translocase of the inner membrane
TIM23	presequence translocase of the inner mitochondrial membrane
TOM	translocase of the outer mitochondrial membrane
UTR	untranslated region
V	Volt
v/v	volume per volume
VDAC	Voltage-dependent anion channel
w/v	weight per volume
WT	wild-type
µg	microgram
µM	micromoles per liter
Δψ	mitochondrial membrane potential

x g	unit of relative centrifugal force (RCF)
XL-MS	crosslink mass-spectrometry
10x His	Decahistidine protein tag for affinity purifications

10. List of figures

Figure 1 Asymmetry of mitochondrial membranes in yeast (adapted from Wollweber et al, 2017).....	9
Figure 2 Organisation of the MICOS/MIB complex at crista junctions (modified from Wollweber et al, 2017)	16
Figure 3 MICOS core subunits are required for efficient adaptation to respiratory metabolism	42
Figure 4 Delayed mitochondrial inner membrane biogenesis in Mic10 mutant yeast during the diauxic shift	43
Figure 5 ATP synthase-bound Mic10 is required for efficient adaptation to respiratory metabolism, but does not rescue MICOS activity	46
Figure 6 Antagonistic effect of Mic26 and Mic27 on Mic10 oligomerisation.	49
Figure 7 Mic26-Mic27 and cardiolipin independently affect Mic10 assembly.	51
Figure 8 Subcomplexes of the human MICOS complex.	54
Figure 9 Effect of MIC10 and MIC60 deletion in HEK293T mitochondria	57
Figure 10 Organisation of the MIC10 subcomplex in human mitochondria	60
Figure 11 The MIB complex and DNAJC11 spatially coordinate β -barrel biogenesis	63
Figure 12 Structure of Mgm1 (as published in Faelber et al., 2019).....	66
Figure 13 Analysis of Mgm1 dimer and tetramer interface mutants.....	68
Figure 14 Mgm1 tetramer mutants exert strong dominant-negative phenotypes.....	70
Figure 15 Hypothetical model of MICOS/DNAJC11 mediated spatial coordination of protein import.....	81

11. List of tables

Table 1 Reagents and critical equipment	21
Table 2 Antibodies.....	25
Table 3 Plasmids.....	27
Table 4 Yeast strains.....	28
Table 5 Mammalian cell lines	31

12. Acknowledgements

The work described here was conducted at the University of Freiburg and the Saarland University Medical Centre in Homburg. I would like to thank Prof. Dr. Martin van der Laan for the opportunity to work in his laboratory and Prof. Dr. Nikolaus Pfanner for the opportunity to start my PhD in his laboratories in Freiburg.

Many colleagues and collaborators have contributed to the work described here. I thank all colleagues in Freiburg, especially “lab 3” for their help and discussions. Particularly, I would like to thank Dr. Susanne Horvath for her help during the first months of my PhD, Dr. Ralf Zerbes for the great collaboration on the initial characterisation of human MICOS knockout cell lines and Dr. Heike Rampelt for the great collaboration on various projects related to the yeast MICOS complex and many insightful discussions during the last few years.

I am grateful to all lab members in Homburg for their contributions to the projects described here and their help in the transition from Freiburg to Homburg. In particular, I thank Dr. Karina von der Malsburg and Dr. Alexander von der Malsburg for countless discussions, their help in setting up the lab in Homburg and the great collaboration on the human MICOS/DNAJC11 project. I also thank Katja Noll and Sibylle Jungbluth, not only for their exceptional effort in keeping the lab running but also for their amazing experimental help. In addition, I thank my lab and office-mates, particularly Tobias Deisemann, Elena May, Valerie Chaumet and Tommy Sroka, for the nice working atmosphere.

During my PhD I was lucky to collaborate with numerous great colleagues. In particular, I thank Prof. Dr. Oliver Daumke and members of his laboratory (especially Dr. Katja Faelber and Dr. Tobias Bock-Bierbaum) for the great collaboration on Mgm1 and MICOS assembly and all co-authors of Faelber et al., 2019 for their outstanding work. Furthermore, I would like to thank Prof. Dr. Johannes Herrmann and his team (especially Felix Boos, Dr. Ajay Ramesh and Dr. Katja Hansen) for the opportunity to contribute to exciting manuscripts and many inspiring discussions.

I am grateful to the Boehringer Ingelheim Fonds for funding my PhD and, more importantly, I thank the entire BIF team for organising amazing retreats where I met many like-minded young scientists. These meetings had a greater influence on my career than I could have imagined.

Finally, I thank all my friends from Freiburg, Edinburgh and elsewhere and my family for their support during the last years.

13. Publications

McCormick B, Craig HE, Chu JY, Carlin LM, Canel M, Wollweber F, Toivakka M, Michael M, Astier AL, Norton L, Lilja J, Felton JM, Sasaki T, Ivaska J, Hers I, Dransfield I, Rossi AG & Vermeren S (2019) A Negative Feedback Loop Regulates Integrin Inactivation and Promotes Neutrophil Recruitment to Inflammatory Sites. *J. Immunol.* 203: 1579–1588

Faelber K*, Dietrich L*, Noel JK#, Wollweber F#, Pfitzner A-K#, Mühleip A, Sánchez R, Kudryashev M, Chiaruttini N, Lilie H, Schlegel J, Rosenbaum E, Hessenberger M, Matthaeus C, Kunz S, von der Malsburg A, Noé F, Roux A, van der Laan M, Kühlbrandt W & Daumke O (2019) Structure and assembly of the mitochondrial membrane remodelling GTPase Mgm1. *Nature* 571: 429–433
(*/# equal contribution)

Boos F, Krämer L, Groh C, Jung F, Haberkant P, Stein F, Wollweber F, Gackstatter A, Zöller E, van der Laan M, Savitski MM, Benes V & Herrmann JM (2019) Mitochondrial protein-induced stress triggers a global adaptive transcriptional programme. *Nat. Cell Biol.* 21: 442–451

Rampelt H*, Wollweber F*, Gerke C, de Boer R, van der Klei IJ, Bohnert M, Pfanner N & van der Laan M (2018) Assembly of the Mitochondrial Cristae Organizer Mic10 Is Regulated by Mic26–Mic27 Antagonism and Cardiolipin. *J. Mol. Biol.* 430: 1883–1890
(* equal contribution)

Wollweber F, von der Malsburg K & van der Laan M (2017) Mitochondrial contact site and cristae organizing system: A central player in membrane shaping and crosstalk. *Biochim. Biophys. Acta - Mol. Cell Res.* 1864: 1481–1489

Ramesh A, Peleh V, Martinez-Caballero S, Wollweber F, Sommer F, van der Laan M, Schroda M, Alexander RT, Campo ML & Herrmann JM (2016) A disulfide bond in the TIM23 complex is crucial for voltage gating and mitochondrial protein import. *J. Cell Biol.* 214: 417–431

Ieva R, Schrempp SG, Opaliński Ł, Wollweber F, Höß P, Heißwolf AK, Gebert M, Zhang Y, Guiard B, Rospert S, Becker T, Chacinska A, Pfanner N & van der Laan M (2014) Mgr2 Functions as Lateral Gatekeeper for Preprotein Sorting in the Mitochondrial Inner Membrane. *Mol. Cell* 56: 641–652

Ieva R, Heißwolf AK, Gebert M, Vögtle F-N, Wollweber F, Mehnert CS, Oeljeklaus S, Warscheid B, Meisinger C, van der Laan M & Pfanner N (2013) Mitochondrial inner membrane protease promotes assembly of presequence translocase by removing a carboxy-terminal targeting sequence. *Nat. Commun.* 4: 2853

14. Curriculum vitae

Aus datenschutzrechtlichen Gründen wird der Lebenslauf in der elektronischen Fassung der Dissertation nicht veröffentlicht.